Stability and Regulation of Delayed Negative Feedbacks in Biochemical Networks

Dissertation
zur Erlangung des akademischen Grades
Doktoringenieur (Dr.-Ing.)

von
Anastasiya Börsch
geboren am 29. September 1988 in Minsk

genehmigt durch die Fakultät für Elektrotechnik und Informationstechnik der
Otto-von-Guericke-Universität Magdeburg

Gutachter:
Prof. Dr. Rolf Findeisen
Prof. Dr. Gerald Warnecke
Dr. Jörg Schaber

eingereicht am 29. Januar 2016
Promotionskolloquium am 4. November 2016

Aknowledgments

Contents

List of symbols and abbreviations

This list serves as a reference for symbols and abbreviations that are not explained at each individual occurrence in the text.

Genes and proteins

GFP	Green fluorescent protein
IκB	Inhibitor of κB
IKK	Inhibitor of nuclear factor κB
Hes1	Hairy and enhancer of split-1 protein
HOG	High osmolarity glycerol
Hog1	High osmolarity glycerol response protein 1
Hog1-PP	Phosphorylated high osmolarity glycerol response protein 1
NF-κB	Nuclear factor "κ-light-chain-enhancer" of activated B-cells
Mdm2	Mouse double minute 2 homolog
p53	Protein 53
TNF-α	Tumor necrosis factor-α

Further abbreviations

DDE	Delay differential equation
DNF	Delayed negative feedback
IPTG	Isopropyl β-D-1-thio-galactopyranoside
NaCl	Sodium Chloride
M	Molar mass
ODE	Ordinary differential equation
SSR	Sum of squared residuals

Abstract

Intracellular networks have a complex structure. Despite their complexity they are formed from a small set of recurring regulation patterns called network motifs. This manuscript is dedicated to studying one of these network motifs called negative feedback.

Negative feedback in combination with time delay can cause several characteristic response patterns of the cellular system including an overdamped response, damped or sustained oscillations. In order to understand this complex behaviour I construct generic two-dimensional models of delayed negative feedback by means of delay differential equations and subject them to mathematical analysis.

As a result, I derive explicit thresholds and boundaries showing how time delay determines characteristic response patterns of delayed negative feedback systems. In addition, I investigate the influence of several design features on the stability of the model equilibrium, i.e., presence of auto-inhibition and/or mass conservation and the kind and/or strength of the delayed negative feedback. I show that auto-inhibition and mass conservation have a stabilizing effect on the model equilibrium. In contrast, increasing abruptness and decreasing feedback threshold have a de-stabilizing effect.

Further, I apply my theoretical analyses to concrete data. I show that adaptation to osmotic stress in yeast is optimal in the sense of minimizing adaptation time without causing oscillatory behaviour, i.e., a critically damped response. I also claim that a slight increase of time delay in NF-κB system might induce a switch from damped to sustained oscillatory behaviour. For the mammalian p53 system I show that an auto-inhibitory feedback can decouple period and amplitude of an oscillatory response, whereas the delayed feedback cannot.

Using my theoretical analysis, I suggest a design of a synthetic intracellular network, which contains delayed negative feedbacks and can switch between adaptive behaviour and sustained oscillations in a controlled manner.

Finally, I present a technique showing how to approximate delay differential equations using ordinary differential equations. The approximated system can be further analysed by means of common mathematical theory and computational software developed for analysis of ordinary differential equations.

Taken together, my thesis provides insights into how time delay and design features of biochemical networks containing delayed negative feedback act together to elicit specific characteristic response patterns of network components. My theoretical framework is useful for engineering synthetic networks and controlling their behaviour in response to external stimulation.

Deutsche Kurzfassung

Die Stabilität und Regelung der verzögerten negativen Rückkopplung in biochemischen Netzwerken

Intrazelluläre Netzwerke haben eine komplexe Struktur. Trotz ihrer Komplexität sind sie aus sich wiederholenden regulären Mustern, die Netzwerkmotive genannt werden, aufgebaut. Dieses Manuskript wird der Untersuchung einer dieser Netzwerkmotiven, der negativen Rückkopplung, gewidmet.

Die negative Rückkopplung in Kombination mit einer Zeitverzögerung kann unterschiedliche charakteristische Antwortmuster des zellulären Systems verursachen, zum Beispiel eine übergedämpften Antwort, gedämpfte Schwingungen oder Dauerschwingungen. Um dieses komplexe Verhalten zu verstehen, konstruiere ich generische zweidimensionale Modelle einer verzögerten negativen Rückkopplung durch verzögerte Differentialgleichungen und unterziehe diese einer mathematischen Analyse.

Als Ergebnis erhalte ich explizite Schwellenwerte und Grenzen, die definieren, wie die Zeitverzögerung das charakteristische Antwortmuster von Negativrückkopplungssystemen definieren. Zusätzlich untersuche ich die Wirkung von bestimmten Systemdesigns auf die Stabilität des Modellgleichgewichts. Das sind die Präsenz von Autoinhibition und/oder Massenerhaltung und die Art und Stärke der verzögerten negativen Rückkopplung. Ich zeige, dass Autoinhibition und Massenerhaltung einen stabilisierenden Effekt auf das Modellgleichgewicht haben. Im Gegensatz dazu haben die wachsende Steilheit und der fallende Rückkopplungsschwellenwert einen destabilisierenden Effekt.

Ich wende meine theoretischen Analysen auf spezifische experimentelle Daten an. Ich zeige, dass die Adaptation auf den osmotischen Stress in der Hefe optimal ist. Das Adaptationsoptimum wird in dem Sinne von Minimierung der Adaptionszeit ohne Oszillationen zu verursachen, d.h. eine kritische gedämpfte Antwort, betrachtet. Ich behaupte, dass eine schwache Erhöhung der Zeitverzögerung in dem NF-κB-System einen Wechsel von einem gedämpften zu einem Dauerschwingungsverhalten verursachen kann. Für das p53 Säugersystem zeige ich, dass die Autoinhibitionsrückkopplung die Periode und Amplitude der oszillatorischen Antwort entkoppeln kann. Im Gegensatz dazu kann die verzögerte negative Rückkopplung dies nicht.

Durch Nutzung meiner theoretischen Analyse schlage ich einen Aufbau von einem synthetischen intrazellulärem Netzwerk vor, das verzögerte negative Rückkopplungen enthält und zwischen dem adaptiven Verhalten und Dauerschwingungen in kontrollierter Form wechseln kann.

Schließlich präsentiere ich eine Technik, wie man verzögerte Differentialgleichungen durch gewöhnliche Differentialgleichungen annähern kann. Das angenäherte System kann weiter durch die gewöhnliche mathematische Theorie und Berechnungssoftware, die für die Analyse von gewöhnlichen Differentialgleichungen entwickelt wurde, analysiert werden.

Zusammengenommen gibt meine Dissertation Einblick, wie die Zeitverzögerung und das Design von biochemischen Netzwerken, die verzögerte negative Rückkopplungen enthalten, zusammen agieren um spezifische charakteristische Antwortmuster von Netzwerkkomponenten hervorzurufen. Meine Theorien sind nützlich für die Entwicklung von synthetischen Netzwerken und Steuerung ihres Verhaltens in Reaktion auf externe Stimulation.

1 Introduction

1.1 Modelling biological systems

Biological systems including organisms, cells and molecules have complex structure and fulfil various functions. Often biological processes happening in these systems are also complex and intuitively unclear. Biologists perform experiments and build hypotheses to understand individual processes. However, it is hard to combine results obtained for distinct processes into a big picture. In this case, mathematical modelling is a useful tool, which can assist in understanding the nature and dynamics of these processes, derive predictions about their behaviour and reveal interactions between their components [53]. The mathematical and computational modelling of complex biological systems is often called "systems biology". Here, I would like to cite the statement of the British biologist Denis Noble concerning systems biology [82]:

"Systems biology...is about putting together rather than taking apart, integration rather than reduction. It requires that we develop ways of thinking about integration that are as rigorous as our reductionist programmes, but different....It means changing our philosophy, in the full sense of the term."

1.1.1 What is a model?

The definition of a model varies depending on the community and research field. In this study, I refer to the model definition provided by the German scientist Edda Klipp [53]:

"In a broad sense, a model is an abstract representation of objects or processes that explains features of these objects or processes..."

The way of abstract representation depends on the purpose of the model. In Fig. 1.1, I depicted several types of models constructed for an example process. In the example process, which may occur in a eukaryotic cell, an activator protein X increases the expression of protein Y after an external cell stimulation S.

Thus, in order to understand molecular details of the process one may construct a *biological model*. This model has a graphical form and contains detailed information about molecular processes preceding the formation of the protein Y. One may acquire this information by performing preliminary experiments and using established biochemical knowledge.

Additionally, a model of a biochemical network may have the form of a *wiring scheme*. The wiring scheme also has a graphical representation. However, in comparison to the biological model, the wiring scheme has a higher level of abstraction
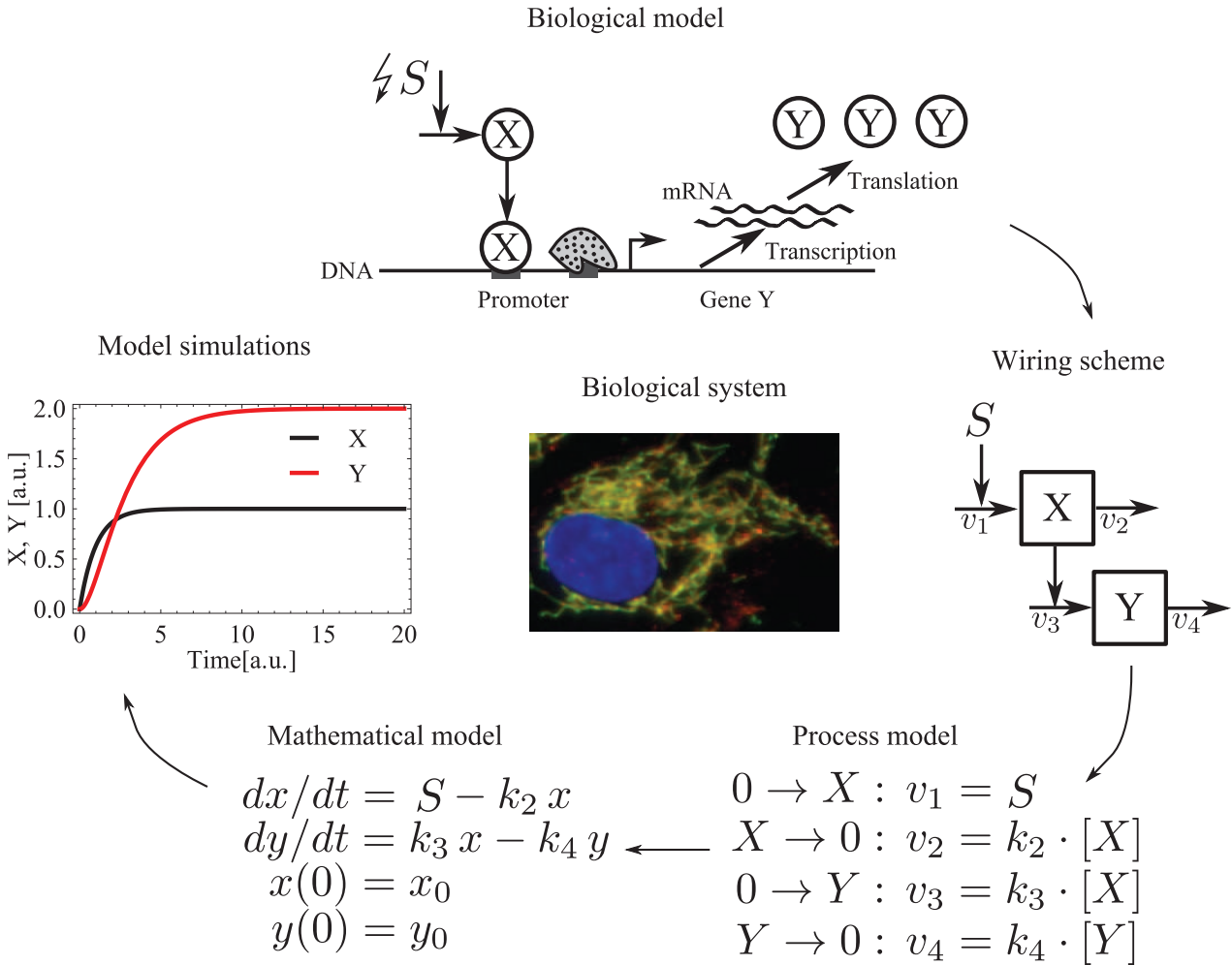
Figure 1.1: Chain of models of a biological process. The process describes how the activator protein X increases the expression of the protein Y after the external cell stimulation S. In order to represent this process, one may construct a biological model, a wiring scheme, a process model or a mathematical model. The biological system, where the example process takes place, is represented by eukaryotic cells.

and represents only the relevant information. At this stage it is up to the modeller to decide on the relevance of the information depending on the objective of the study. In my example, I am interested in the dynamics of proteins X and Y as well as the biochemical reactions and modifying influences between them. To this end, I omit the information, how the active protein X binds the promoter of the gene Y, how transcription and translation processes occur, etc.

Based on the wiring scheme one may construct a *process model*. The process model describes individual processes, which occur in the system, in the form of chemical reactions. Reaction rates are designated by variables v_i, $i = 1, \ldots, 4$. The parameter $k_2 > 0$ designates the degradation rate of protein X. Parameters $k_3 > 0$ and $k_4 > 0$ designate activation and degradation rates of protein Y. Activation and degradation rates can be either experimentally measured or fitted based on the available experimental data.

The process model can be formulated into a *mathematical model*. For this purpose one may apply a variety of methods including Markov chains [1], Petri nets [16], boolean networks [103], ordinary [88, 92] and delay [76] differential equations, etc. The choice of the method depends on the objective of the study and available experimental data. In Fig. 1.1 I depicted one of several possible dynamic models of the example process by means of ordinary differential equations. Here, variables x and y designate the amount of proteins X and Y, respectively, changing over time in the cell. I assume that the initial amount of proteins before stimulation have values $x_0 \geq 0$ and $y_0 \geq 0$. The mathematical model can be further analysed and simulated with certain parameter values.

As a result, I presented a chain of models for the same biological process starting with the biological model and ending with the mathematical model. The kind of model used depends on the purpose of the modeller and objective of the study.

1.1.2 Why mathematical models?

Modelling is a subjective procedure, since the modeller decides what and how to put in the model. However, a proper model is able to represent specific parts of a real system and gain new insights into its functioning. In this context, I would like to mention the statement of the British statistician George Box concerning modelling [18]:

"Essentially, all models are wrong, but some are useful."

Thus, combining experiments and mathematical modelling leads to many advantages for investigating complex biological systems in comparison with purely experimental studies [53]:

- Mathematical modelling requires rigorous formulation of the verbal hypothesis. This clarifies the concept of the study and specifies the research problem.

- Mathematical modelling reveals gaps in the knowledge of a specific system. During the modelling process the modeller defines components and interactions to be specified experimentally.

- Mathematical modelling provides quantitative as well as qualitative predictions of the system behaviour. Model simulations may indicate, which components at which conditions and time points should be measured to support or reject the hypothesis.

- Theoretical and numerical analyses of mathematical models may reveal mechanisms underlying complex behaviour of the biological system, e.g., bistability, oscillations, etc.

- Mathematical modelling is cheap and fast in comparison with experiments.

- Well designed mathematical models are re-usable and can be completely or partly embedded in other models.

Thus, I may conclude that mathematical modelling in combination with experiments is a powerful tool for approaching research problems of complex biological systems.

1.1.3 Differential equations

Using differential equations is an effective way to mathematically model the evolution of biochemical systems in continuous time [2, 54, 100]. There exist several types of differential equations such as ordinary differential equations [20], delay differential equations [25, 95], partial differential equations [29] and differential algebraic equations [57]. Depending on the purpose of the model the investigator decides which kind of equations should be applied. In this thesis, I construct mathematical models using ordinary and delay differential equations.

Ordinary differential equations (ODEs)
ODEs contain only one independent variable, the time t, and describe the dynamic behaviour of a deterministic system on the same time scale in vector notation:

$$\begin{aligned} \frac{dx}{dt} &= f(t, p, x(t)), \\ x(0) &= \phi, \end{aligned}$$

where $x(t) = (x_1(t), x_2(t), \ldots, x_n(t))^T$ is a vector of system components, $f = (f_1, f_2, \ldots, f_n)^T$ is a vector of functions representing interactions between components $x_i(t)$, the vector $p = (p_1, p_2, \ldots, p_m)^T$ represents parameters and the vector $\phi = (\phi_1, \phi_2, \ldots, \phi_n)^T$ is a non-negative constant vector describing initial values.

Delay differential equations (DDEs)
Similarly to ODEs, DDEs contain only one independent variable, the time t. However, DDEs also include an explicit time delay τ. As a result, time derivatives at the current time depend not only on the solution at the current time, but also on the solution at the previous time:

$$\begin{aligned} \frac{dx}{dt} &= f(t, p, x(t), x(t - \tau)), \\ x(t) &= \phi(t), \, -\tau \leq t \leq 0, \end{aligned}$$

where $\tau \in \mathbb{R}_{>0}$ designates a time delay and $\phi(t) = (\phi_1(t), \phi_2(t), \ldots, \phi_n(t))^T$ is the vector of continuous functions satisfying $\phi_i \colon [-\tau, 0] \mapsto \mathbb{R}_{\geq 0}, \, i = 1, \ldots, n$.

1.1.4 Parameter estimation

Mathematical model can demonstrate different behaviour depending on parameter values. However, it is necessary that a mathematical model is able to approximate and predict the behaviour of the concrete biological system. Therefore the error between model simulations and available experimental data obtained for the concrete biological system should be minimized. This can be achieved by estimating parameter values of the mathematical model.

There are many approaches to estimate model parameters [65, 93]. In this thesis, I consider parameter values to be optimal if they minimize the sum of squared residuals SSR, i.e.:

$$SSR(p) = \sum_{i=1}^{k} \left(x(t_i, p) - x_i \right)^2,$$

where $p = (p_1, p_2, \ldots, p_m)^T$ denotes a vector of parameters to be estimated, $x(t, p)$ is a numerical solution that depends on parameters p, x_i is a measured data value at the time point t_i, k is the number of data points.

For minimizing $SSR(p)$ with respect to parameter values I utilize the numerical function *NMinimize* in Mathematica 9, which, by default, uses the "Nelder-Mead" method [78]. In case "Nelder-Mead" performs poorly, it automatically switches to the "Differential evolution" method [98]. The parameter optimization process is assumed to have converged to a local minimum, if the difference between the new best and the old best function value $SSR(p)$, as well as the distance between the new best and the old best parameter values, are less than a tolerance of 10^{-8}.

1.1.5 Mathematical analysis

The constructed model can be subjected to further mathematical analyses in order to explain the complex behaviour of the biological system of interest.

The kind and complexity of analysis depend on model properties. The model is said to be linear if all the x_i on the right-hand side of model equations appear to the first power only. Otherwise, the model is non-linear [100]. In comparison to linear, most non-linear systems of differential equations are impossible to solve analytically and are difficult to analyse. However, the majority of biological interactions, including processes presented in this thesis, occur in a non-linear fashion [2, 105]. This requires non-linear equations for modelling and, consequently, special analysis techniques.

Stability of steady states

In the absence of stress the biological system is considered to be in steady state (or equilibrium). This means that values of model components remain constant in time:

$$\frac{dx}{dt} = 0.$$

Depending on the biological system and on the model there can exist multiple steady states. Determining the stability of steady states is the key to the analysis of non-linear systems [95, 100].

In this thesis, I perform theoretical stability analysis of mathematical models described by two autonomous non-linear delay differential equations (DDEs) of the form:

$$\begin{aligned}
\frac{dx}{dt} &= f(p, x(t), x(t - \tau)), \\
x(t) &= \phi(t), \ -\tau \leq t \leq 0,
\end{aligned} \tag{1.1}$$

where $x(t) = (x_1(t), x_2(t))^T$ is a vector of system components; $x(t - \tau) = (x_1(t - \tau), x_2(t - \tau))^T$ is a vector of system components delayed by the time τ; $f = (f_1, f_2)^T$ is a vector of continuously differentiable functions representing interactions between components $x_1(t)$, $x_2(t)$, $x_1(t - \tau)$ and $x_2(t - \tau)$; the vector $p = (p_1, p_2, \ldots, p_m)^T$ represents parameters; the vector $\phi(t) = (\phi_1(t), \phi_2(t))^T$ is a vector of functions having constant non-negative values for $t \in [-\tau, 0]$.

Thus, the steady state x_s of the model (1.1) satisfies

$$f(p, x_s, x_s) = 0.$$

For the model (1.1), the steady state x_s is *stable*, if for any $\varepsilon > 0$, there exists $\delta > 0$ such that $||\phi|| < \delta$ implies that $||x(t - \tau)|| < \varepsilon$ for $t \geq 0$ and $x(t \leq 0) = \phi$. The steady state x_s is *asymptotically stable*, if it is stable and if there exists $\gamma > 0$ such that any $||\phi|| < \gamma$ implies that $x(t) \to x_s$ for $t \to \infty$ and $x(t \leq 0) = \phi(t)$. Finally, the steady state x_s is *unstable*, if it is not stable [95].

In other words, the steady state x_s is defined to be stable, if sufficiently small disturbances away from it damp out in time. If disturbances grow in time, then the steady state is unstable [100].

Let $\zeta = x - x_s$ be a small perturbation away from x_s. In order to check whether the perturbation ζ grows or decays, I describe its dynamics by means of DDEs:

$$\frac{d\zeta}{dt} = \frac{dx}{dt} = f(p, x, x_\tau) = f(p, x_s + \zeta, x_s + \zeta_\tau), \tag{1.2}$$

where delayed variables $x(t - \tau)$ and $\zeta(t - \tau)$ are denoted as x_τ and ζ_τ, respectively. Using Taylor's expansion about the steady state x_s leads to the following expression:

$$f(p, x_s + \zeta, x_s + \zeta_\tau) \approx \underbrace{f(p, x_s, x_s)}_{=0} + \underbrace{\frac{\partial f}{\partial \zeta}(x_s, x_s)}_{A} \zeta + \underbrace{\frac{\partial f}{\partial \zeta_\tau}(x_s, x_s)}_{B} \zeta_\tau,$$

where A and B are two-dimensional matrices.

Thus, the equation (1.2) can be approximated by the following equation:

$$\frac{d\zeta}{dt} = A\,\zeta(t) + B\,\zeta(t-\tau). \tag{1.3}$$

The equation (1.3) is called the linearised equation about the equilibrium x_s. To seek exponentially growing solutions of (1.3), I represent them in the form:

$$\zeta(t) = \psi\,e^{\lambda t},$$

where λ is a complex number, v is a vector of complex numbers.

Substituting this vector in (1.3) results in the following equation:

$$\lambda\,I_2 = A + B\,e^{-\lambda\tau},$$

where I_2 is the identity matrix of the size two.

Thus, $\zeta(t) = \psi\,e^{\lambda t}$ is a non-zero solution of (1.3), if λ is a solution of the characteristic equation:

$$P(\lambda,\tau) = \det(\lambda\,I_2 - A - B\,e^{-\lambda\tau}). \tag{1.4}$$

Solutions of the characteristic equation are called characteristic roots. If there are no characteristic roots λ on the imaginary axis, then dynamics of the system (1.3) near the equilibrium $\zeta_s = (0,0)^T$ is locally topologically equivalent to the dynamics of the model (1.1) near the equilibrium x_s [58]. Namely, there exists a homeomorphism $h\colon \mathbb{R}^2 \mapsto \mathbb{R}^2$ that is defined in a small neigbourhood $U \subset \mathbb{R}^2$ of ζ_s, satisfies $x_s = h(\zeta_s)$ and maps orbits of the system (1.3) in U onto orbits of the model (1.1) in $W = f(U) \subset \mathbb{R}^2$ preserving the direction of time. For example, if ζ produces sustained oscillations about the equilibrium ζ_s, then x also demonstrates sustained oscillations about the equilibrium x_s.

Thus, if any characteristic root has a positive real part, then the perturbation ζ exponentially grows in time and the steady state is unstable. If all characteristic roots have negative real parts, then the perturbation ζ exponentially decays in time and the steady state is stable. If leading characteristic roots are zero, then the stability can not be determined using the first order of the linearisation.

In biological terms, the stability of the steady state can be interpreted as the ability of the biological system to return to its initial state after small changes in component values.

Bifurcation analysis

Changing parameter values can change the number of steady states and their stability. This may result in a qualitative change in the model dynamics called bifurcation [58, 100, 105]. To detect bifurcations one may perform a bifurcation analysis of the model. The model parameter, which is varied for the bifurcation analysis, is called a control parameter. The value of the control parameter at which bifurcation occurs is called

the bifurcation point [100].

There are several types of bifurcations, which may arise under variation of the control parameter [58, 100]. The *saddle-node bifurcation* is the basic mechanism by which steady states are created and destroyed. For presenting this kind of bifurcation I introduce the following ordinary differential equation (ODE):

$$\frac{dx}{dt} = r + x^2, \tag{1.5}$$

where $x(t)$ is a time-dependent variable and r is a parameter. The bifurcation diagram for (1.5) is presented in Fig. 1.2A. In this figure, the steady state of the system is designated by x_s, branches of stable and unstable steady states are designated by solid and dashed blue curves, respectively.

In several models, the steady state always exists independent of parameter values. However, under parameter variation the stability of the steady state can be changed constituting the *transcritical bifurcation*. An example of the ODE with the transcritical bifurcation has the following form:

$$\frac{dx}{dt} = rx - x^2. \tag{1.6}$$

The bifurcation diagram corresponding to the transcritical bifurcation is depicted in Fig. 1.2B.

When the *pitchfork bifurcation* occurs, steady states appear and disappear in symmetrical pairs. The pitchfork bifurcation can be subcritical or supercritical. For presenting the supercritical pitchfork bifurcation I use the following ODE:

$$\frac{dx}{dt} = rx - x^3. \tag{1.7}$$

A
Saddle-node bifurcation

B
Transcritical bifurcation

C
Pitchfork bifurcation (supercritical)
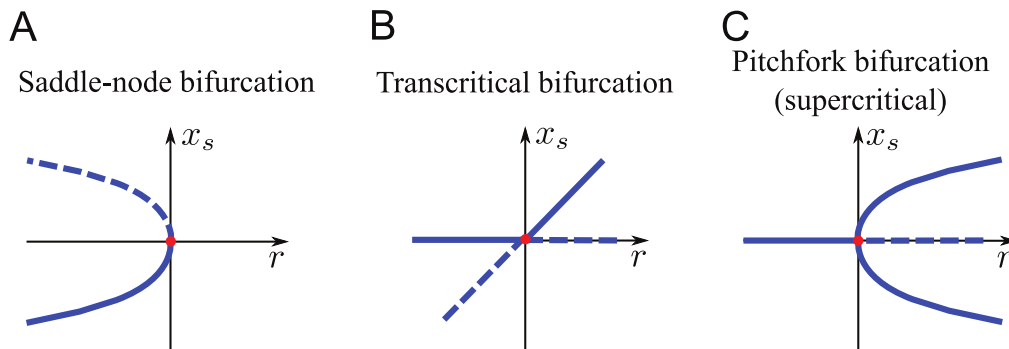
Figure 1.2: Bifurcation diagrams. (A) Saddle-node bifurcation. (B) Transcritical bifurcation. (C) Supercritical pitchfork bifurcation. Values of steady states x_s of corresponding ODEs (1.5)-(1.7) depend on the parameter value r. Bifurcation points ($r = 0$) are designated by red dots. Branches of stable steady states are designated by solid blue curves, branches of unstable steady states are designated by dashed blue curves.
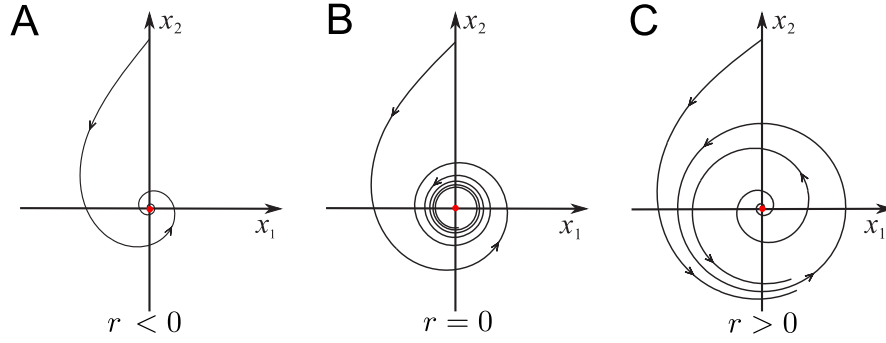
Figure 1.3: Phase portraits of the system (1.8) **undergoing the supercritical Hopf bifurcation with respect to** r. (A) For $r < 0$ the steady state is stable. (B) For the parameter $r = 0$ the Hopf bifurcation occurs. (C) The parameter $r < 0$ causes the instability of the steady state and the system (1.8) has a periodic orbit. The steady state $x_s = (0, 0)^T$ is designated by red dots. The figure was taken from [58].

The bifurcation diagram presenting the supercritical pitchfork bifurcation is shown in Fig. 1.2C.

There also exists a separate type of bifurcation called *Hopf bifurcation*. The Hopf bifurcation turns on or off sustained oscillations in model components under variation of a parameter. Like pitchfork bifurcations, Hopf bifurcations exist in both sub- and supercritical variations. An example of the two-dimensional ODE system with the supercritical Hopf bifurcation has the following form:

$$
\begin{aligned}
\frac{dx_1}{dt} &= r\,x_1 - x_2 - x_1(x_1^2 + x_2^2), \\
\frac{dx_2}{dt} &= x_1 + r\,x_2 - x_2(x_1^2 + x_2^2),
\end{aligned}
\tag{1.8}
$$

where $(x_1(t), x_2(t))^T$ is a vector of time-dependent variables and r is the parameter. Several phase portraits of the system (1.8) depending on the parameter r are presented in Fig. 1.3. The location of the steady state $x_s = (0, 0)^T$ is designated by red dots. In case $r < 0$, the steady state x_s is stable (see Fig. 1.3A). In case $r > 0$, the steady state x_s is unstable and the system (1.8) has a periodic orbit (see Fig. 1.3C). In case $r = 0$, the supercritical Hopf bifurcation occurs (see Fig. 1.3B).

For detecting the Hopf bifurcation in both ODE and DDE models one should derive the characteristic polynomial of the model and calculate characteristic roots with respect to the control parameter r [21, 58, 95, 100]. If there exists a pair of complex characteristic roots $\lambda(r)_{1,2} = \alpha(r) \pm i\omega(r)$ that crosses the imaginary axis for some value of $r = r_m$:

$$
\lambda(r_m)_{1,2} = \pm i\omega,\ \omega > 0
$$

and the *Hopf transversality condition* at $r = r_m$ holds:

$$\frac{d\alpha}{dr}(r_m) > 0,$$

then one may conclude that the Hopf bifurcation occurs at the marginal value $r = r_m$.

Simulations of models presented in this thesis indicate that these models exhibit supercritical Hopf bifurcations presented in Fig. 1.3. Therefore, in the following chapters when I refer to Hopf bifurcations, I mean supercritical Hopf bifurcations.

In fact, the introduced differential equations (1.5)-(1.8) constitute normal forms of bifurcation types, which they presented above [58, 100]. Namely, these equations are locally topologically equivalent near the origin to systems exhibiting the respective type of bifurcations. In other words, each system with a bifurcation can be approximated by the corresponding normal form near the bifurcation point.

The bifurcation analysis is widely used to reveal mechanisms, e.g., bistability, and key parameters and components underlying complex behaviour of the biological system.

Sensitivity analysis

In comparison to bifurcation analysis, sensitivity analysis is performed to detect the quantitative change in the model dynamics under a specific parameter variation [22]. Thus, the investigator perturbs one certain parameter of the model and observes how this perturbation affects model characteristics, e.g., the dynamics of some model component or the value of a bifurcation point [40, 96].

In mathematical terms the sensitivity of a model characteristic to a specific perturbation can be presented in the following way [31]:

$$S = \frac{\Delta O}{O} \cdot \frac{p}{\Delta p},$$

where O is the output and p is the perturbed parameter. The output O can be any model element or characteristic, e.g., bifurcation point, adaptation time, etc. With ΔO and Δp I designate differences between the perturbed and unperturbed values of O and p, respectively. If $|S| \approx 1$ holds, then the perturbation ratio in the parameter p equals its effect in the output O. The relation $|S| >> 1$ means the sensitivity of the output O to the perturbation in the parameter p. Moreover, if $S > 0$ holds, then an inhibition of p will induce the inhibition of O. Otherwise, an inhibition of p results in the amplification of O, and vice versa.

In this thesis, I present sensitivity analysis graphically. Namely, I vary parameter values of the model within a defined range. For each varied parameter value I calculate a model characteristic of interest. Obtained results are further depicted on the same graph. Using this graph one may conclude how parameter values influence the model characteristic of interest. Additionally, this may reveal a parameter, which demon-

strates the highest impact on the model characteristic of interest. This information can be further used for performing experiments and predicting the behaviour of the biological system under certain conditions encoded in parameter values.

Robustness analysis

The robustness analysis clarifies if the biological system is able to keep its performance under a wide range of conditions [51, 52, 96]. In contrast to sensitivity, robustness is the insensitivity of a particular property of the biological system to intrinsic or extrinsic noise [22, 67].

For performing a robustness analysis of a concrete system the type of perturbations should be determined [22]. A simple method for examining the robustness of biological systems is a Monte-Carlo simulation [26, 50]. This method is based on the random sampling of model parameters according to a particular probability distribution and repeated simulation of the system for sampled parameters.

In this thesis, I perform Monte-Carlo analysis of mathematical models described by DDE systems having the general form (1.1). To this end, all fitted components of the parameter vector p and time delay τ of considered models are simultaneously varied N times:

$$\breve{p} = U[p \cdot r_1, p \cdot r_2],$$
$$\breve{\tau} = U[\tau \cdot r_1, \tau \cdot r_2],$$

where $\breve{p}$ is a perturbed parameter vector p, $\breve{\tau}$ is a perturbed time delay τ and $U[a, b]$ designates the limitation of the uniform distribution for random sampling of p and τ within $r1 \cdot 100\%$ and $r2 \cdot 100\%$ of their respective fitted values.

Then, for each perturbed parameter set I calculate model characteristics of interest. For example, for each perturbed parameter set of one of considered models I calculate Hopf bifurcation points of time delay $\breve{\tau}_m^i$ for $i = 1, \ldots, N$ and obtain their mean value:

$$< \breve{\tau}_m > = \frac{1}{N} \sum_{i=1}^{N} \breve{\tau}_m^i.$$

Finally, I compare model characteristics for fitted and perturbed parameter values. For the presented example, I compare the value of the Hopf bifurcation point τ_m calculated for fitted parameter values with the value $< \breve{\tau}_m >$ calculated for perturbed parameter values. The low change in the model characteristic under parameter variation indicates the robustness of a corresponding property of the biological system when subjected to a defined noise. In contrast, the high variation of the model characteristic shows that this particular property of the biological system is not robust to the noise.

1.2 Design principles of intracellular networks

Living cell can be considered as a system that governs its behaviour and its interaction with the environment. According to the definition of Uri Alon [2]:

"The cell is an integrated device made of several thousand types of interacting proteins."

Every protein is a small molecule, which fulfils a certain function in the cell. Proteins interact with each other, with external signals and with DNA constituting different kinds of intracellular networks. These networks regulate processes happening inside the cell and allow the cell to adapt to environmental changes.

There exist several types of intracellular networks such as sensory [3] and developmental [24] transcription networks, protein-protein interaction networks [97], signal transduction networks [89] and metabolic networks [72]. They differ from each other by modes of interaction between biomolecules as well as by velocities of functioning [2]. For example, transcription networks tend to have slow dynamics with processes happening on the scale of hours. In contrast, signal transduction networks usually function on the time scale of seconds to minutes.

Despite the aforementioned differences, networks function together. For example, the output of a signal transduction pathway, which belongs to a signal transduction network, is often a transcription factor belonging to a transcription network. In this way, signal transduction and transcription networks create a joint network [2].

Intracellular networks have a complex structure [2, 3, 94, 105]. In Fig. 1.4 a transcription network in the bacterium *E. coli* is depicted. The network consists of red nodes representing genes and black edges representing transcriptional regulation of one gene by the protein product of another gene [32].

Many studies showed that in spite of their complexity intracellular networks are composed from a small set of recurring regulation patterns called network motifs [2, 3, 73, 94, 105]. Some examples of network motifs are depicted in Fig. 1.5. Here, X, Y and Z mimic some network components, e.g., genes, proteins, metabolites, etc. Arrows mimic interactions between network components: sharp arrows mimic activation or production, blunt arrows mimic inhibition or degradation. As an example, one may interpret the motif from Fig. 1.5E as follows: the activator X activates Z and Y, the inhibitor Y inhibits Z.

Several network motifs, e.g., simple regulation (see Fig. 1.5A), are present in all network types [2, 3]. Some network motifs have been detected in several network types. For example, positive and negative auto-regulation (see Fig. 1.5B and C) and feedforward loops (see Fig. 1.5D and E) were detected in sensory and developmental networks [2, 3]. Some network motifs are found to be present only in a specific network type. For example, the diamond network motif seems to be restricted to signal transduction networks (see Fig. 1.5F) [2, 3].

It was shown that similar to separate networks, joint networks also have charac-
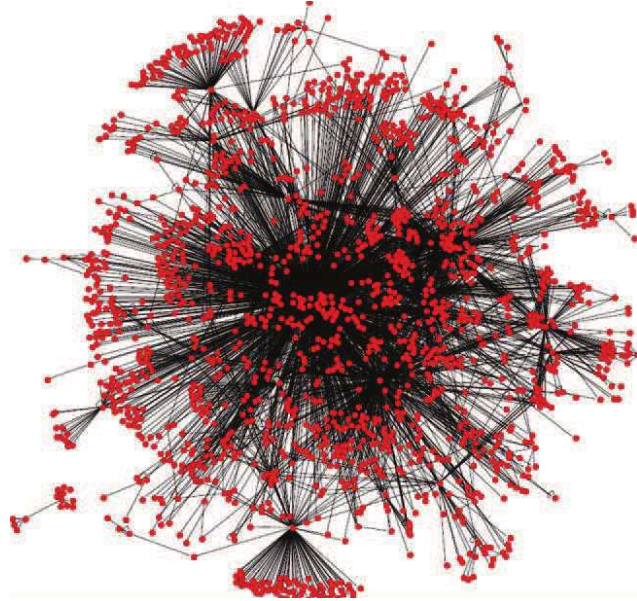
Figure 1.4: Example of a transcription network in *E. coli***.** Red nodes represent genes and black edges represent transcriptional regulation of one gene by the protein product of another gene. The figure was taken from [32].
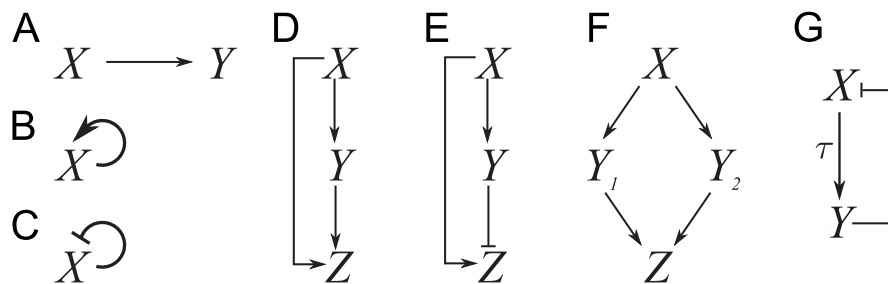
Figure 1.5: Examples of network motifs. (A) Simple regulation. (B) Positive auto-regulation. (C) Negative auto-regulation. (D) Coherent feedforward loop type 1. (E) Incoherent feedforward loop type 1. (F) Diamond network motif. (G) Composite network motif: negative feedback loop. The activation occurs with time delay τ. Designation: sharp arrows mimic activation, blunt arrows mimic repression.

teristic network patterns called composite network motifs [110]. The example of a very common composite network motif is a negative feedback loop [2] presented in Fig. 1.5G. In the joint network, the negative feedback loop is a hybrid of two types of interactions. The network component X activates Y on transcriptional level on a slow time scale. Then Y feeds back inhibiting X on the protein level on a rapid time scale. One may conclude that in comparison with the rapid inhibition, the activation of Y occurs with time delay. In Fig. 1.5G time delay is designated with the Greek letter τ. Note that negative feedbacks are also present in separate networks, e.g., sensory and developmental networks and signal transduction networks, however, not as often as in joint networks [2].

1.3 Mathematical modelling of biochemical reactions

It is believed that each network motif fulfils specific information-processing functions [3, 41, 105]. Once embedded in networks, these simple pathways are able to generate complex behaviour of network components, e.g., bistable switches or oscillations [105]. To approximate this behaviour, one may construct mathematical models of network motifs [2, 105]. Obtained models can be further subjected to mathematical analysis to explain the dynamics of components of the intracellular network. In this section, I introduce basic principles for constructing mathematical models of biochemical reactions underlying network motifs.

Law of mass action

The simplest way to describe kinetics of biochemical reactions is the law of mass action. It states that the reaction rate, i.e., the velocity by which the execution of the reaction changes the concentrations of its substrates, is proportional to the concentration of reactants to the power of the molecularity [53].

As an example, I consider a chemical equation of a reversible reaction, where molecules X and Y bind to form two molecules of Z:

$$X + Y \rightleftharpoons 2Z.$$
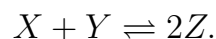
If the reaction obeys the law of mass reaction, then its reaction rate can be described in the following way:

$$v = v_1 - v_2 = k_1\, X\, Y - k_2\, Z^2,$$

where v_1 and v_2 represent rates of forward and backward reactions, respectively.

Correspondingly, the dynamics of concentrations of X, Y and Z can be formulated using the following ODEs:

$$\begin{aligned}
\frac{dX}{dt} &= -v, \\
\frac{dY}{dt} &= -v, \\
\frac{dZ}{dt} &= 2v.
\end{aligned}$$

These equations can be further solved analytically or numerically providing the time course of X, Y and Z.

Michaelis-Menten kinetics

Chemical reactions can be catalysed by enzymes. In this case, the reaction rate may saturate at a certain concentration of the substrate. The saturation effect can be described by Michaelis-Menten kinetics [53].

The following chemical equation describes a transformation of a substrate X into the product Y in the presence of an enzyme E:

$$X + E \rightarrow Y + E.$$
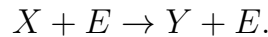
The Michaelis-Menten reaction rate of this reaction has the following form:

$$v = V_{max} \frac{X}{K_m + X},$$

where V_{max} designates the maximal velocity and K_m designates the substrate concentration, which yields the half-maximal reaction rate.

Hill kinetics

Molecules may act together to increase reaction rates in a non-linear way. This process is often called cooperativity. In order to model biochemical reactions of this kind one may use Hill kinetics [2], which can be deduced using a simple reaction scheme:

$$n\,X + E \rightleftharpoons n\,X\,E \xrightarrow{v} n\,X\,E + Y.$$
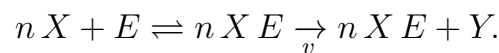
The Hill reaction rate is of the form:

$$v = V_{max} \frac{X^n}{K_m{}^n + X^n},$$

where V_{max} designates the maximal velocity and K_m designates the substrate concentration, which yields the half-maximal reaction rate, n is the Hill coefficient mimicking the cooperativity in a binding process.

Thus, for modelling the reaction rate mimicking inhibition one may use a decreasing step function called a reverse Hill function (see Fig. 1.6):

$$S_1(X) \quad = \quad \frac{K_m{}^n}{K_m{}^n + X^n}. \tag{1.9}$$

For modelling the reaction rate mimicking activation one may use an increasing step function called a Hill function (see Fig. 1.6):

$$S_2(X) = \frac{X^n}{K_m{}^n + X^n}. \tag{1.10}$$

For both functions S_1 and S_2, parameter $K_m > 0$ designates the substrate concentration, which yields the half-maximal reaction rate, and parameter $n \geq 1$ designates the Hill coefficient, which describes the cooperativity rate of molecules.
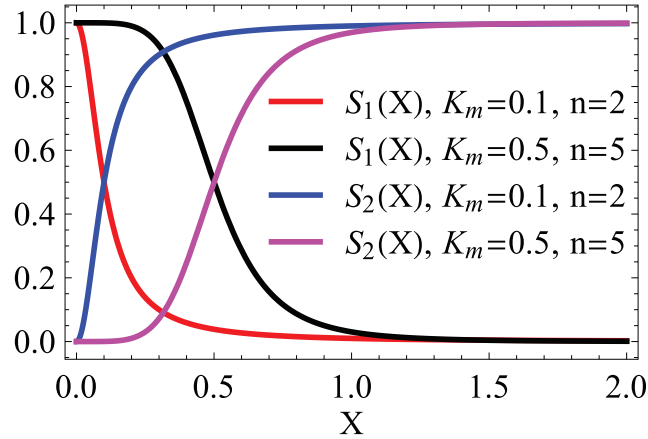
Figure 1.6: Plots of functions S_1 (1.9) and S_2 (1.10). Parameters $(K_m, n) = (0.1, 2)$ and $(K_m, n) = (0.5, 5)$ were used for performing simulations.

1.4 General notions on feedback

In control theory, the term feedback refers to a situation in which two or more dynamical systems are connected together such that each system influences the other and their dynamics are strongly coupled. As a result, the first system influences the second and the second system influences the first leading to a circular argument [23].

The use of feedback is widespread in the design of electronic amplifiers, oscillators, and stateful logic circuit elements. Also biological systems make an extensive use of feedbacks on scales ranging from molecules to cells to organisms to ecosystems. As a trivial example of a feedback mechanism in the human organism one may consider the regulation of the glucose level in the bloodstream. In this system the interplay between insulin and glucagon, i.e., a hormone having an effect opposite to insulin, keeps the blood-glucose concentration constant [23].

The complicated interaction between feedback components often induces counter-intuitive behaviour and requires formal methods to explain the observed dynamics [23, 104]. This complicated behaviour often becomes the aim of research for many scientists. In this context, it is important to mention the studies of David Angeli and Eduardo Sontag [5, 6], who investigated numerous properties of biochemical feedback systems. Namely, they provided concrete methods for detecting multistability, bifurcations and hysteresis in biochemical positive feedback systems. In addition, they studied oscillations in monotone systems under negative feedback.

Feedbacks have diverse properties. For example, they provide robustness to uncertainty, change a dynamics of the system and may give rise to instability if designed not properly [23]. Because of these properties feedbacks are extensively used for engineering electrical, mechanical as well as biological systems. For further detailed information about feedback systems refer to [9].

1.5 Delayed negative feedback

In intracellular networks, feedback mechanisms are present in the form of positive and negative feedback loops [2, 3, 49, 63, 90, 104, 105]. This thesis is dedicated to studying the dynamics of biochemical networks containing a negative feedback loop. The importance of this study is raised by the fact that negative feedbacks have been observed in a wealth of biochemical networks ranging from the mammalian cell cycle [30, 83] to bacterial adaptation [55, 111] and stress response in mammals [17] and yeast [54, 91]. Negative feedback control principles are even used to engineer artificial biological systems in bacteria and mammalian cells [27, 99, 109]. Investigating negative feedback loops allows to explain, how these systems function, and develop methods to modify and control their behaviour.

In biochemical networks, negative feedback occurs when the output of the process negatively influences its input (see Fig. 1.7). The negative feedback system subtracts the measurement of the output from the required value and uses the obtained result to regulate the input of the process. In this way negative feedback reduces the difference between actual and required values of the output.

Note that despite the simplicity of this definition the mechanism of the negative feedback can differ from system to system. For example, negative feedback can act through sequestering molecules from particular cellular compartments, e.g., nucleus, cytoplasm or cell membrane, where they can react with other molecules [44]. In addition, negative feedback may act through activating or deactivating molecules, e.g., through post-translational modifications [91]. Negative feedback may also act through blocking and activating the transcription of molecules [99] or through subjecting molecules to degradation, e.g., through ubiquitination [75].

In biochemical networks, negative feedback can serve several objectives such as stabilizing the abundance of biochemical species [2, 42, 101, 105], inducing oscillations [27, 48, 84, 104], modifying response times [3, 69] and mediating adaptation [68, 81, 111].

In many intracellular networks negative feedback operates together with time delay [76]. Time delay may have a different origin. For example, time delay may arise in joint networks due to the different velocities of interactions between feedback components as shown in Fig. 1.5G. Indeed, the transcriptional interaction, where X activates Y, occurs on a slow time scale, whereas the protein-protein interaction, where Y inhibits X, occurs on a rapid time scale. As a result, the activation of Y is delayed in
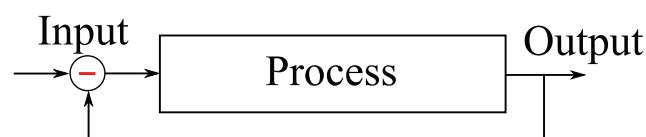

Figure 1.7: General definition of the negative feedback.

comparison to the inhibition of X. Time delay may also appear due to the cascade of reactions happening between sensing the input and producing the output.

It is widely accepted that negative feedback in conjunction with a time delay may lead to oscillatory behaviour [37, 39, 70]. Oscillations brought about by delayed negative feedback (DNF) have been observed and analysed in a range of biological systems, e.g., the mammalian p53 system [36, 59, 86], the NF-κB system [7, 44, 79] or the Hes1 transcription factor [15, 76]. However, the role of oscillations in the aforementioned biochemical DNF systems remains unclear. It is also conceivable that in biological systems mediating adaptive responses oscillatory behaviour might be inappropriate. For example, in the hyperthermia treatment of cancer, large-amplitude temperature oscillations could result in tissue damage or patient discomfort [102].

Mathematical modelling is a common method used for investigating often non-trivial dynamics of negative feedbacks. First fundamental study of stability of DNF intracellular systems by means of mathematical modelling was performed by Brittish scientist Brian Goodwin in 1965 [38]. The purpose of this study was to illustrate the type of periodic behaviour, which may arise in biological systems. In 1968 J.S. Griffith continued Goodwin's study and developed a necessary condition for negative feedback systems to give rise to sustained oscillations [39]. In these studies the time delay was induced by including several intermediate components inside of the feedback loop. In 1982 discrete time delays were explicitly included in mathematical models of negative feedbacks [21]. In these models time delay was considered as a bifurcation parameter. Unfortunately, none of presented models was parametrized with respect to real biological data. In 2000 it was shown that not only time delay but also ultrasensitivity of the negative feedback may induce oscillatory dynamics of intracellular components [48]. In 2008 a computational study was published, where it was investigated how the interaction between positive and negative feedbacks influences the dynamics of intracellular systems [104]. Despite impressive numerical simulations, no theoretical analysis of considered models was provided. Recently, two studies [80, 92] investigated stability and resistance of DNF systems modelled with three ordinary differential equations (ODEs). They showed that nested negative feedbacks inside of DNF may suppress oscillations of biochemical species. However, this studies provided no insight into how time delay influences the behaviour of these systems.

In this thesis, I derive explicit thresholds and boundaries showing how time delay determines characteristic response patterns of biochemical networks containing DNF. In addition, I investigate how the combination of time delay and certain design features influences the dynamics of intracellular DNF systems. Thus, I consider not only the presence of a nested negative feedback but also the presence of mass conservation and the type of DNF mechanism. To this end, several mathematical models of DNF systems are developed and analysed. I demonstrate that my theoretical results can be used to study concrete cellular systems both adaptive as well as oscillatory. This is based on the fact that my models are capable to recapitulate measured dynamics of these

systems in a quantitative manner. Thus, my theoretical result can be parametrized to study real systems. Despite its simplicity my theoretical framework facilitates novel insights into the functioning of the high osmolarity glycerol pathway mediating osmo-adaptation in yeast [69], as well as NF-κB and p53 oscillations in mammalian cells [44, 64]. Specifically, I show that adaptation to osmotic stress in yeast is optimal in the sense of minimizing adaptation time without causing oscillatory behaviour, i.e., a critically damped response. Additionally, a slight increase of time delay in NF-κB system might induce a switch from damped to sustained oscillatory behaviour. Further, I apply my theoretical analysis to explore under what conditions sustained oscillations of p53 model can be suppressed by the activation of a nested auto-inhibitory feedback.

Finally, I propose a design of a synthetic intracellular network, which contains DNFs and is able to switch between adaptive behaviour and sustained oscillations in a controlled manner.

1.6 Outline

This thesis has the following structure:

Chapter 2 introduces generic models of six alternative delayed negative feedback (DNF) systems, which differ in the type of inhibition and presence of signalling components. Models are described by two-dimensional delay differential systems, which are further subjected to mathematical analysis with respect to time delay. Obtained theoretical results are applied to study concrete biological systems containing DNF. These are the high osmolarity glycerol (HOG) pathway in yeast and the NF-κB system in mammalian cells. The main results described in this chapter are partly presented in [62].

Chapter 3 focuses on investigating the ability of design features of DNF systems to suppress unwanted oscillations. As alternative designs, the mechanism of DNF, strength of DNF and presence of mass conservation of biochemical components were considered. Based on the obtained results, a design of synthetic auto-inhibitory feedback was suggested to suppress oscillations in the mammalian p53 system. The main results described in this chapter are partly presented in [19, 92].

Chapter 4 presents a design of a synthetic intracellular network, which contains DNFs and can switch between adaptive and oscillatory responses in a controlled manner.

Chapter 5 describes a technique to show how to approximate delay differential equations by means of ordinary differential equations. This technique is applied to approximate parametrized HOG and p53 models, which demonstrate adaptive behaviour and sustained oscillations, respectively.

Chapter 6 draws conclusions about the work and presents an outlook for future research.

2 Role of time delay in systems containing delayed negative feedback

2.1 Introduction

The first fundamental study on stability of intracellular DNF systems states that the occurrence of negative feedback in combination with time delay make it highly probable that molecular species in cells will undergo sustained oscillations [38]. Later on, numerous mathematical models of biochemical delayed negative feedback (DNF) systems were created and subjected to rigorous mathematical analysis to explain their behaviour [30, 39, 48, 80, 92, 111]. These models were described by ordinary differential equations (ODEs), where the time delay was mimicked by intermediate processes preceding the inhibition of the input.

In several DNF systems time delay arises due to the different velocities of interactions between components of the biochemical network [2, 3]. Indeed, interactions, which occur on a slow time scale, are delayed in comparison to interactions, which occur on a rapid time scale.

To study the role of time delay in DNF systems, I model a range of DNF systems using two-dimensional differential equations with time delay τ as a parameter. Architectures of considered models mimic biochemical networks differing in the kind of negative feedback and presence of mass conservation for model components (see Fig. 2.1). By both theoretical and numerical analyses I describe the role of time delay in shaping cellular response patterns of biochemical systems. Specifically, I derive explicit delay thresholds and boundaries beyond which the system's response patterns change leading to overdamped, damped oscillatory or sustained oscillatory behaviour.

I demonstrate that my theoretical results can be used to study concrete cellular systems both adaptive as well as oscillatory. This is based on the fact that my models are capable of recapitulating the measured dynamics of these systems in a quantitative manner. Thus, my theoretical result can be parametrized to study real systems. I show that despite its simplicity my theoretical framework facilitates novel insights into the functioning of the HOG pathway mediating osmo-adaptation in yeast [69] as well as NF-κB oscillations in mammalian cells [44].

2.2 Mathematical modelling of delayed negative feedbacks with DDEs

I consider a range of two-dimensional DNF models that represent generic cellular signal-response networks (see Fig. 2.1). The model choice is motivated by biological DNF systems able to produce adaptive and/or oscillatory response to stimulation [15, 44, 48, 64, 76, 91, 111]. Using mathematical modelling I represent core DNF structures underlying these biochemical networks. Resulting models differ in the architecture of the delayed feedback, i.e., input-inhibition or output-activation, and presence of mass conservation for model components.

Models presented in Fig. 2.1 have the following mathematical formulations by means of delay differential equations:

Model 1: DNF with input-inhibition and without mass conservation (see Fig. 2.1A):

$$
\begin{aligned}
\frac{dC}{dt} &= I\, S_1(R)\, F(C) - \alpha\, C,\\
\frac{dR}{dt} &= \eta\, C(\cdot - \tau) - \beta\, R.
\end{aligned}
\tag{2.1}
$$

Model 2: DNF with input-inhibition and with mass conservation for the model component C (see Fig. 2.1B):

$$
\begin{aligned}
\frac{dC}{dt} &= I\, S_1(R)\, F(C)\, (1 - C) - \alpha\, C,\\
\frac{dR}{dt} &= \eta\, C(\cdot - \tau) - \beta\, R.
\end{aligned}
\tag{2.2}
$$

Model 3: DNF with input-inhibition and with mass conservation for model components C and R (see Fig. 2.1C):

$$
\begin{aligned}
\frac{dC}{dt} &= I\, S_1(R)\, F(C)\, (1 - C) - \alpha\, C,\\
\frac{dR}{dt} &= \eta\, C(\cdot - \tau)\, (1 - R) - \beta\, R.
\end{aligned}
\tag{2.3}
$$

Model 4: DNF with output-activation and without mass conservation (see Fig. 2.1D):

$$
\begin{aligned}
\frac{dC}{dt} &= I\, F(C) - \alpha\, C - \delta\, C\, S_2(R),\\
\frac{dR}{dt} &= \eta\, C(\cdot - \tau) - \beta\, R.
\end{aligned}
\tag{2.4}
$$
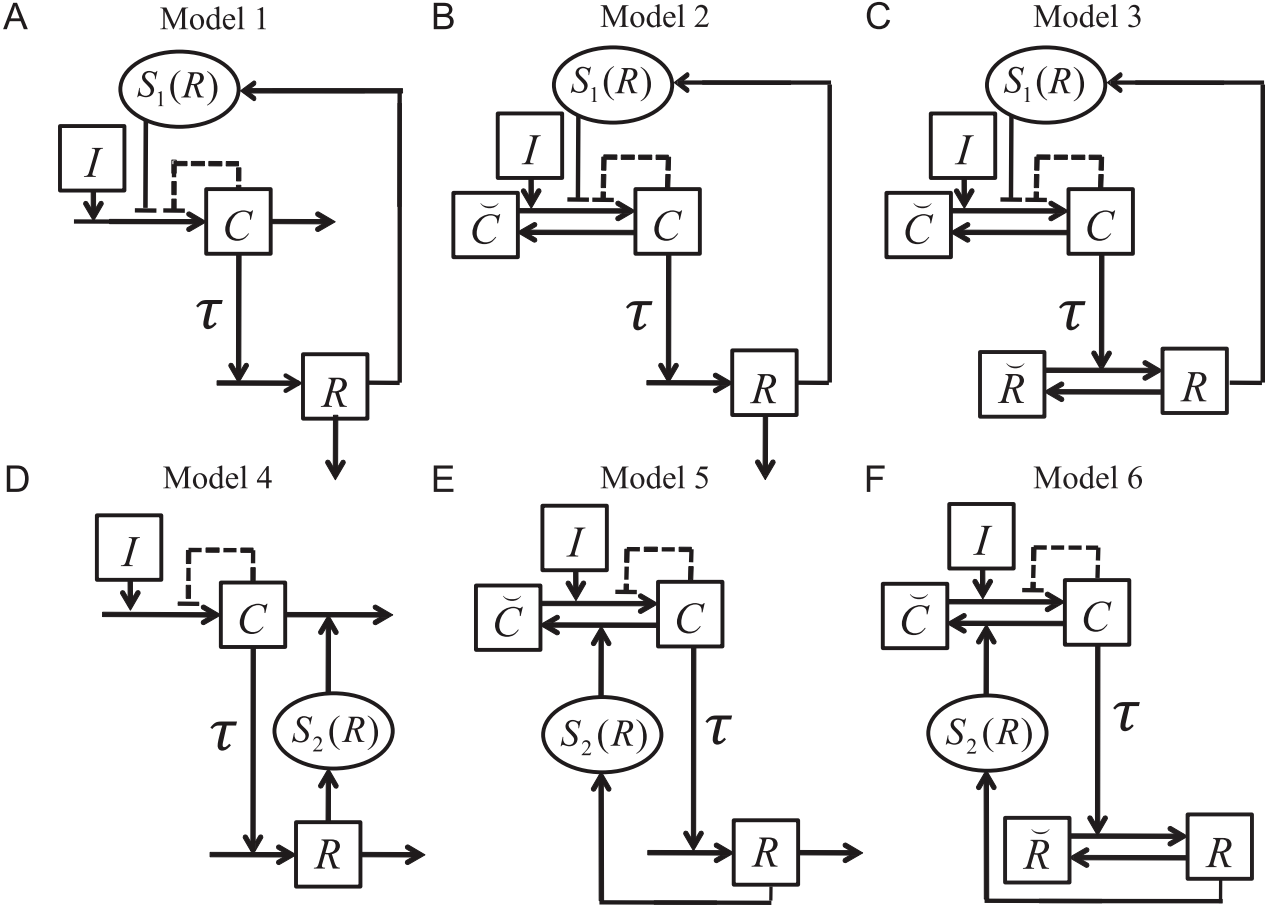
Figure 2.1: Generic signal-response models with DNF. Squares indicate model variables, circles indicate model functions. Arrows between and to components indicate biochemical reactions, arrows on arrows indicate modifying influences and arrows to functions indicate the respective influence on the function. The models differ in the architecture of the DNF as well as in the presence of mass conservation for components C and R. (A) Model with input-inhibition as DNF and without mass conservation. (B) Model with input-inhibition as DNF and with mass conservation for the model component C. (C) Model with input-inhibition as DNF and with mass conservation for both model components C and R. (D) Model with output-activation as DNF and without mass conservation. (E) Model with output-activation as DNF and with mass conservation for the model component C. (F) Model with output-activation as DNF and with mass conservation for both model components C and R. In all models the time delay τ is before activation of the response variable R. Dashed lines indicate an alternative auto-inhibitory feedback.

Model 5: DNF with output-activation and with mass conservation for the model component C (see Fig. 2.1E):

$$\begin{aligned}
\frac{dC}{dt} &= I\,F(C)\,(1-C) - \alpha\,C - \delta\,C\,S_2(R), \\
\frac{dR}{dt} &= \eta\,C(\cdot - \tau) - \beta\,R.
\end{aligned} \qquad (2.5)$$

Model 6: DNF with output-activation and with mass conservation for model components C and R (see Fig. 2.1F):

$$\begin{aligned}
\frac{dC}{dt} &= I\,F(C)\,(1-C) - \alpha\,C - \delta\,C\,S_2(R), \\
\frac{dR}{dt} &= \eta\,C(\cdot - \tau)\,(1-R) - \beta\,R.
\end{aligned} \tag{2.6}$$

The function $S_1\colon [0,\infty) \to \mathbb{R}_+$ is twice continuously differentiable and monotonically decreasing with R. The function $S_2\colon [0,\infty) \to \mathbb{R}_+$ is twice continuously differentiable and monotonically increasing with R. The twice continuously differentiable monotonically decreasing function $F\colon [0,\infty) \to (0,1]$ mimics an optional auto-inhibitory feedback.

Parameters of Models 1-6 have real positive constant values. For convenience, I combine them in the vector p:

$$p = (I, \alpha, \beta, \eta, \delta)^T. \tag{2.7}$$

Note that all model parameters represent lumped biological processes and therefore have only limited physical or biological meaning. For Models 1-3 the parameter δ equals 0.

In all models the input I defines some constant stimulus (e.g., radiation, osmotic stress, tumor necrosis factor-α (TNF-α), see below) that activates a gene transcription network (see Fig. 2.1A and D), represented by the model variable C, or a signalling cascade (see Fig. 2.1B, C, E and F). The component C in turn activates the response variable R with a certain time delay τ. Time delay can be motivated by processes like transport, transcription, translation or by the cascade of reactions happening between sensing the input and producing the response R. Subsequently, the response R negatively feeds back into its own activation through S_1 or S_2, respectively, thereby mediating DNF.

Note that the response R mediates DNF through different mechanisms depending on the considered model. In models from Fig. 2.1A-C the response variable R has inhibiting influence on C by means of the function $S_1(R)$. Therefore, I refer to this situation as input-inhibition. In models from Fig. 2.1D-F the DNF mediated by the response R acts through activating the degradation of C by means of the function $S_2(R)$. I refer to this model structure as output-activation.

I refer to models from Fig. 2.1A and D as a transcription network, because C is not reversibly converted into different states, but rather produced and degraded. Both input-inhibition and output-activation architectures are also considered together with so-called signalling components (see Fig. 2.1B, C, E and F). In Models 2, 3, 5 and 6 the component C, which in turn activates the response R, originates from another component $\breve{C}$ to which it is constitutively converted back. This construction mimics a

fast and reversible post-translational protein modification, e.g., phosphorylation. As a result, the total protein content stays unchanged over time, as it is often the case in signalling cascades:

$$\frac{dC}{dt} + \frac{d\breve{C}}{dt} = 0,$$
$$C + \breve{C} \equiv const = 1. \tag{2.8}$$

Here, the constant is assumed to be unity. I refer to this feature as mass conservation. Using the mass conservation allows to exclude the variable $\breve{C}$ from Models 2, 3, 5 and 6 reducing their dimension to two. For example, the following system of equations for Model 2 is reduced to get the system (2.2):

$$\frac{dC}{dt} = I\, S_1(R)\, F(C)\, \breve{C} - \alpha\, C,$$
$$\frac{d\breve{C}}{dt} = -\, I\, S_1(R)\, F(C)\, \breve{C} + \alpha\, C,$$
$$\frac{dR}{dt} = \eta\, C(\cdot - \tau) - \beta\, R.$$

In Models 3 and 6 two pairs of components C, $\breve{C}$ and R and $\breve{R}$ undergo mass conservation. As a result, two variables $\breve{C}$ and $\breve{R}$ are excluded from these models to get systems (2.3) and (2.6) using the following transformation:

$$\breve{C} = 1 - C,$$
$$\breve{R} = 1 - R.$$

In the following section, I present theoretical analysis of Models 1-6 showing how time delay determines characteristic response patterns of delayed negative feedback systems.

2.3 How time delay determines characteristic response patterns

Models 1-6 are non-linear and can not be solved analytically. In order to understand their dynamics I investigate the stability of their steady states applying the analysis introduced in Section 1.1.5. In this section, most derived formulas apply to all Models 1-6, respectively. For readability, I do not make an explicit distinction between models, unless necessary.

2.3.1 Existence and uniqueness of steady states

Using Proposition 1 I demonstrate the existence and uniqueness of steady states $E = (C_s, R_s)^T$ of Models 1-6.

Proposition 1. Steady states $E = (C_s, R_s)^T$ of Models 1-6 exist and are unique.

Proof. I define the relation between equilibrium components R_s and C_s for Models 1-6. For this I equate the right hand side of the differential equation $\dfrac{dR}{dt}$ to 0 and solve it with respect to R_s:

$$R_s = \frac{\eta}{\beta} C_s \text{ for Models } 1, 2, 4 \text{ and } 5,$$

$$R_s = \frac{\eta \, C_s}{\eta \, C_s + \beta} \text{ for Models } 3 \text{ and } 6. \tag{2.9}$$

Note that in both cases R_s increases with C_s. Further, for each Model 1-6 I equate the right hand side of the differential equation $\dfrac{dC}{dt}$ to 0 and substitute R_s (2.9):

$$\underbrace{I \, S_1 \left(\frac{\eta}{\beta} C_s \right) \cdot F(C_s)}_{\theta_1(C_s)} = \underbrace{\alpha \, C_s}_{\theta_2(C_s)} \text{ for Model 1,} \tag{2.10}$$

$$\underbrace{I \, S_1 \left(\frac{\eta}{\beta} C_s \right) (1 - C_s) \cdot F(C_s)}_{\theta_1(C_s)} = \underbrace{\alpha \, C_s}_{\theta_2(C_s)} \text{ for Model 2,} \tag{2.11}$$

$$\underbrace{I \, S_1 \left(\frac{\eta \, C_s}{\eta \, C_s + \beta} \right) (1 - C_s) \cdot F(C_s)}_{\theta_1(C_s)} = \underbrace{\alpha \, C_s}_{\theta_2(C_s)} \text{ for Model 3,} \tag{2.12}$$

$$\underbrace{I}_{\theta_1(C_s)} \cdot F(C_s) = \underbrace{\alpha \, C_s + \delta \, C_s \, S_2 \left(\frac{\eta}{\beta} C_s \right)}_{\theta_2(C_s)} \text{ for Model 4,} \tag{2.13}$$

$$\underbrace{I \, (1 - C_s)}_{\theta_1(C_s)} \cdot F(C_s) = \underbrace{\alpha \, C_s + \delta \, C_s \, S_2 \left(\frac{\eta}{\beta} C_s \right)}_{\theta_2(C_s)} \text{ for Model 5,} \tag{2.14}$$

$$\underbrace{I \, (1 - C_s)}_{\theta_1(C_s)} \cdot F(C_s) = \underbrace{\alpha \, C_s + \delta \, C_s \, S_2 \left(\frac{\eta \, C_s}{\eta \, C_s + \beta} \right)}_{\theta_2(C_s)} \text{ for Model 6.} \tag{2.15}$$

Thus, for each model I derive the equation defining the equilibrium component C_s in the form:

$$\theta_1(C_s) \cdot F(C_s) = \theta_2(C_s). \tag{2.16}$$

According to (2.16), the equilibrium component C_s can be found as the intersection of functions $\theta_1 \cdot F$ and θ_2. For considered models the function θ_1 is either constant or a decreasing function with respect to C_s and θ_2 is an increasing non-bounded function with respect to C_s. As a result, the equilibrium component C_s always exists and is unique. According to (2.9), the same conclusion holds for the equilibrium component R_s. $\qquad \square$

Note that steady states $E = (C_s, R_s)^T$ implicitly depend on the parameter vector p (2.7) including the input I. Therefore, Models 1-6 are not able to show a perfect adaptation.

2.3.2 Characteristic response patterns of models

The linearisation of Models 1-6 about the respective steady states E results in the system (2.17), which describes the dynamics of a steady state perturbation $\zeta(t) = (C(t) - C_s, R(t) - R_s)^T$. Linearisation matrices A and B are obtained by linearising Models 1-6 about non-delayed and delayed model components, respectively.

$$\frac{d\zeta}{dt} = \underbrace{\begin{pmatrix} -x & -y/\gamma \\ 0 & -z \end{pmatrix}}_{A} \zeta(t) + \underbrace{\begin{pmatrix} 0 & 0 \\ \gamma & 0 \end{pmatrix}}_{B} \zeta(t-\tau), \tag{2.17}$$

where for Model 1, I have

$$\begin{aligned} x &= I\, S_1(R_s)|F'(C_s)| + \alpha > 0, \\ y &= \eta\, I\, |S_1'(R_s)|\, F(C_s) > 0, \\ z &= \beta > 0, \\ \gamma &= \eta. \end{aligned} \tag{2.18}$$

for Model 2, I have

$$\begin{aligned} x &= I\, S_1(R_s)\left[F(C_s) + (1-C_s)\,|F'(C_s)|\right] + \alpha > 0, \\ y &= \eta\, I\, |S_1'(R_s)|\, (1-C_s)\, F(C_s) > 0, \\ z &= \beta > 0, \\ \gamma &= \eta. \end{aligned} \tag{2.19}$$

for Model 3, I have

$$\begin{aligned} x &= I\, S_1(R_s)\left[F(C_s) + (1-C_s)\,|F'(C_s)|\right] + \alpha > 0, \\ y &= \eta\, I\, |S_1'(R_s)|\, (1-C_s)\, (1-R_s)\, F(C_s) > 0, \\ z &= \eta\, C_s + \beta > 0, \\ \gamma &= \eta\, (1-R_s). \end{aligned} \tag{2.20}$$

for Model 4, I have

$$\begin{aligned} x &= I\, |F'(C_s)| + \alpha + \delta\, S_2(R_s) > 0, \\ y &= \eta\, \delta\, C_s\, S_2'(R_s) > 0, \\ z &= \beta > 0, \\ \gamma &= \eta. \end{aligned} \tag{2.21}$$

for Model 5, I have

$$
\begin{aligned}
x &= I\left[F(C_s) + (1 - C_s)\,|F'(C_s)|\,\right] + \alpha + \delta S_2\,(R_s) > 0, \\
y &= \eta\,\delta\,C_s\,S_2'\,(R_s) > 0, \\
z &= \beta > 0, \\
\gamma &= \eta.
\end{aligned}
\tag{2.22}
$$

for Model 6, I have

$$
\begin{aligned}
x &= I\left[F(C_s) + (1 - C_s)\,|F'(C_s)|\,\right] + \alpha + \delta S_2\,(R_s) > 0, \\
y &= \eta\,\delta\,C_s\,S_2'\,(R_s)\,(1 - R_s) > 0, \\
z &= \eta\,C_s + \beta > 0, \\
\gamma &= \eta\,(1 - R_s).
\end{aligned}
\tag{2.23}
$$

The transcendental characteristic equation of the system (2.17) has the form:

$$
P(\lambda, \tau) = \det(\lambda\,I_2 - A - B\,e^{-\lambda\tau}) = (\lambda + x)(\lambda + z) + y\,e^{-\lambda\tau} = 0,
\tag{2.24}
$$

where I_2 is the two-dimensional identity matrix.

Roots λ of the equation (2.24) decide on the stability of steady states E (see Section 1.1.5). The characteristic equation (2.24) has the infinite number of root branches [8, 61]. However, there are two root branches that are associated with the two dominant roots λ_1 and λ_2, which determine the dynamics of the system (2.17). Therefore, in order to analyse how the time delay τ influences the dynamics of the perturbation $\zeta(t)$ and, as a result, the dynamics of Models 1-6, I consider the dependence between the time delay τ and dominant roots λ_1, λ_2.

For obtaining λ_1, λ_2 I intersect the following functions (see Fig. 2.2):

$$
\begin{aligned}
p_1(\lambda) &= (\lambda + x)(\lambda + z), \\
p_2(\lambda, \tau) &= -y\,e^{-\lambda\tau}.
\end{aligned}
$$

These functions constitute the transcendental characteristic equation (2.24):

$$
P(\lambda, \tau) = p_1(\lambda) - p_2(\lambda, \tau) = 0.
$$

The function $p_1(\lambda)$ does not depend on τ and represents a parabola that faces upward, has negative roots $-x$, $-z$ and a vertex with coordinates $(\lambda_v, p_1(\lambda_v)) = \left(-(x + z)/2, -(x - z)^2/4\right)$ (see Fig. 2.2).

The function $p_2(\lambda, \tau)$ is a negative function that equals $-y$ for $\tau = 0$ or $\lambda = 0$, increases with λ for $\tau > 0$, decreases with τ for $\lambda \in (-\infty, 0)$ and increases with τ for $\lambda \in (0, +\infty)$ (see Fig. 2.2).

Thus, if real roots λ_1, λ_2 exist, then they are both negative. Moreover, the necessary and sufficient condition for existence of real roots λ_1, λ_2 is that for $\tau = 0$ the vertex of
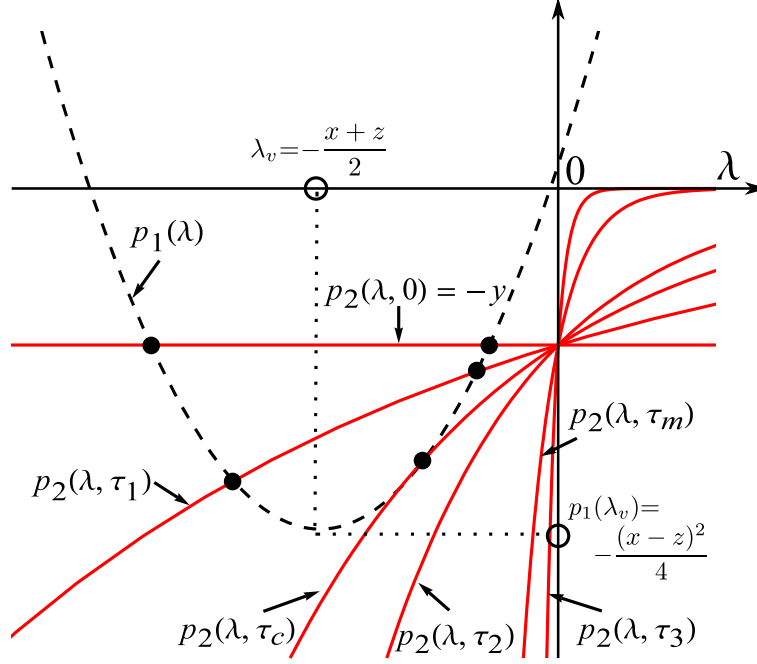
Figure 2.2: The plot of functions $p_1(\lambda)$ and $p_2(\lambda, \tau)$. The plot of functions $p_1(\lambda) = (\lambda + x)(\lambda + z)$ (*black dashed*) and $p_2(\lambda, \tau) = -y\,e^{-\lambda\tau}$ (*red solid*), which constitute the characteristic equation $P(\lambda, \tau) = p_1(\lambda) - p_2(\lambda, \tau) = 0$ (2.24). The plot of $p_2(\lambda, \tau)$ is represented for several values of τ: $\tau = 0$, $\tau_1 \in (0, \tau_c)$, $\tau = \tau_c$, $\tau_2 \in (\tau_c, \tau_m)$, $\tau = \tau_m$, $\tau_3 > \tau_m$. Black dots designate intersections of $p_1(\lambda)$ and $p_2(\lambda, \tau)$ that correspond to real dominant roots λ_1, λ_2 of $P(\lambda, \tau)$. Dotted lines with open circles designate coordinates of the vertex of the parabola $p_1(\lambda)$.

the parabola p_1 is lower than $p_2(\lambda, 0) = -y$, i.e., $-(x-z)^2/4 < -y$, which is equivalent to $(x - z)^2 > 4\,y$ (see Fig. 2.2).

According to properties of $p_1(\lambda)$ and $p_2(\lambda, \tau)$, roots λ_1, λ_2 may have either real negative or complex conjugate values and induce the following response patterns of the system (2.17) depending on the value of time delay τ (see Fig. 2.3 and Table 2.1):

1. If $(x - z)^2 > 4\,y$ holds, then there exists a critical time delay τ_c such that:

   a) For $0 \le \tau < \tau_c$, roots λ_1 and λ_2 have distinct real negative values and the system (2.17) produces an overdamped response (see *white and red regions* in Fig. 2.3).

   b) For $\tau = \tau_c$, $\lambda_1 = \lambda_2 = \lambda_c$ with a negative real value. At this threshold the system (2.17) produces a so-called critical damping response, beyond which damped oscillations occur.

   c) For $\tau > \tau_c$ roots λ_1 and λ_2 have complex conjugate values. Here, two alternative response patterns are possible:

      i. If $x\,z \ge y$ holds, then λ_1 and λ_2 have a negative real part that converges

to 0 for $\tau \to \infty$. In this case the system (2.17) produces a damped oscillatory response for any $\tau > \tau_c$ (see *red region* in Fig. 2.3).

   ii. If $x\,z < y$ holds, then there exists a marginal time delay τ_m (the Hopf bifurcation point) such that the negative real part of λ_1, λ_2 increases with $\tau < \tau_m$, reaches 0 for $\tau = \tau_m$ and turns to positive for $\tau > \tau_m$. In this case the system (2.17) produces a damped oscillatory response for any $\tau_c < \tau < \tau_m$ and a sustained oscillatory response for any $\tau \geq \tau_m$ (see *white region* in Fig. 2.3).

2. If $(x - z)^2 < 4\,y$ holds, λ_1 and λ_2 have complex conjugate values for any $\tau \geq 0$ and the dynamics of the model depends on the relation between $x\,z$ and y:

   a) If $x\,z \geq y$ holds, then λ_1 and λ_2 have a negative real part that converges to 0 for $\tau \to \infty$. In this case the system (2.17) produces a damped oscillatory response for any τ (see *grey region* in Fig. 2.3).

   b) If $x\,z < y$ holds, then there exists a marginal time delay τ_m such that the negative real part of λ_1, λ_2 increases with $\tau < \tau_m$, reaches 0 for $\tau = \tau_m$ and turns to positive for $\tau > \tau_m$. In this case the system (2.17) produces a damped oscillatory response for any $\tau < \tau_m$ and a sustained oscillatory response for any $\tau \geq \tau_m$ (see *blue region* in Fig. 2.3).

3. If $(x - z)^2 = 4\,y$ holds, then for $\tau = 0$ roots $\lambda_1 = \lambda_2$ have a negative real value and the system (2.17) produces a critical damping response. For $\tau > 0$ roots λ_1 and λ_2 have complex conjugate values and the dynamics of the system (2.17) depends on the relation between $x\,z$ and y as described in 2.a and 2.b.

For derivation of the value of τ_c refer to Section 2.3.3. For derivation of the relation between $x\,z$ and y and the value of τ_m refer to the Section 2.3.4.

Table 2.1: Characteristic response patterns of the system (2.17) depending on the value of time delay τ and values of x, y, z.

	$(x-z)^2 > 4y$	$(x-z)^2 < 4y$	$(x-z)^2 = 4y$
	$\exists\,\tau_c$ such that • for $0 \leq \tau < \tau_c$: overdamped response, • for $\tau = \tau_c$: critical damping.		For $\tau = 0$ critical damping.
$x\,z \geq y$	For $\tau > \tau_c$: damped oscillations.	For any $\tau \geq 0$: damped oscillations.	For any $\tau > 0$: damped oscillations.
$x\,z < y$	$\exists\,\tau_m$ such that • for $\tau_c < \tau < \tau_m$: damped oscillations, • for $\tau \geq \tau_m$: sustained oscillations.	$\exists\,\tau_m$ such that • for $0 \leq \tau < \tau_m$: damped oscillations, • for $\tau \geq \tau_m$: sustained oscillations.	$\exists\,\tau_m$ such that • for $0 < \tau < \tau_m$: damped oscillations, • for $\tau \geq \tau_m$: sustained oscillations.

Designations: cells are color-coded with respect to regions of Fig. 2.3.
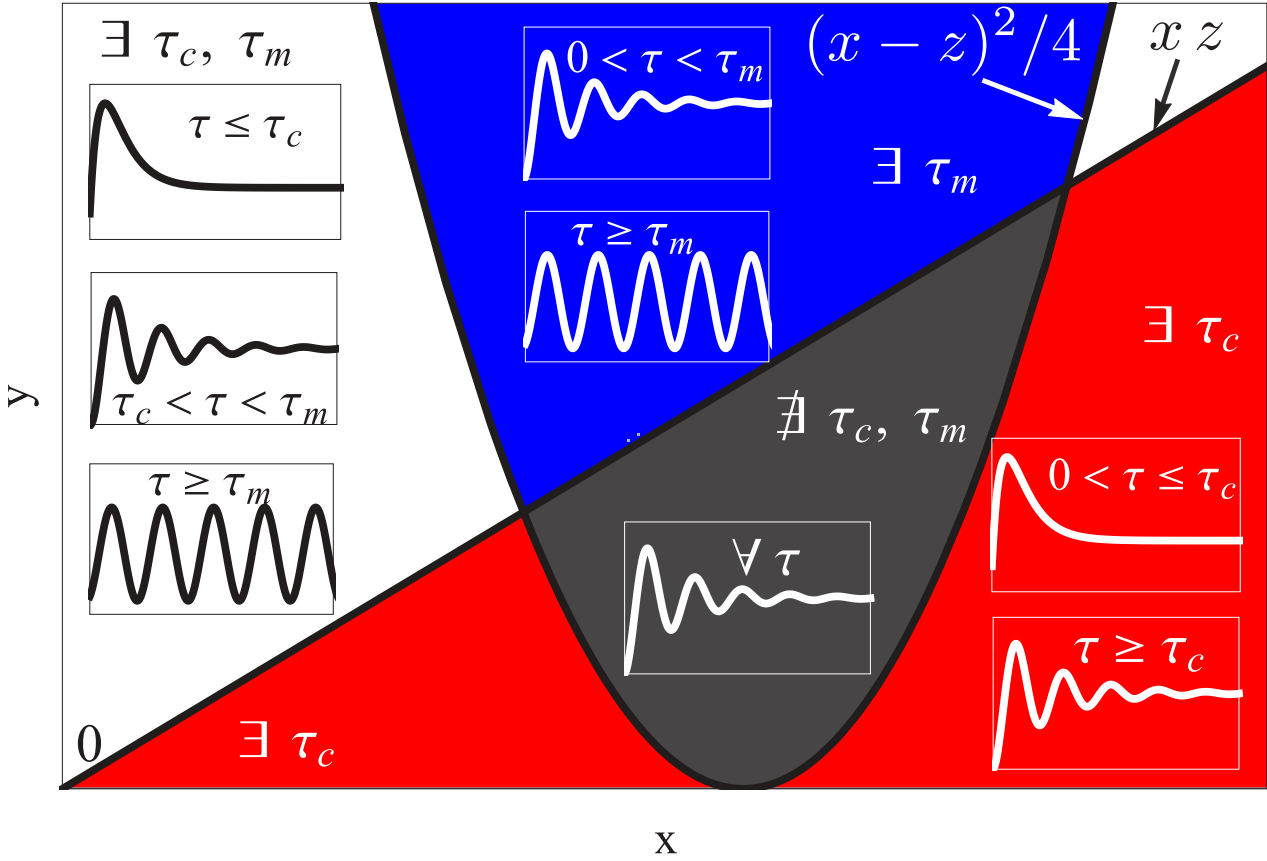
Figure 2.3: Schematic visualization of regions, where τ_c and τ_m exist, and possible dynamics of the steady state perturbation. Existence of τ_c and τ_m depends on relations between $(x-z)^2/4$ and y and xz and y, respectively: if $(x-z)^2/4 > y$ and $xz > y$ hold (*red region*), then only τ_c exists; if $(x-z)^2/4 > y$ and $xz < y$ hold (*white region*), then both τ_c and τ_m exist; if $(x-z)^2/4 < y$ and $xz < y$ hold (*blue region*), then only τ_m exists; if $(x-z)^2/4 < y$ and $xz > y$ hold (*grey region*), then neither τ_c nor τ_m exists. For each region I depict schematically the possible dynamics of the system (2.17) with respect to τ.

In Fig. 2.3 I visualize schematically regions of values of x and y, where τ_c and τ_m exist. Additionally, for each region I depict schematically the possible dynamics of the system (2.17) and, as a result, the possible dynamics of Models 1-6 with respect to τ. I also summarize these results in Table 2.1 with colours corresponding to Fig. 2.3.

Thus, the value of time delay τ and values of x, y and z determine the type of response (overdamped, critical damping, damped oscillatory or sustained oscillatory) of Models 1-6. In the following sections, I provide quantification of the critical value of time delay τ_c and marginal value of time delay τ_m.

2.3.3 Quantification of τ_c

If the condition $(x-z)^2 > 4y$ for the existence of τ_c is satisfied, τ_c corresponds to the twice-repeated root λ_c of $P(\lambda, \tau)$ and can be calculated by solving the system of

equations with respect to τ:

$$
\begin{aligned}
P(\lambda, \tau) &= (\lambda + x)(\lambda + z) + y\, e^{-\lambda \tau} = 0, \\
\frac{\partial\, P(\lambda, \tau)}{\partial\, \lambda} &= 2\,\lambda + x + z - y\,\tau\, e^{-\lambda \tau} = 0.
\end{aligned}
\tag{2.25}
$$

The above system consists of transcendental equations and can not be solved explicitly. However, I was able to derive an estimation for τ_c. According to properties of functions $p_1(\lambda)$, $p_2(\lambda, \tau)$ presented in the section above, they might be tangent to each other at the point (λ_c, τ_c) if and only if the condition $\lambda_c \geq \lambda_v$ is satisfied (see Fig. 2.2). Therefore, the following inequality holds:

$$
p_1(\lambda_v) = -\frac{(x - z)^2}{4} \geq -y\, e^{\frac{\tau_c(x + z)}{2}} = p_2(\lambda_v, \tau_c).
$$

Thus, I estimate τ_c using the following inequality (2.26):

$$
\tau_c \geq \tilde{\tau}_c(x, y, z) = \frac{2\left(\ln(x - z)^2 - \ln 4\, y\right)}{x + z}.
\tag{2.26}
$$

2.3.4 Quantification of τ_m

In this section, I provide a detailed Hopf bifurcation analysis of the linearised system (2.17) with quantification of τ_m.

First, I designate the number of roots of the characteristic polynomial (2.24) in the right half-plane for some time delay τ by $M(\tau)$:

$$
M(\tau) = \#\{\lambda : Re(\lambda) \geq 0 \text{ and } P(\lambda, \tau) = 0\}.
$$

The lemma (without number) from [21] says that as τ varies, $M(\tau)$ can change only if a characteristic root λ with $Re(\lambda) = 0$ appears on or crosses the imaginary axis. Thus, the only way that $M(\tau) \neq M(\tau')$ for $\tau < \tau'$ is, if there exists a marginal value τ_m between τ and τ', such that $P(\lambda_m, \tau_m) = 0$ and $Re(\lambda_m) = 0$ [21, 95].

To this end, I consider a root of the characteristic polynomial in the form $\lambda_m = i\,\omega_m$, where $\omega_m > 0$, and substitute the latter into (2.24):

$$
P(i\,\omega_m, \tau_m) = x\,z - \omega_m^2 + i\,(x + z)\,\omega_m + y\, e^{-i\,\omega_m \tau_m} = 0.
$$

Using Euler's formula I get an expression $e^{-i\,\omega_m \tau_m} = \cos(\omega_m \tau_m) - i\sin(\omega_m \tau_m)$ that I substitute in the formula above:

$$
x\,z - \omega_m^2 + i\,(x + z)\,\omega_m + y\,(\cos(\omega_m \tau_m) - i\sin(\omega_m \tau_m)) = 0.
\tag{2.27}
$$

Satisfying (2.27) the real and imaginary parts should both be equal to zero:

$$x\,z - \omega_m^2 + y\cos(\omega_m \tau_m) = 0, \tag{2.28}$$

$$(x + z)\,\omega_m - y\sin(\omega_m \tau_m) = 0. \tag{2.29}$$

I bring $y\cos(\omega_m \tau_m)$ and $y\sin(\omega_m \tau_m)$ to the right hand side of the respective equations and square both sides:

$$\left(x\,z - \omega_m^2\right)^2 = \left(-y\cos(\omega_m \tau_m)\right)^2,$$

$$(x + z)^2\,\omega_m{}^2 = \left(y\sin(\omega_m \tau_m)\right)^2.$$

Then, I sum both equations and use the fact that $\left(-y\cos(\omega_m \tau_m)\right)^2 + \left(y\sin(\omega_m \tau_m)\right)^2 = y^2$:

$$\omega_m^4 + (x^2 + z^2)\omega_m^2 + x^2\,z^2 - y^2 = 0. \tag{2.30}$$

The equation (2.30) has real non-zero roots if and only if $x\,z < y$. Otherwise, τ_m does not exist and the equilibrium (C_s, R_s) is absolutely stable. I assume that $x\,z < y$ holds and define the discriminant D by

$$D = (x^2 + z^2)^2 - 4(x^2\,z^2 - y^2). \tag{2.31}$$

Then, I find

$$\omega_{m\pm}^2 = \frac{1}{2}\left(-x^2 - z^2 \pm \sqrt{D}\right).$$

Hence, I obtain the expression for ω_m^2 and ω_m, respectively:

$$\omega_m^2 = \frac{1}{2}\left(-x^2 - z^2 + \sqrt{D}\right), \quad \omega_m = \sqrt{\frac{1}{2}\left(-x^2 - z^2 + \sqrt{D}\right)}.$$

Further, I define τ_m. For this I substitute ω_m into (2.28) and (2.29):

$$\cos(\omega_m \tau_m) = \frac{1}{2\,y}\left(-(x + z)^2 + \sqrt{D}\right), \tag{2.32}$$

$$\sin(\omega_m \tau_m) = \frac{x + z}{y}\,\omega_m > 0. \tag{2.33}$$

Thus, I express the value of τ_m:

$$\tau_m(n) = \frac{1}{\omega_m}\left[\arccos\left(\frac{1}{2\,y}\left(-(x + z)^2 + \sqrt{D}\right)\right) + 2\pi n\right], \quad n = 0,\,1,\,2,\,...$$

Since $\sin(\omega_m \tau_m) > 0$ holds, I conclude that if $\left(-(x + z)^2 + \sqrt{D}\right) > 0$, then $\arccos\left(\frac{1}{2\,y}\left(-(x + z)^2 + \sqrt{D}\right)\right) \in \left(0, \frac{\pi}{2}\right)$, otherwise $\arccos\left(\frac{1}{2\,y}(-(x + z)^2 + \sqrt{D})\right) \in \left(\frac{\pi}{2}, \pi\right)$. In both cases, the smallest time delay, which causes a purely imaginary pair of

roots $\lambda_{1,2} = \pm i\omega_m$, is

$$\tau_m = \frac{1}{\omega_m} \arccos\left(\frac{1}{2\,y}\left(-(x+z)^2 + \sqrt{D}\right)\right). \tag{2.34}$$

As a result, I proved the stability of the equilibrium (C_s, R_s) for any $\tau \in [0, \tau_m)$. Indeed, roots of $P(\lambda, 0)$ are either real negative or have a negative real part (see above).

Then, according to Lemma from [21], $M(\tau) = 0$ for any $\tau \in [0, \tau_m)$. Hence, for any $\tau \in [0, \tau_m)$ the equilibrium (C_s, R_s) is asymptotically stable.

Finally, I check if a Hopf bifurcation occurs at $\tau = \tau_m$. For this I differentiate the characteristic polynomial (2.24) with respect to τ and equate it to zero:

$$2\lambda\frac{d\lambda}{d\tau} + (x+z)\frac{d\lambda}{d\tau} = y\,e^{-\lambda\tau}\left(\tau\frac{d\lambda}{d\tau} + \lambda\right).$$

Then, I express $\dfrac{d\lambda}{d\tau}$:

$$\frac{d\lambda}{d\tau} = \frac{y\,\lambda}{e^{\lambda\tau}\,(x+z+2\lambda) - y\,\tau}.$$

I substitute $\lambda = i\omega_m$ into the expression for $\dfrac{d\lambda}{d\tau}$ and use Euler's formula again:

$$\frac{d\lambda}{d\tau}(\tau) = \frac{i\,\omega_m\,y\cos(\omega_m\tau) + \omega_m\,y\sin(\omega_m\tau)}{x + z - y\,\tau\cos(\omega_m\tau) + i\,(2\omega_m + \tau y\sin(\omega_m\tau))}.$$

I substitute the expression for τ_m (2.34), used (2.32) and (2.33), multiply the top and the bottom by the conjugate of the denominator, take the real part and get:

$$\frac{dRe(\lambda)}{d\tau}(\tau_m) = \frac{\sqrt{D}\,\omega_m^2}{(x + z - y\,\tau_m\cos(\omega_m\tau_m))^2 + (2\,\omega_m + \tau_m\,y\,\sin(\omega_m\tau_m))^2} > 0. \tag{2.35}$$

The positivity of (2.35) guarantees that the hypotheses of the implicit function theorem hold. Hence, I conclude that for $\tau \approx \tau_m$ the root of the characteristic polynomial (2.24) $\lambda_m = i\omega_m$ crosses the imaginary axis from left to right.

According to Proposition 6.5 from [95], for $\tau \geq \tau_m$ the equilibrium (C_s, R_s) is unstable.

2.4 Application

In the following sections I apply Models 2 and 4 to concrete experimental data demonstrating the ability of my theoretical framework to gain novel insights into the functioning of concrete biochemical systems. Specifically, I apply Model 2 to the high osmolarity glycerol pathway in yeast and Model 4 to the NF-κB system in mammalian cells.

2.4.1 High osmolarity glycerol system

The high osmolarity glycerol (HOG) pathway in yeast is a stress-activated protein kinase (SAPK) pathway that serves as a prototype signalling system for eukaryotes. This pathway is necessary and sufficient to adapt yeast cells to high external osmolarity. A key component of the pathway is the SAPK Hog1, which is rapidly phosphorylated upon hyper-osmotic shock. Phosphorylated Hog1 translocates to the nucleus activating transcription factors that lead to the synthesis of enzymes facilitating the accumulation of the osmolyte glycerol. Internal glycerol balances and re-establishes pre-stress internal and external water potential differences [45, 69, 91].

Several models of the HOG pathway with different complexity have been already published [69, 91, 92]. Here, I transform the three-dimensional generic HOG model from [92] into a 2-dimensional model, where I replace transcription and translation processes that are needed for the glycerol production by their duration τ. Since I study the role of time delay in the HOG pathway, I omit nested negative feedbacks leaving only delayed glycerol-mediated negative feedback. Thus, I obtain Model 2 from Fig. 2.1B.

In Model 2, phosphorylated Hog1 (Hog1-PP), glycerol and external osmotic shock [M NaCl] correspond to C, R and I, respectively.

In order to define a signal function S_1 mediating a DNF I consider an auxiliary component A used in [92] for the three-dimensional HOG model. The component A mimics a cellular sensor, which reacts to an external stimulus I and transduces a signal to the component C. I adapt the dynamics of A from [92]:

$$\frac{dA}{dt} = I + T_0 - \rho A(t) - \xi R(t) \frac{A(t)}{K_m + A(t)}, \tag{2.36}$$

where T_0 is a base signal, ρ, ξ and K_m are positive parameters.

Then I define $S_1(I, R)$ as the equilibrium of (2.36), which is scaled by the parameter $\mu > 0$:

$$S_1(I, R) = \mu \frac{\sqrt{(-K_m \rho + I - \xi R + T_0)^2 + 4\rho(K_m I + K_m T_0)} - K_m\rho + I - \xi R + T_0}{2\rho}. \tag{2.37}$$

Note that for small values of K_m ($K_m \to 0$) the system (2.2) senses the positive difference between the scaled external stimulus $I + T_0$ and the scaled response R (see Fig. 2.4):

$$\lim_{K_m \to 0} S_1(I, R) = \mu \frac{|I + T_0 - \xi R| + I + T_0 - \xi R}{2\rho} = \mu \max\left(\frac{I + T_0 - \xi R}{\rho}, 0\right).$$

Thus, I may conclude that the signal function S_1 is a linear function of the scaled external stimulus $I + T_0$ and the scaled response R, which is basically the function
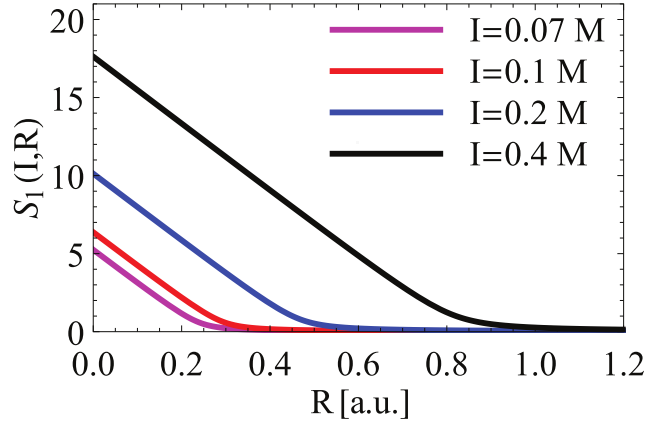
Figure 2.4: Plot of the signal function $S_1(I, R)$ (2.37)**.** Parameters from Table B.1 and $I = 0.07, 0.1, 0.2, 0.4$ M are used.
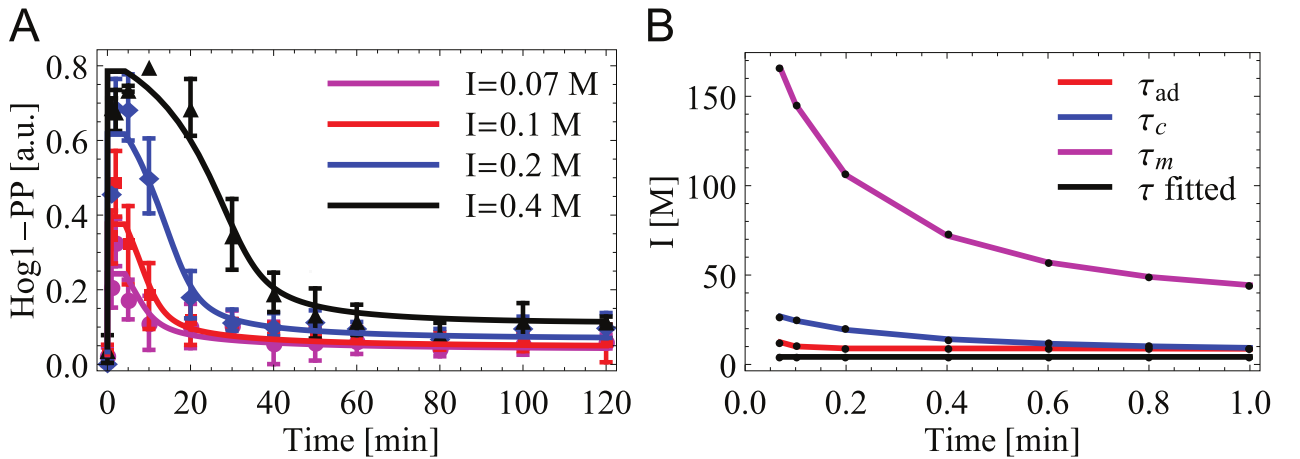
Figure 2.5: Simulation and response analysis of the HOG model. (A) Simulation of the HOG model (2.2) with parameters from Table B.1, dots – experimental data from [69]. (B) Calculation of τ_c, τ_m and τ_{ad} for several values of stimulus $I = 0.07, 0.1, 0.2, 0.4, 0.6, 0.8, 1$ M designated by dots.

used for the generic 4-dimensional model in [91] in a differentiable positive form.

After the definition of the DNF function $S_1(I, R)$ the parameter vector p (2.7) of Model 2 has the following extended form:

$$ p_{ext} = (I, \alpha, \beta, \eta, K_m, \mu, \rho, \xi, T_0)^T . $$

I fit the parameter vector p_{ext} of the HOG model (2.2) to experimental data from [69] for salt shocks $I = 0.07, 0.1, 0.2, 0.4$ M (see Table B.1). Corresponding simulations of the fitted HOG model (2.2) are represented in Fig. 2.5A. The model is not only able to recapitulate measured Hog1 dynamics for different conditions, but the fitted optimal solution is also robust with respect to noise in the fitted parameters (see Fig. A.1). The integrated response varies only around 8% assuming a parameter noise of $\pm 10\%$ (see Appendix A). Further, I analyse the influence of τ on the response patterns of

the HOG model (2.2) for stimulus values $I = 0.07, 0.1, 0.2, 0.4, 0.6, 0.8, 1$ M. As a result, for considered values of I both critical and marginal time delays, τ_c and τ_m, exist (see Fig. 2.5B). The fitted time delay $\tau = 4.2$ min is less than both τ_c and τ_m for all values of I (see Fig. 2.5B). According to the derived theory, the relation $0 < \tau < \tau_c$ corresponds to an overdamped response, which is also supported by experimental data (see Fig. 2.5A).

The fitted time delay τ has a large distance to τ_m for all considered I (see Fig. 2.5B). Therefore, the HOG system robustly produces a strongly overdamped response and crosses the steady state only once at early time points ($t < 5$ min), even if perturbations in time delay arise. Thus, it is unlikely that damped oscillations occur. Indeed, τ_c is about 2-7 times higher than the fitted τ.

In addition, I conduct a Monte-Carlo analysis of the HOG model (2.2) to check the robustness of the overdamped response to perturbations in all parameter values. For this, I simultaneously vary all parameters including time delay τ within 80% and 120% of their fitted values for $N = 8000$ times. The value of external stimulus I is randomly sampled in the range $[0.07, 1]$ M using the uniform distribution for $N = 8000$ times. As a result, for HOG model (2.2) I create $N = 8000$ sampled parameters sets. For each sampled parameter set I calculate the critical time delay τ_c. For all sampled parameter sets, the critical time delay τ_c varies between 6.3 min and 45.6 min and is always greater than the respective sampled τ. Thus, HOG model (2.2) produces an overdamped response for all generated parameter sets. This analysis leads to the conclusion that HOG system in yeast produces a robust overdamped response with respect to osmotic stress and it is unlikely that it produces damped or sustained oscillations for the considered external stimulus I in the range $[0.07, 1]$ M.

Calculation of time delay minimizing the adaptation time

Further, I numerically calculate values of the time delay τ_{ad} minimizing the adaptation time of the HOG model (2.2) for stimulus $I \in [0.07, 1]$ M (see Fig. 2.5B):

$$
\begin{aligned}
\tau_{ad} = &\arg\min_{\tau \in [0, \tau_c]} t \\
\text{s.t. } &|C(t) - C_s| < 5 \times 10^{-7}, \\
&|C(t-1) - C_s| > 5 \times 10^{-7}, \\
&t \in \{1, 2, 3, ..., 1000\}.
\end{aligned}
\tag{2.38}
$$

For calculating τ_{ad} I perform the following steps:

1. For fixed values of $I \in [0.07, 1]$ M and $\tau \in [0, \tau_c]$ I simulate the HOG model (2.2) with parameters from Table B.1 on the time interval $t \in [0, 1000]$ min. Searching for τ_{ad} at the interval $[0, \tau_c]$ allows the exclusion of damped and sustained oscillatory responses of the HOG model.

2. I assign $t_i = 1000$ min to be the starting time point for searching the adaptation time of the component $C(t)$ of the HOG model (2.2). At this time point conditions $|C(t_i) - C_s| < 5 \times 10^{-7}$ and $|C(t_i - 1) - C_s| < 5 \times 10^{-7}$ are fulfilled for all considered values of I and τ.

3. I decrease t_i and check conditions (2.38). If conditions (2.38) are satisfied for the time point t_i, I designate t_i as the adaptation time of the HOG model (2.2). The corresponding value of time delay is designated as the optimal time delay τ_{ad}, which induces the shortest adaptation time of the HOG model (2.2) for the fixed stimulus I. Otherwise, I decrease t_i until conditions (2.38) are satisfied.

As an example, in Fig. 2.6A I plot the adaptation time of the HOG model (2.2) for $\tau \in [2, 14]$ min and $I = 0.4$ M. The value of τ_{ad} corresponds to the minimum of the adaptation time on the graph. In Fig. 2.6B I display simulations of the HOG model (2.2) for $I = 0.4$ M using the optimal time delay $\tau_{ad} = 8.95$ min as well as two representative time delay values $\tau = 3$ min and $\tau = 13$ min, which are less and greater than τ_{ad}, respectively.

Fig. 2.6B shows that simulation of the HOG model (2.2) demonstrates no equilibrium undershooting for both $\tau = 3$ min and $\tau = \tau_{ad} = 8.95$ min. However, the model with $\tau = 3$ min needs more time to approach the equilibrium with the accuracy 5×10^{-7} than the model with $\tau = \tau_{ad} = 8.95$ min. For $\tau = 13$ min the simulation of the HOG model (2.2) crosses the equilibrium twice before reaching it.

Thus, the obtained values of τ_{ad} for $I \in [0.07, 1]$ M are depicted in Fig. 2.5B. Namely, τ_{ad} is equal to 12.4 min for $I \in [0.07, 1]$ M and is about 9 min for other I. Hence, values of τ_{ad} are relatively close to the fitted τ for all considered I (see Fig. 2.5B). Therefore, I may conclude that the HOG system employs an optimal intrinsic time

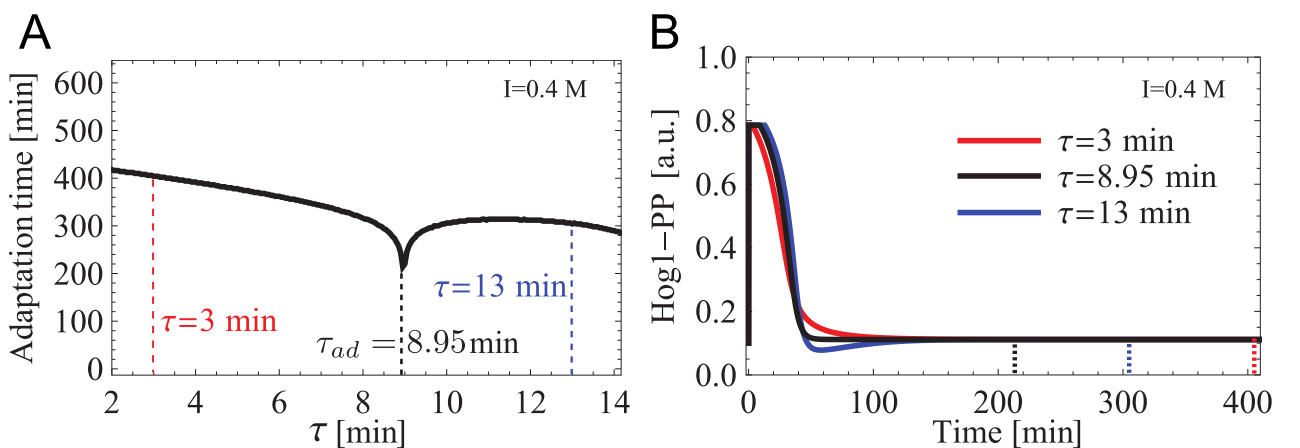**Figure 2.6: Calculating $\boldsymbol{\tau_{ad}}$.** (A) The adaptation time of Hog1-PP for $\tau \in [2, 14]$ min for $I = 0.4$ M. (B) Simulations of the HOG model (2.2) for $I = 0.4$ M with $\tau = 3, 8.95, 13$ min. The colour-coded dashed lines correspond to time values needed for the model simulation to approach the equilibrium C_s with the accuracy 5×10^{-7}.

delay τ for producing glycerol. Indeed, the time delay minimizes the time the system needs to adapt to new osmotic conditions. I call this property "optimal adaptation".

Dependence between adaptation time and model parameters

Next, I investigate how the adaptation time of the HOG model (2.2) depends on activation and degradation parameters α, β, μ, η within the range of 0.1 and 10 times their respective fitted value. As the representative stimulus level I consider $I = 0.4$ M (see Fig. 2.7A). Among the analysed parameters the only parameter, whose change may lead to a substantial decrease in adaptation time, is the degradation rate β of the response R. However, increasing β leads to increasing the steady state C_s that corresponds to the level of phosphorylated Hog1 (see Fig. 2.7B). Yeast cells tend to keep the level of phosphorylated Hog1 low because it is a sign of stress and, in fact, incomplete adaptation. Thus, the value of β is a trade-off between fast adaptation and complete adaptation indicated by elevated steady state Hog1 activation.

Taken together, my study showed that the HOG system produces a robust over-damped response and demonstrates optimal adaptation after osmotic shock. Additionally, the model predicted that increasing the glycerol degradation rate may lead to decreasing adaptation time of the HOG system at the expense of incomplete adaptation, which is indicated by increased steady states of phosphorylated Hog1.
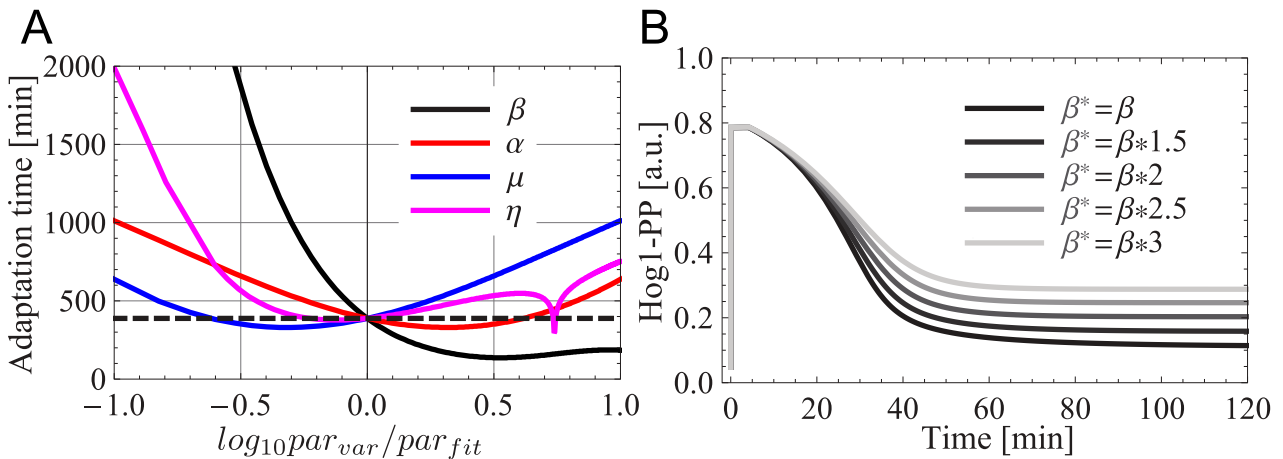
Figure 2.7: **Dependence between the adaptation time of the HOG model** (2.2) **and model parameters for $I = 0.4$ M.** (A) Dependence between the adaptation time of the HOG model and parameter values α, β, μ, η. Dashed line – adaptation time of the model with fitted parameters from Table B.1; par_{var} and par_{fit} designate varied and fitted parameter values, respectively. (B) Simulation of the HOG model (2.2) with parameters from Table B.1 and several values of degradation parameter $\beta^* = \beta$, 1.5β, 2β, 2.5β, 3β.

2.4.2 NF-κB system

The transcription factor NF-κB regulates a variety of genes that are responsible for inter- and intracellular signalling, cell growth, survival, apoptosis and cellular stress responses [35, 85]. Briefly, NF-κB is held inactive in the cytoplasm by three IκB isoforms. Cell stimulation by, e.g., tumour necrosis factor-α (TNF-α) activates the IκB kinase complex, leading to phosphorylation and degradation of IκB proteins. Free NF-κB translocates to the nucleus, activating genes, including IκBα and IκBϵ, which in turn relocates to the cytoplasm inactivating NF-κB.

In order to describe the NF-κB regulation in mammalian cells, an ODE model with negative feedbacks was presented in [44]. Recently, this model was reduced by employing two explicit time delays needed for activating genes of IκBα and IκBϵ [66]. Using theoretical analysis the authors showed that the oscillatory frequency in NF-κB dynamics is not a function of the stimulus but the time delay.

I wondered how the time delay affects the response of the NF-κB system with respect to a stimulus in general. Since my theoretical framework is applicable to systems with a single DNF, I consider the mutant NF-κB system containing only the IκBα feedback loop [44]. In the mutant system, the external stimulation activates NF-κB, which induces the synthesis of IκBα, which in its turn binds NF-κB and deactivates it. According to studies [44, 66], the IκB-α–NF-κB signalling pathway can be described by Model 4 from Fig. 2.1D.

I designate concentrations of NF-κB and IκB-α by C and R, respectively. In order to get the NF-κB model (2.4) without external stimulus in a non-zero steady state I present the input I in the form (2.39). Here, the input I is a scaled sum of external signal I^*, e.g. TNF-α, and base signal T_0 with the scaling factor $\mu > 0$:

$$I = \mu\left(I^* + T_0\right). \tag{2.39}$$

The negative feedback by output-activation is modelled by a Hill function (1.10). After the definition of the DNF function $S_2(R)$ the parameter vector p (2.7) of Model 4 has the following extended form:

$$p_{ext} = \left(I^*, \alpha, \beta, \eta, K_m, n, \mu, \delta, T_0\right)^T.$$

I estimate parameters p_{ext} of the NF-κB model (2.4) using experimental data from [44] (see Fig. S1 therein). The resulting parameter values are represented in Table B.1. The corresponding data and simulations are displayed in Fig. 2.8A. The model recapitulates measured NF-κB dynamics for a TNF-α stimulus of $I^* = 10$ ng/ml. Moreover, the fitted optimal solution is also robust with respect to noise in the fitted parameters (see Fig. A.1). The integrated first transient response varies only by 6.4% assuming a parameter noise of $\pm 10\%$ (see Appendix A).

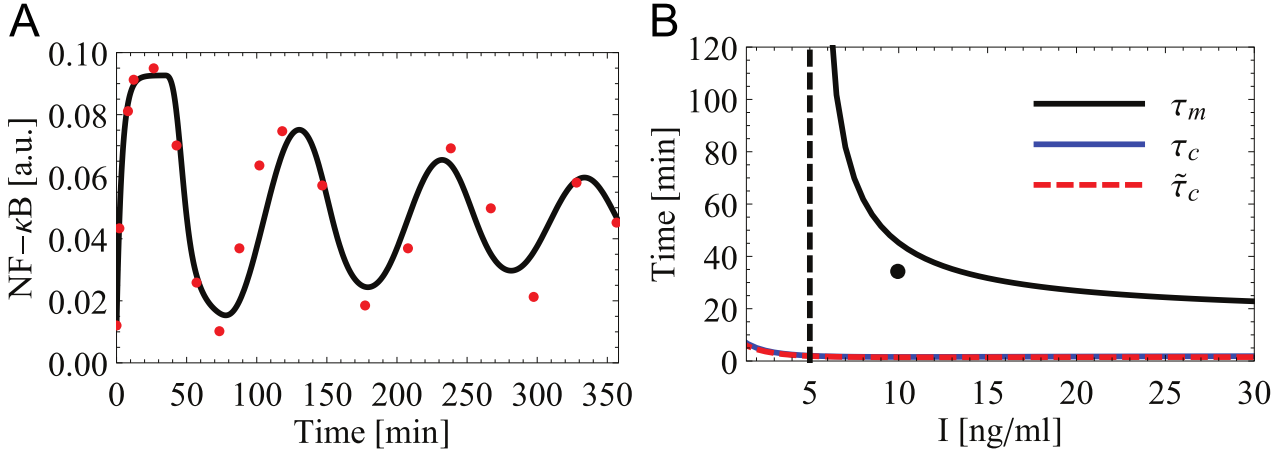Further, I investigate how time delay influences the response of the NF-κB

Figure 2.8: Simulation and response analysis of the NF-κB model. (A) Simulation of the NF-κB model (2.4) with parameters from Table B.1, dots – – experimental data from [44], Fig. S1 therein. (B) Dependence between the stimulus value I and τ_c, $\tilde{\tau}_c$, τ_m. The dot corresponds to fitted parameter values $I^* = 10$ ng/ml and $\tau = 34.5$ min. The black dashed line corresponds to the value $I_s^* = 5.4$ ng/ml such that for any $I^* \in [0, I_s^*]$ the NF-κB model (2.4) is asymptotically stable for any $\tau \geq 0$.

model (2.4) with parameters from Table B.1 for stimulus values $I^* \in [0, 20]$ (see Fig. 2.8B). The numerical analysis shows that there exists a stimulus value $I_s^* \approx 5.4$ ng/ml such that for $I^* \in [0, I_s^*]$ only τ_c exists. For $I^* > I_s^*$ there exist both τ_c and τ_m. Note that both τ_c and τ_m decrease with I^*.

The value of the stimulus TNF-α $I^* = 10$ ng/ml, which was used in [44] for obtaining data in Fig. 2.8A, is greater than $I_s^* = 5.4$ ng/ml. Therefore, for $I^* = 10$ ng/ml there exist both $\tau_c = 1.56$ min and $\tau_m = 45.2$ min. Since the relation $\tau_c < \tau = 34.5\,\text{min} < \tau_m$ holds (see Fig. 2.8B), the NF-κB model (2.4) produces a damped oscillatory response, which corresponds well to experimental data (see Fig. 2.8A).

In comparison to τ_c, the fitted τ is close to τ_m (see Fig. 2.8B). This might facilitate both damped and sustained oscillatory dynamics upon small changes in parameter values. To this end, I check the robustness of the NF-κB characteristic response to parameter perturbations by performing Monte-Carlo analysis. I sample all parameter values including time delay τ and external stimulus I within 80% and 120% of their fitted values for $N = 8000$ times. Then for each sampled parameter set I calculate the marginal time delay τ_m if it exists. Thus, Monte-Carlo analysis shows that for about 78% of sampled parameter sets τ_m is greater than the corresponding sampled τ and the model demonstrates damped oscillatory behaviour. Nevertheless, for about 16 % of parameter sets τ_m is less than τ and the model demonstrates sustained oscillatory behaviour. For about 6 % of parameter sets τ_m does not exist and the model demonstrates damped oscillatory behaviour. Thus, given the intrinsic noise in protein expression, mimicked by Monte-Carlo analysis, both damped and sustained oscilla-

tory response patterns might co-exist. The probability of the two response patterns with respect to random parameter perturbations is determined by the strength of the stimulus. For $I^* = 10$ ng/ml damped oscillations dominate the response. For higher stimuli the Hopf bifurcation threshold decreases making sustained oscillations more likely to arise (see Fig. 2.8B).

Thus, the NF-κB system upon TNF-α is prone to damped oscillatory behaviour. However, the NF-κB system may also switch to sustained oscillations upon small changes in parameter values or increasing stimulus.

2.5 Discussion

In biological systems adaptive behaviour is often mediated and controlled by negative feedbacks, which inevitably come with time delays due to the time needed to transcribe biochemical information into concentrations of relevant compounds. Such delayed negative feedbacks (DNFs) are able to demonstrate adaptive as well as oscillatory dynamics [12, 15, 21, 36, 38, 44, 76].

In this chapter, I addressed the question of how time delay influences the response pattern of DNF systems. For generalization, I investigated several alternatives of DNF systems:

- systems with two types of DNF represented by signal input-inhibition and output-activation, respectively,

- systems without mass conservation and with mass conservation for one or two components.

Then I implemented the described systems using delay differential equations and perform mathematical analyses with respect to time delay. As a result, for all considered model structures the model response depends on the value of parameters, including time delay, and exhibits one of the following response characteristics: overdamped, critical damping, damped oscillatory or sustained oscillatory response.

I applied my general framework to concrete data of adaptive and oscillatory biological systems to study the role of time delay within DNFs. I studied two different systems with overdamped and damped oscillatory behaviour, respectively, i.e., the HOG system in yeast and the NF-κB and in mammals.

The application of my theoretical framework to the HOG pathway reveals an aspect of the adaptation process that I called optimal adaptation. The HOG system employs a time delay that is close to the value, which minimizes both the adaptation time and the number of over- and undershoots of the final steady state after stimulation. It would be interesting to see whether this feature of optimal adaptation also applies to other adaptive biochemical networks. My framework is suitable for such an analysis.

In addition, my analyses suggested that time delay in the NF-κB system is close to the bifurcation threshold. This property might facilitate both damped and sustained oscillatory dynamics upon small changes in the value of time delay. This way cell fate decisions might be tuned depending on network dynamics.

Based on design specification, several synthetic gene-regulatory networks have been proposed in order to generate artificial oscillations in bacteria [27, 99]. Mathematical modelling has been instrumental in this design process and time delay is recognized as a key design principle for constructing robust oscillators [99]. My framework allows to better address the role of delay, because it can be studied as a separate parameter. For example, in a specific network design a first estimate of the delay needed to provoke a certain response pattern can be obtained and, accordingly, the length of a gene-regulatory cascade can be projected.

3 Repressing oscillations in delayed negative feedback systems

3.1 Introduction

In the previous chapter, I demonstrated that oscillatory dynamics of biochemical compounds can be induced in intracellular delayed negative feedback (DNF) systems. However, in biological networks mediating adaptive responses oscillatory behaviour might be inappropriate. For example, in the hyperthermia treatment of cancer, large-amplitude temperature oscillations could result in tissue damage or patient discomfort [102]. Therefore, I wondered if there exist any cellular mechanisms or network design features that may suppress oscillatory dynamics of intracellular components.

The recent study [80] demonstrated that nested negative feedbacks may suppress oscillations of biochemical species involved in a delayed negative feedback. However, this study provided no insight into how time delay influences the dynamics of DNF systems and interacts with nested negative feedbacks. In one of studies with my contribution [92] it was proved that nested negative feedbacks can modify the resistance of a DNF system, i.e, the distance between model parameters and certain thresholds beyond which sustained oscillations occur. In this chapter, I continue this research and investigate how the combination of time delay and certain network design features influences the dynamics of biochemical DNF systems after external stimulation. Using Models 1-6 presented in Fig. 2.1 I study if the following network design features may repress oscillations of components of biochemical networks:

- presence of a nested negative (auto-inhibitory) feedback as it was described in [80, 92],

- presence of mass conservation for biochemical compounds,

- mechanism of DNF, i.e., input-inhibition or output-activation.

I subject these models to computational and theoretical stability analyses. My computational analyses demonstrate that the presence of auto-inhibition and mass conservation have a stabilizing influence on the model equilibrium independent of the strength of DNF. In contrast, increasing steepness and decreasing threshold of the DNF have a de-stabilizing effect on the model equilibrium. For modelling DNF Hill functions (1.9) and (1.10) were used. In terms of Hill functions, steepness and threshold correspond to the Hill coefficient n and half-saturation constant K_m, respectively. Along with computational studies theoretical analyses show that nested

auto-inhibitory feedbacks may increase the range of time delay, where the equilibrium is stable, through the steepness of the feedback function.

The developed theoretical framework is applied to study the oscillating p53 system in mammalian cells [64].

3.2 Design features stabilizing biochemical delayed negative feedback systems

According to recent studies [80, 91], nested auto-inhibitory feedbacks can repress oscillatory dynamics of simple biochemical networks containing a non-linear DNF. I investigate how other design features influence the dynamics of two-dimensional DNF systems. For this analysis I consider generic DNF Models 1-6 formulated in Section 2.2. Thus, in addition to auto-inhibition I consider the presence of the following model designs:

- Mechanism of DNF: input-inhibition (Models 1-3) or output-activation (Models 4-6),

- Presence of mass conservation for biochemical compounds (Models $1, 4$ without mass conservation, Models $2, 5$ with mass conservation for one component, Models $3, 6$ with mass conservation for both components),

- Strength of DNF: strong or weak.

I also consider how the following combinations of delayed and auto-inhibitory negative feedbacks influence the dynamics of DNF networks:

- Weak DNF with and without auto-inhibition,

- Strong DNF with and without auto-inhibition.

For analysing the influence of these design features on the dynamics of Models 1-6 I perform Monte-Carlo analysis of these models. In this study, Monte-Carlo analysis implies random sampling of model parameters in the certain range with the subsequent calculation of model characteristics of interest for every sampled parameter set (see section 1.1.5). In order to perform this analysis, I define concrete DNF functions, i.e., S_1 and S_2, and auto-inhibition function F.

I define a reverse Hill function as the input-inhibition DNF function $S_1(R)$ (1.9). As the output-activation function $S_2(R)$ I define a Hill function (1.10). For both functions S_1 and S_2, $K_m > 0$ is the half-saturation constant, characterizing the activation threshold beyond which the feedback takes effect, and $n \geq 1$ is the Hill coefficient, characterizing how abruptly the feedback takes effect after having passed the activation threshold. Thus, parameters K_m and n specify the strength of the DNF: the
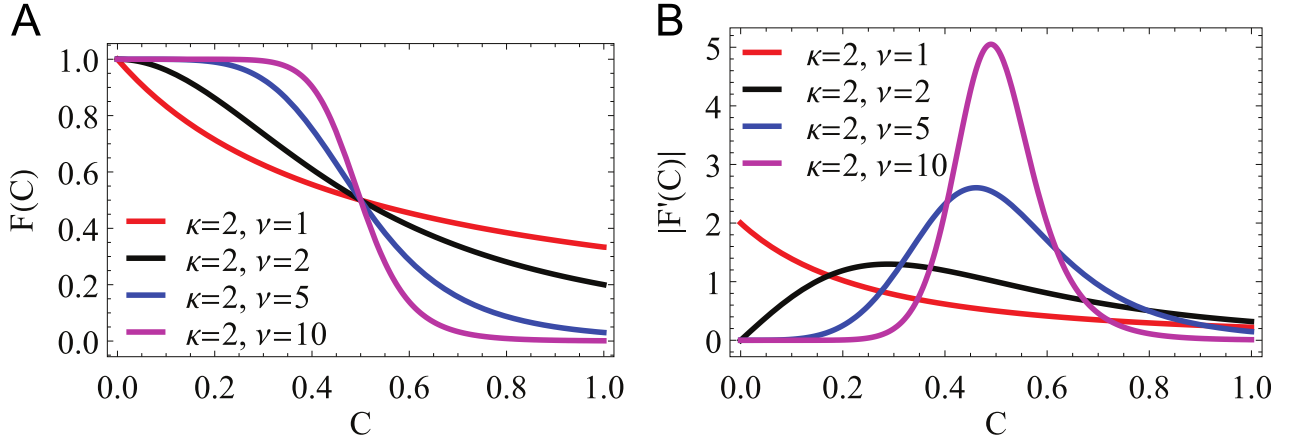
Figure 3.1: Reverse Hill function. (A) Plot of the reverse Hill function $F(C)$ (3.1). (B) Absolute value of the derivative of the reverse Hill function with the fixed κ and different values of ν.

lower the activation threshold K_m and the higher the steepness n are, the stronger the DNF is. Note that applying the same parameters make functions S_1 and S_2 symmetric allowing a fair comparison of the influence of input-inhibition and output-activation on the model stability (see Fig. 1.6).

As the auto-inhibitory feedback I employ a reverse Hill function $F(C)$ having the following form (see Fig. 3.1):

$$F(C) = \frac{1}{1 + (\kappa\,C)^{\nu}}, \ \nu \geq 1, \ \kappa \geq 0. \tag{3.1}$$

After the definition of functions S_1, S_2 and F the parameter vector p (2.7) of Models 1-6 has the following extended form:

$$p_{ext} = (I, \alpha, \beta, \eta, \delta, K_m, n, \kappa, \nu)^T.$$

Next, I randomly generate values of the parameter vector p_{ext} in the way that all Models 1-6 without auto-inhibition, i.e., $\kappa = 0$, have similar values of the marginal time delay τ_m (2.34). These are $I = 1.74$, $\alpha = 0.66$, $\beta = 1.32$, $\delta = 282$, $\eta = 1$, $n = 2.72$, $K_m = 0.015$. These parameter values lead to $\tau_m = 1.21$, $\tau_m = 1.27$, $\tau_m = 1.37$, $\tau_m = 1.22$, $\tau_m = 1.25$, $\tau_m = 1.25$ for Models 1-6, respectively. This parameter set guarantees that any value of time delay τ has the similar distance to the Hopf bifurcation point τ_m for all considered Models 1-6. Simulations of Models 1-6 with these parameters and $\tau = 3.5$ are depicted in Fig. 3.2.
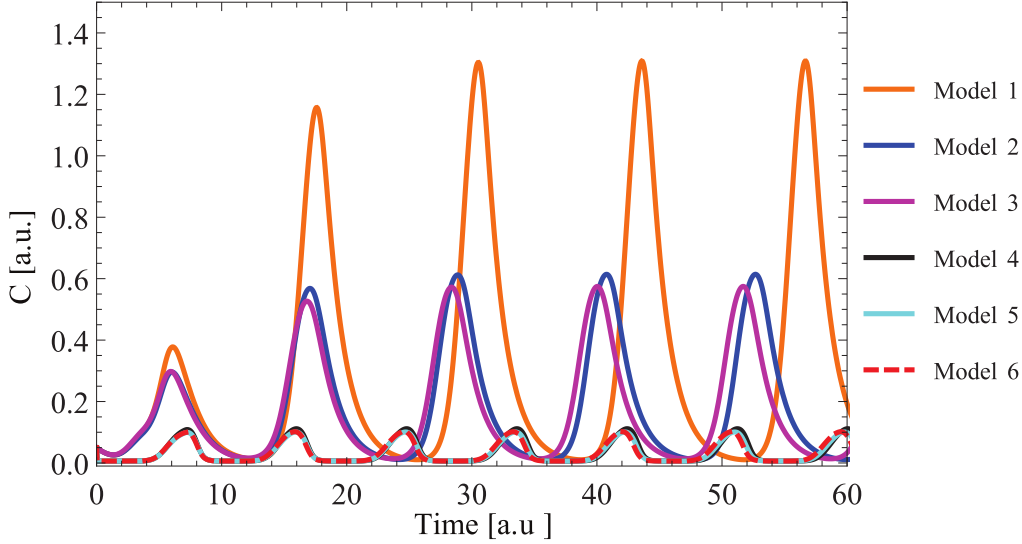
Figure 3.2: Simulation of Models 1-6 without auto-inhibition. Parameter values $I = 1.74$, $\alpha = 0.66$, $\beta = 1.32$, $\delta = 282$, $\eta = 1$, $n = 2.72$, $K_m = 0.015$, $\tau = 3.5$, $\kappa = 0$ were used.

Further, for every defined parameter value, except the input I, I assign a sampling range for the Monte-Carlo analysis. The value of the input $I = 1.74$ stays fixed assuming that the external stimulus is constant for all simulations. Then I randomly sample parameter values α, β, δ, η in the range from 0.1 to 10 times their respective values $N = 10000$ times. Parameter values n, K_m, ν, κ are sampled in the following way:

(i) in the case of weak DNF without auto-inhibition ($\kappa = 0$) I sample parameters n in the range from $n = 1$ to its chosen value $n = 2.72$ and K_m in the range from 10 to 20 times its value $N = 10000$ times.

(ii) in the case of strong DNF without auto-inhibition ($\kappa = 0$) I sample n in the range from 1 to 2 times its value and K_m in the range from 0.1 to 10 times its value $N = 10000$ times.

(iii) in the case of weak DNF with auto-inhibition I sample n and K_m as in (i), κ in the interval $[0.1, 10]$, ν in the interval $[1, 20]$ $N = 10000$ times.

(iv) in the case of strong DNF with auto-inhibition I sample n and K_m as in (ii), κ in the interval $[0.1, 10]$, ν in the interval $[1, 20]$ $N = 10000$ times.

Thus, for each Model 1-6 and each combination of DNF and auto-inhibition I sample 10000 parameter sets p_{ext}. Further, for each parameter set I calculate x, y and z according to (2.18)-(2.23) for Models 1-6, respectively. Then I define the percentage of parameter sets for which $x z \geq y$ holds meaning the absolute stability of the model equilibrium (see Fig. 3.3A). For the rest of the parameter sets, which do not induce absolute stability, I calculate the mean value of the marginal time delay τ_m (3.2) (see Fig. 3.3B).

Fig. 3.3A and B shows that considered models with auto-inhibition have higher
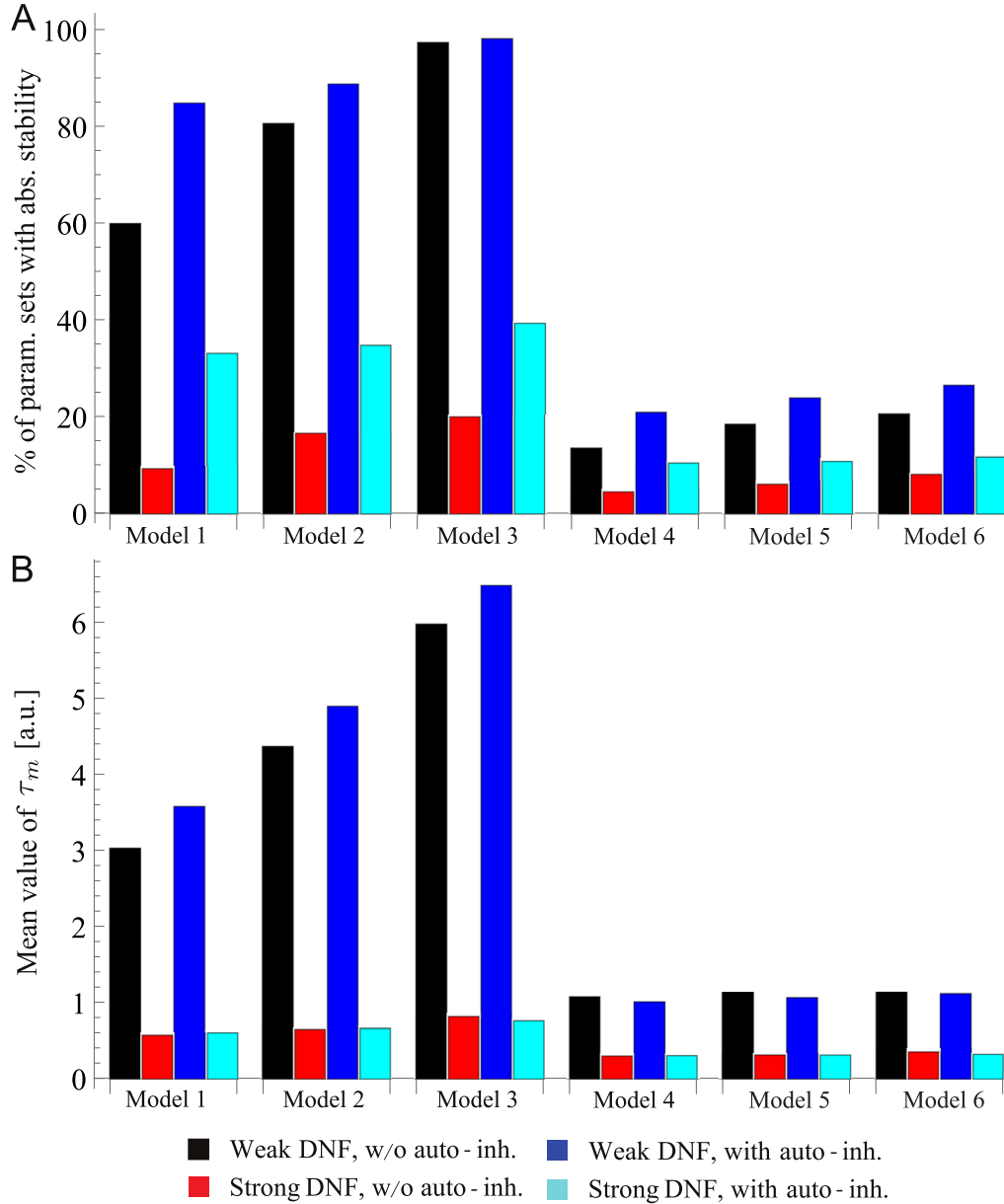
Figure 3.3: Stability analysis of Monte-Carlo simulations of Models 1-6.
(A) The percentage of parameter sets, which induces absolute stability. (B) The
mean value of marginal time delay τ_m. Model parameters are randomly sampled
10000 times in the certain range. The range is defined according to assumptions
about model characteristics: strength of DNF (strong or weak) and presence of
auto-inhibition.

percentage of parameter sets leading to absolute stability and higher mean value of τ_m
than the same models without auto-inhibition. This observation supports conclusions
of previous studies [80, 91], which claim that auto-inhibitory feedbacks may repress
oscillatory dynamics in networks containing DNF.

Additionally, for models with weak DNF there is a higher percentage of parameter
sets, which induce absolute stability of the model equilibrium, than for models with
the strong one. The same holds for the mean value of τ_m: models with weak DNF

have a higher mean value of τ_m than models with the strong DNF.

Interestingly, mass conservation demonstrates a stabilizing influence on model equilibria. Indeed, models with mass conservation for one component have a higher percentage of parameter sets leading to absolute stability of the model equilibrium and higher mean value of τ_m than respective models without mass conservation. In addition, models with mass conservation for both components have higher percentage of parameter sets leading to absolute stability of the model equilibrium than corresponding models with mass conservation for one component. In order to detect the influence of mass conservation on τ_m, for all models I quantify the dependence between τ_m and every parameter value. First I vary a parameter value in the range from 0.1 to 10 times its respective chosen value leaving the rest of the parameter values fixed. Then I quantify τ_m using resulting parameter sets with one varied parameter (see Fig. 3.4). This analysis shows that for the considered range of parameter values mass conservation influences τ_m only through changing the sensitivity of the half-saturation rate K_m leaving the sensitivity of other parameters almost unchanged. Thus, the sensitivity analysis indicates that mass conservation stabilizes the model equilibrium through changing the sensitivity of the half-saturation rate K_m of DNF (Fig. 3.4A).

Concerning the mechanism of DNF, Monte-Carlo analysis shows that Models 1-3 with input-inhibition have higher percentage of parameter sets leading to absolute stability and higher mean value of τ_m than Models 4-6 with output-activation (see Fig. 3.3A and B). However, I was not able to support these results applying Monte-Carlo analysis to the parameter set $I = 0.48$, $\alpha = 0.14$, $\beta = 0.44$, $\delta = 83.71$, $\eta = 1$, $n = 10$, $K_m = 0.9$, which I call the alternative parameter set. Refer to Fig. 3.5A for simulations of Models 1 and 4 using the alternative parameter set and $\tau = 10$. In contrast, for the alternative parameter set Model 1 with input-inhibition has a higher value of τ_m, i.e., $\tau_m = 1.27$, than Model 4 with output-activation, i.e., $\tau_m = 0.36$. According to values of τ_m one could expect that models with input-inhibition might have a higher percentage of parameter sets, which induce absolute stability, than models with output-activation. Nevertheless, for this parameter set Monte-Carlo analysis showed that models with input-inhibition have approximately the same percentage of parameter sets leading to absolute stability as corresponding models with output-activation (see Fig. 3.5). Note that for the alternative parameter set the rest of the conclusions presented above remained unchanged.

Taken together, I may conclude that auto-inhibition and mass conservation have a stabilizing influence on the model equilibrium independent of the strength of DNF and allow systems with DNF to adapt to an external stimulus without producing sustained oscillations.
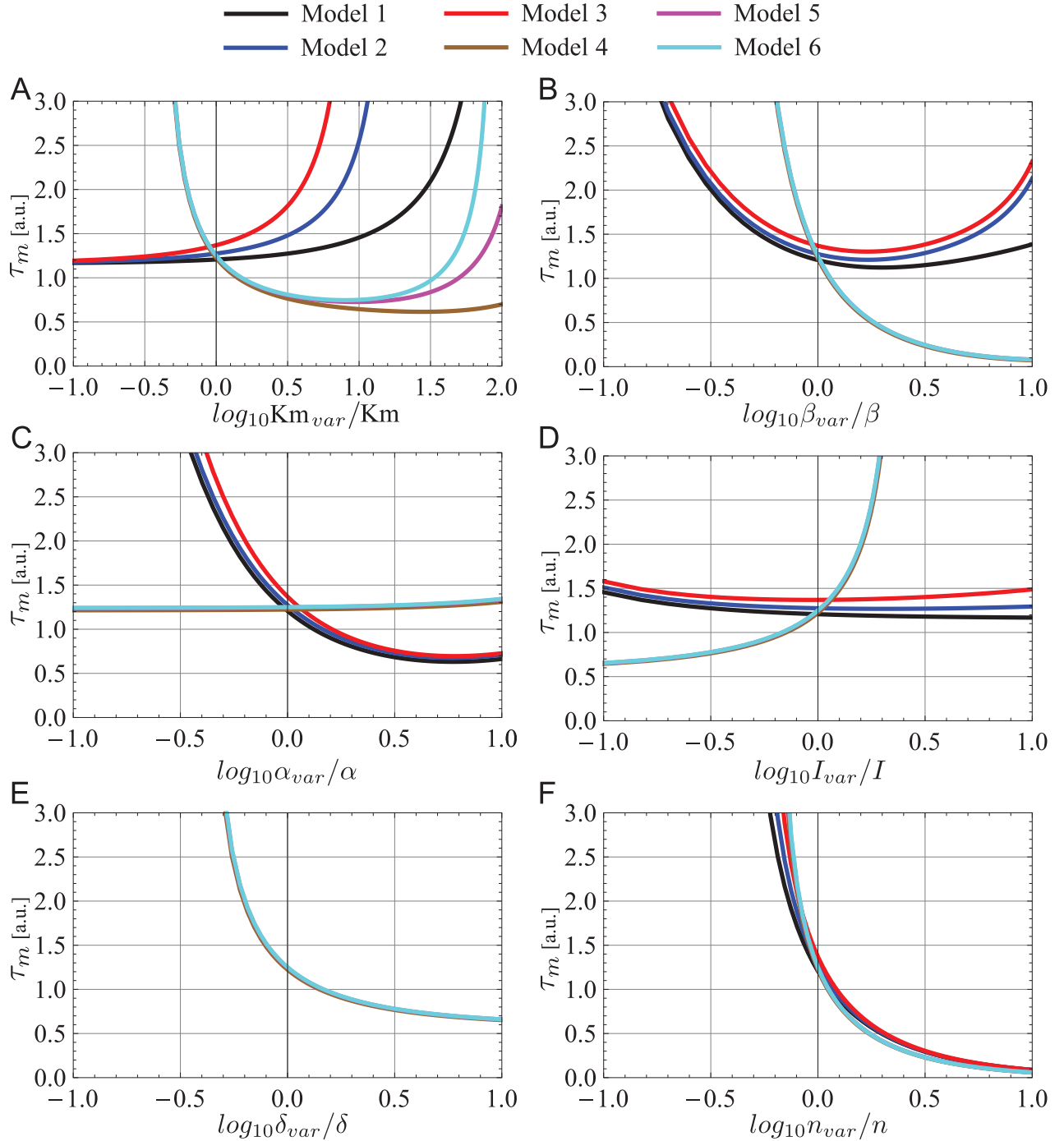
Figure 3.4: The dependence between τ_m and parameter values of Models 1-6. (A) K_m. (B) β. (C) α. (D) I. (E) δ. (F) n. With par_{var} and par I designate varied and initial chosen parameter values. These are $I = 1.74$, $\alpha = 0.66$, $\beta = 1.32$, $\delta = 282$, $\eta = 1$, $n = 2.72$, $K_m = 0.015$. For (A) I vary the parameter K_m in the range from 0.1 to 100 times its respective chosen value. For (B-F) I vary the value of each parameter in the range from 0.1 to 10 times its respective chosen value.

A

B
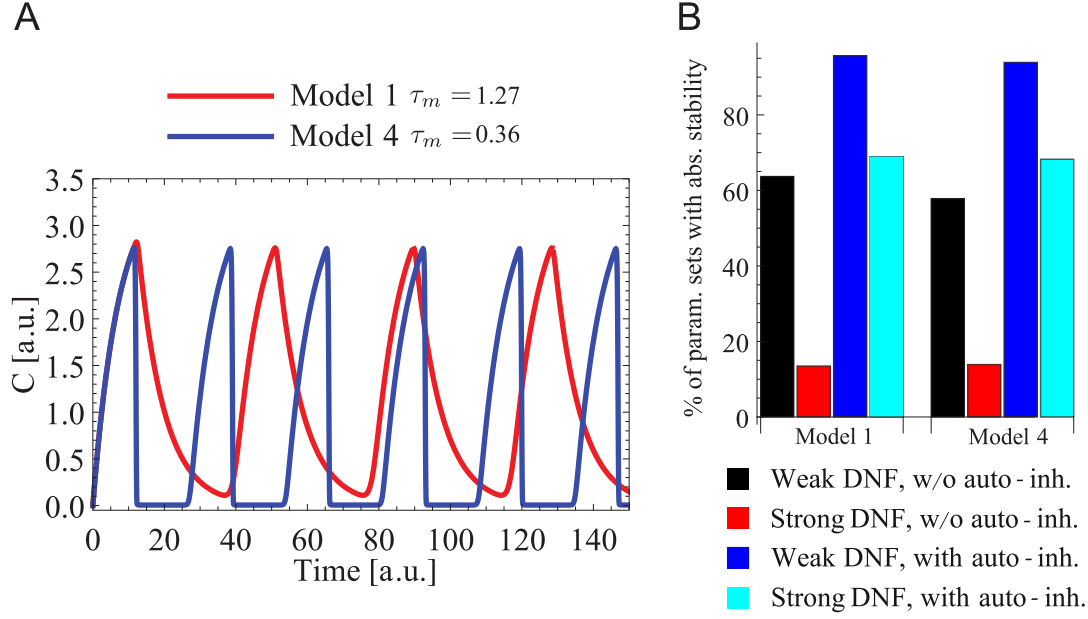
Figure 3.5: Results of Monte-Carlo analysis of Models 1 and 4 with the alternative parameter set. As the alternative parameter set I apply $I = 0.48$, $\alpha = 0.14$, $\beta = 0.44$, $\delta = 83.71$, $\eta = 1$, $n = 10$, $K_m = 0.9$, $\tau = 10$ without auto-inhibition ($\kappa = 0$). (A) Simulation of Models 1 and 4. (B) Stability analysis of Monte-Carlo simulations of Models 1 and 4. Model parameters are randomly sampled 10000 times in the certain range. The range is defined according to assumptions about model characteristics: strength of DNF (strong or weak) and presence of auto-inhibition. The percentage of parameter sets, which induces absolute stability, is quantified.

3.3 Auto-inhibition increases the value of the marginal time delay

In the previous section, the computational analysis showed that auto-inhibition may suppress oscillatory behaviour of DNF components. In this section, I present a theoretical evidence of this phenomenon.

First, I consider the marginal time delay τ_m (2.34) as the function of x, y and z:

$$\tau_m(x, y, z) = f(x, y, z) \cdot g(x, y, z), \tag{3.2}$$

where

$$
\begin{aligned}
f(x, y, z) &= \frac{\sqrt{2}}{\sqrt{-x^2 - z^2 + \sqrt{(x^2 + z^2)^2 + 4(y^2 - x^2 z^2)}}} > 0, \\
g(x, y, z) &= \arccos \frac{-(x + z)^2 + \sqrt{(x^2 + z^2)^2 + 4(y^2 - x^2 z^2)}}{2y} > 0.
\end{aligned}
\tag{3.3}
$$

Assuming $x\,z < y$ and using D from (2.31), I obtain derivatives of functions f and g

with respect to x, y and z:

$$\frac{\partial f}{\partial x}(x,y,z) = \frac{\sqrt{2}x\left(\sqrt{D}-\left(x^2-z^2\right)\right)}{\sqrt{D}\left(\sqrt{D}-x^2-z^2\right)^{3/2}} > 0,$$

$$\frac{\partial g}{\partial x}(x,y,z) = \frac{2(x+z)\left(\sqrt{D}-x^2+xz\right)}{\sqrt{D}\sqrt{4y^2-\left((x+z)^2-\sqrt{D}\right)^2}} > 0,$$

$$\frac{\partial f}{\partial z}(x,y,z) = \frac{\sqrt{2}z\left(\sqrt{D}+\left(x^2-z^2\right)\right)}{\sqrt{D}\left(\sqrt{D}-x^2-z^2\right)^{3/2}} > 0,$$

$$\frac{\partial g}{\partial z}(x,y,z) = \frac{2(x+z)\left(\sqrt{D}-z^2+xz\right)}{\sqrt{D}\sqrt{4y^2-\left((x+z)^2-\sqrt{D}\right)^2}} > 0, \tag{3.4}$$

$$\frac{\partial f}{\partial y}(x,y,z) = -\frac{2\sqrt{2}y}{\sqrt{D}\left(\sqrt{D}-x^2-z^2\right)^{3/2}} < 0,$$

$$\frac{\partial g}{\partial y}(x,y,z) = -\frac{(x+z)^2\left(-x^2-z^2+2xz+\sqrt{D}\right)}{\sqrt{D}y\sqrt{4y^2-\left((x+z)^2-\sqrt{D}\right)^2}} < 0.$$

Using the definition of functions f and g (3.3) and relations (3.4) I conclude that $f(x,y,z)$ and $g(x,y,z)$ are both positive functions, which increase with x and z and decrease with y. Consequently, $\tau_m(x,y,z)$ follows the same pattern. Using the relation between the equilibria of models (2.1)-(2.6) with and without auto-inhibitory feedback and properties of feedback functions F, S_1, S_2 described in Section 2.2, I calculate lower and upper bounds of x, y and z. Further, I show how these bounds can be increased or decreased changing the value of τ_m.

First, for each Model 1-6 I calculate lower and upper bounds of x, y and z. According to the proof of Proposition 1 (see Section 2.3.1) the equilibria $E = (C_s, R_s)^T$ of models (2.1)-(2.6) with auto-inhibitory feedback can be found as the intersection of functions $\theta_1 \cdot F$ and θ_2 (see Fig. 3.6). In case the auto-inhibitory feedback is not present in the system ($F(C) \equiv 1$), the equilibrium component $\widehat{C}_s$ of the model without auto-inhibition is always greater than the equilibrium component C_s of the model with auto-inhibition (see Fig. 3.6). According to (2.9), the same conclusion holds for equilibrium components R_s and $\widehat{R}_s$ of models with and without auto-inhibition, respectively.

Taking into account relations $C_s \leq \widehat{C}_s$ and $R_s \leq \widehat{R}_s$ and properties of feedback functions F, S_1, S_2 described in Section 2.2 I obtain the following estimations of x, y, z:

$$0 < \varepsilon_{lb}(|F'(C_s)|) < x < \varepsilon_{ub}(|F'(C_s)|),$$

$$0 < y < \sigma, \tag{3.5}$$

$$0 < \zeta_{lb} \leq z \leq \zeta_{ub}.$$
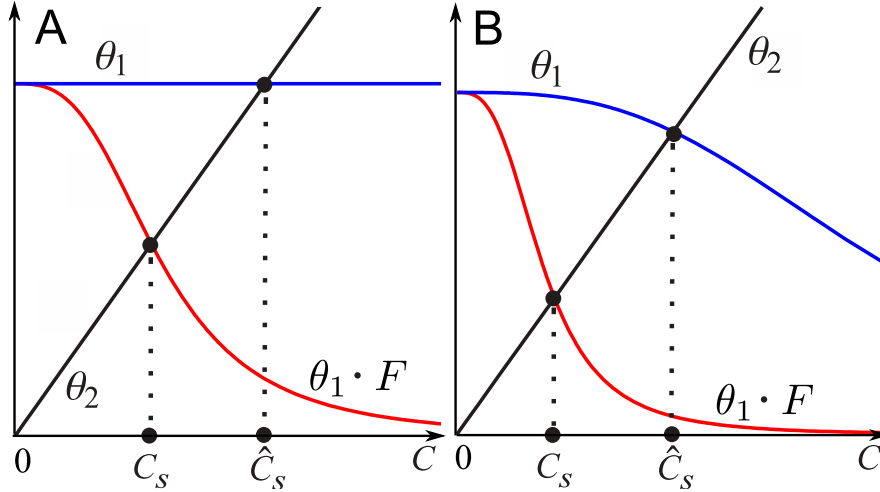
Figure 3.6: Schematic intersection of functions $\boldsymbol{\theta_1}$, $\boldsymbol{\theta_1 \cdot F}$ and $\boldsymbol{\theta_2}$. Functions θ_1 and θ_2 are introduced to find equilibrium components of Models 1-6. (A) To find equilibrium components C_s and $\widehat{C}_s$ for Model 4. (B) To find equilibrium components C_s and $\widehat{C}_s$ for Models $1, 2, 3, 5$ and 6.

Refer to Table 3.1 for values of ε_{lb}, ε_{ub}, σ, ζ_{lb}, ζ_{ub} for each Model 1-6. Note that both the lower and upper bound of x, i.e., ε_{lb} and ε_{ub}, are increasing with $|F'(C_s)|$ for Models 1-6. Therefore, one can always increase a given x by choosing an appropriate value for $|F'(C_s)|$. The value of y is positive and less than σ independent of the auto-inhibitory function F. Consequently, according to (3.4), one can always increase τ_m by increasing $|F'(C_s)|$.

Taken together, I showed that increasing the steepness of the auto-inhibitory feedback may increase the Hopf bifurcation threshold of the time delay τ_m and decrease the range of values of time delay $\tau \in [\tau_m, \infty)$, where sustained oscillations occur.

Table 3.1: Lower and upper bounds of x, y, z for Models 1-6.

Model 1
$\varepsilon_{lb} = I\,S_1(\widehat{R}_s)|F'(C_s)| + \alpha,$
$\varepsilon_{ub} = I\,S_1(0)|F'(C_s)| + \alpha,$
$\sigma = \eta\,I\,\max_{R\in[0,\widehat{R}_s]}|S_1'(R)|,$
$\zeta_{lb} = \zeta_{ub} = \beta.$

Model 2
$\varepsilon_{lb} = I\,S_1(\widehat{R}_s)\,(1 - \widehat{C}_s)|F'(C_s)| + \alpha,$
$\varepsilon_{ub} = I\,S_1(0)\,[1 + |F'(C_s)|] + \alpha,$
$\sigma = \eta\,I\,\max_{R\in[0,\widehat{R}_s]}|S_1'(R)|,$
$\zeta_{lb} = \zeta_{ub} = \beta.$

Model 3
$\varepsilon_{lb} = I\,S_1(\widehat{R}_s)\,(1 - \widehat{C}_s)|F'(C_s)| + \alpha,$
$\varepsilon_{ub} = I\,S_1(0)\,[1 + |F'(C_s)|] + \alpha,$
$\sigma = \eta\,I\,\max_{R\in[0,\widehat{R}_s]}|S_1'(R)|,$
$\zeta_{lb} = \beta,$
$\zeta_{ub} = \beta + \eta\,\widehat{C}_s.$

Model 4
$\varepsilon_{lb} = I\,|F'(C_s)| + \alpha + \delta\,S_2(0),$
$\varepsilon_{ub} = I\,|F'(C_s)| + \alpha + \delta\,S_2(\widehat{R}_s),$
$\sigma = \eta\,\delta\,\widehat{C}_s\,\max_{R\in[0,\widehat{R}_s]}|S_2'(R)|,$
$\zeta_{lb} = \zeta_{ub} = \beta.$

Model 5
$\varepsilon_{lb} = I\,(1 - \widehat{C}_s)|F'(C_s)| + \alpha + \delta\,S_2(0),$
$\varepsilon_{ub} = I\,[1 + |F'(C_s)|] + \alpha + \delta\,S_2(\widehat{R}_s),$
$\sigma = \eta\,\delta\,\widehat{C}_s\,\max_{R\in[0,\widehat{R}_s]}|S_2'(R)|,$
$\zeta_{lb} = \zeta_{ub} = \beta.$

Model 6
$\varepsilon_{lb} = I\,(1 - \widehat{C}_s)|F'(C_s)| + \alpha + \delta\,S_2(0),$
$\varepsilon_{ub} = I\,[1 + |F'(C_s)|] + \alpha + \delta\,S_2(\widehat{R}_s),$
$\sigma = \eta\,\delta\,\widehat{C}_s\,\max_{R\in[0,\widehat{R}_s]}|S_2'(R)|,$
$\zeta_{lb} = \beta,$
$\zeta_{ub} = \beta + \eta\,\widehat{C}_s.$

3.4 Application to p53 system

In this section Model 4 is used to mimic the oscillatory dynamics of the mammalian p53 system. Obtained theoretical results will be applied to design a nested negative feedback for suppressing oscillations in this system. In addition, the simulation of the p53 model will be used to explain how time delay and nested negative feedback influence period and amplitude of oscillations in this system.

3.4.1 Modelling oscillating p53 system

The tumor suppressor protein p53 is activated in response to many stress signals and activates various stress-response programs including cell-cycle arrest, senescence and apoptosis [12]. It is also well established that p53 acts within a negative feedback loop, including Mdm2 as the negative regulator of p53: p53 transcriptionally activates Mdm2, which in turn targets p53 for degradation [56, 59].

Several mathematical models of the p53-Mdm2 feedback loop have been published [36, 64, 76, 92]. One of these models (model III from Table 1 in [36]) is a particular case of Model 4 from Fig. 2.1D with $F(C) \equiv 1$. Therefore, I wondered, whether my theoretical framework would be able to explain measured p53 dynamics upon DNA damage. In my designations C and R correspond to p53 and Mdm2, respectively. The input I is defined here as a scaled DNA damage signal measured in arbitrary units. The negative feedback by output-activation is modelled by a nonlinear Hill function $S_2(R)$ (1.10). After the definition of the DNF function $S_2(R)$ the parameter vector p (2.7) of Model 4 has the following extended form:

$$p_{ext} = (I, \alpha, \beta, \eta, K_m, n, \delta)^T .$$

I fit parameters of the p53 model (2.4) to the experimental data of an averaged oscillation pattern of the p53-Mdm2 system after DNA damage from [36] (see Fig. S6 therein). The results of the fit are presented in Table B.1. Fig. 3.7A shows the simulation of the p53 model (2.4) with fitted parameters. The model is able to recapitulate measured p53 dynamics after DNA damage. Moreover, the fitted optimal solution is robust with respect to noise in the fitted parameters. The integrated first transient response varies only by 8.7% assuming a parameter noise of $\pm 10\%$ (see Appendix A).

The model analysis shows that the fitted time delay $\tau = 1.37$ h is almost two times larger than the corresponding $\tau_m = 0.76$ h that is calculated for the fitted DNA damage signal $I = 0.23$ (see Fig. 3.7B). Therefore, the p53 model (2.4) with fitted parameters from Table B.1 produces a sustained oscillatory response.
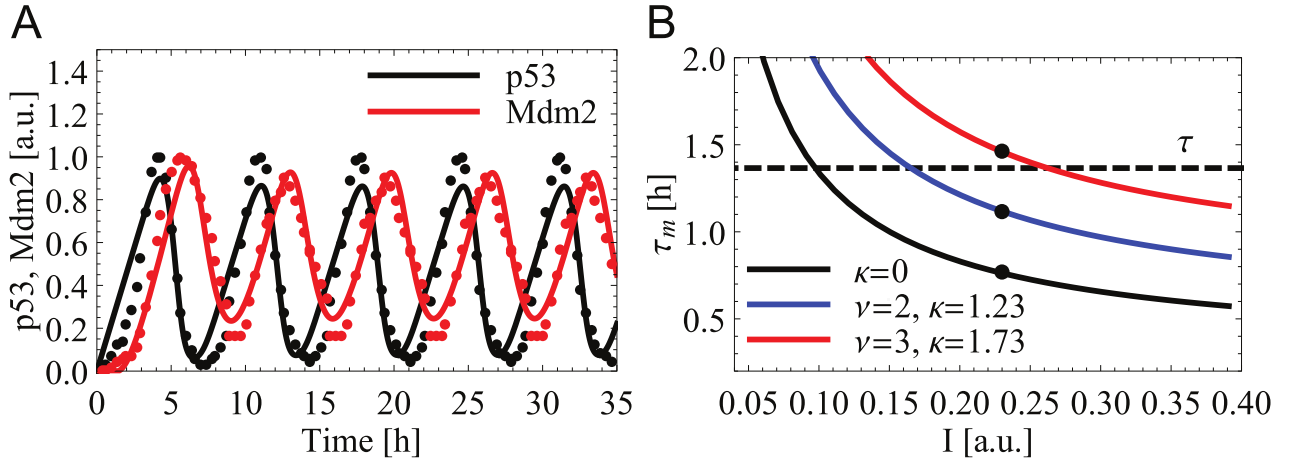
A

B

Figure 3.7: Simulation and response analysis of the p53 model. (A) Simulation of the p53 model (2.4) with fitted parameters from Table B.1, dots – experimental data from [36], Fig. S6 therein. (B) Dependence between the stimulus value I and τ_m for the p53 model (2.4) with fitted parameters from Table B.1 without and with synthetically activated auto-inhibitory feedback $F(C)$ (with $\nu = 2$, $\kappa = 1.23$ and $\nu = 3$, $\kappa = 1.73$). Dots designate values of τ_m calculated for the fitted value of $I = 0.23$ for the p53 model (2.4) with and without auto-inhibitory feedback.

3.4.2 Repressing oscillations in the p53 system

It was earlier reported that distinct p53 dynamics such as oscillations or sustained activation may lead to different cell fate decisions [12, 86]. Applying my theoretical analysis, I explore under what conditions sustained oscillations of p53 model (2.4) can be suppressed leading to a possible change of the cell fate. As a suppressing mechanism nested auto-inhibitory feedback F to the model component C is included preserving all values of fitted parameters.

My theoretical analysis suggests that the marginal time delay τ_m, beyond which any time delay leads to sustained oscillations, can be increased by increasing the slope of the auto-inhibitory feedback function at the equilibrium $|F'(C_s)|$. Here, I present a numerical study that will allow an increase in $|F'(C_s)|$ and, consequently, τ_m for the p53 model (2.4).

For the auto-inhibitory feedback function I utilize a reverse Hill function $F(C)$ (3.1). For the reverse Hill function, an obvious choice to increase the slope is increasing the Hill coefficient ν. Therefore, I make ν a free positive parameter, which value I choose. For simplicity I consider only integer values of ν. Then I adjust κ and equilibrium (C_s, R_s) to maximize $|F'(C_s)|$, which is equivalent to solving the equation $F''(C_s) = 0$. Thus, for the fixed value of ν I solve the following system of equations with respect to (C_s, R_s, κ) using fitted parameter values $(\alpha, \beta, \delta, \eta, K_m, n)$ from Table B.1:

$$
\begin{aligned}
F''(C_s) &= \frac{\nu(\kappa\, C_s)^\nu \left((\nu+1)(\kappa\, C_s)^\nu - \nu + 1\right)}{C_s^2 \left((\kappa\, C_s)^\nu + 1\right)^3} = 0, \\
0 &= I\, F(C_s) - \alpha\, C_s - \delta\, C_s\, S_2(R_s), \\
0 &= \eta\, C_s - \beta\, R_s.
\end{aligned}
\tag{3.6}
$$

Then, I quantify τ_m using (3.2). If τ_m is less than τ, I increase ν, solve the system (3.6) with respect to (C_s, R_s, κ) and quantify τ_m again.

Fig. 3.8 demonstrates results of the application of the algorithm to the p53 model. In Fig. 3.8A I illustrate the graph of the slope $|F'(C)|$ for several values of ν and adjusted values of κ. One can see that $|F'(C_s)|$ is increasing with increasing ν, whereas the value of C_s is only slightly decreasing (indicated by black dots in Fig. 3.8A). Consequently, τ_m is also increasing with respect to the Hill coefficient ν (see Fig. 3.8B). For $\nu \geq 3$ the equilibrium is asymptotically stable. For $\nu > 8$ the equilibrium is absolutely stable. Thus, the relation between ν, $|F'(C)|$ and τ_m demonstrated in Fig. 3.8 matches well with the theoretical analysis presented above.

In Fig. 3.9 I depict simulations of the p53 model with fitted parameters from Table B.1 and synthetically activated auto-inhibitory feedback $F(C)$ (3.1) with $\nu = 3$, $\kappa = 1.73$. One can see that the model with auto-inhibitory feedback produces damped instead of sustained oscillations.

Further, I investigate the stability of the equilibrium of the p53 model with and without synthetically activated feedback with respect to several parameters. In Fig. 3.10A and B I show that increasing the Hill coefficient ν and adjusting κ leads to decreas-
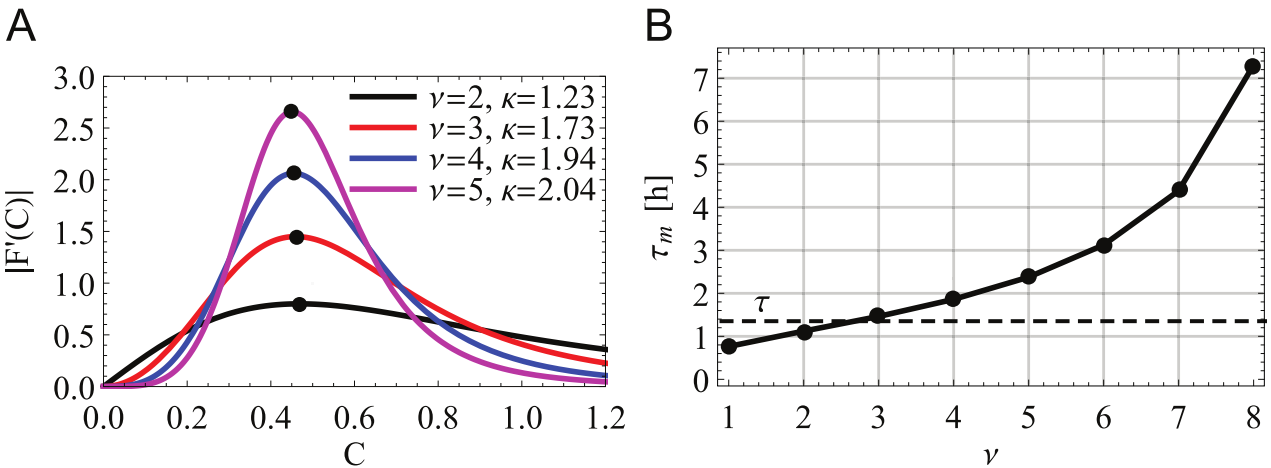
Figure 3.8: Influence of the synthetically activated auto-inhibitory feedback $\boldsymbol{F(C)}$ on the stability of the p53 model. (A) Absolute value of the derivative of $F(C)$ for $\nu = 2, 3, 4, 5$ and adjusted values of κ. Dots – absolute values of the derivative at the equilibrium point C_s. (B) Dependency between τ_m and Hill coefficient ν. The dashed line designates the value of the fitted time delay τ.
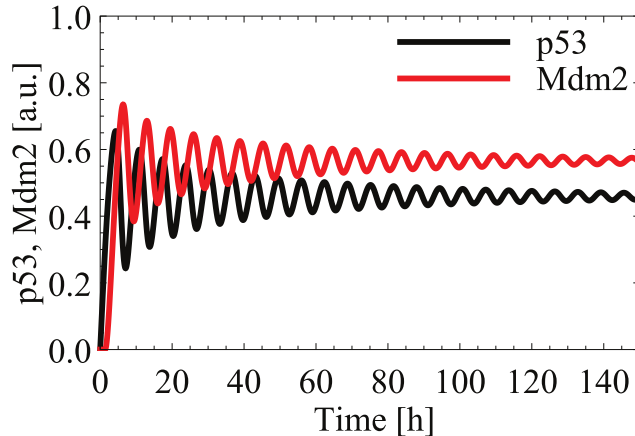
Figure 3.9: Simulation of the p53 model with synthetically activated auto-inhibitory feedback. Simulation of the p53 model with fitted parameters from Table B.1 and synthetically activated auto-inhibitory feedback $F(C)$ (3.1) with $\nu = 3$, $\kappa = 1.73$.

ing the parameter region, where oscillations occur. Fig. 3.10C demonstrates that τ_m increases with respect to κ for both $\nu = 2$ (*blue*) and $\nu = 3$ (*red*). These results correspond well to the recent study [92], which stated that nested negative feedbacks lead to increasing resistance of the DNF system. In addition, Fig. 3.10A illustrates that τ_m increases with respect to α thus indicating the stabilizing property of α and possibly explaining such a small fitted parameter value. On the other hand, τ_m decreases with respect to I (see Fig. 3.7B).

In a similar DNF system it was shown that the period of oscillations increases with the Hill coefficient n of the DNF function for a given time delay [15]. This inspired me to conduct a similar analysis for the p53 system. Fig. 3.11 demonstrates that the auto-inhibitory feedback with parameters $\nu = 3$, $\kappa = 1.73$ decreases and stabilizes the amplitude of oscillations, whereas the amplitude of oscillations increases with respect to the Hill coefficient n of the DNF function $S_2(R)$ (1.10). Moreover, increasing the steepness of the DNF has no substantial influence on the increase of the period with τ. The period of oscillations is a linear function of time delay τ, irrespective of values of ν, κ and n. Thus, opposed to the delayed feedback, the auto-inhibitory feedback has the potential to de-couple the increase of amplitude and period of oscillations with respect to τ. Moreover, auto-inhibitory and delayed negative feedbacks have opposing influence on the amplitude of oscillations.

Taken together, this analysis showed that for the p53 model (2.4) an auto-inhibitory feedback can be a potential mechanism increasing the marginal time delay τ_m, decreasing the amplitude of oscillations and turning sustained oscillations into damped oscillations.
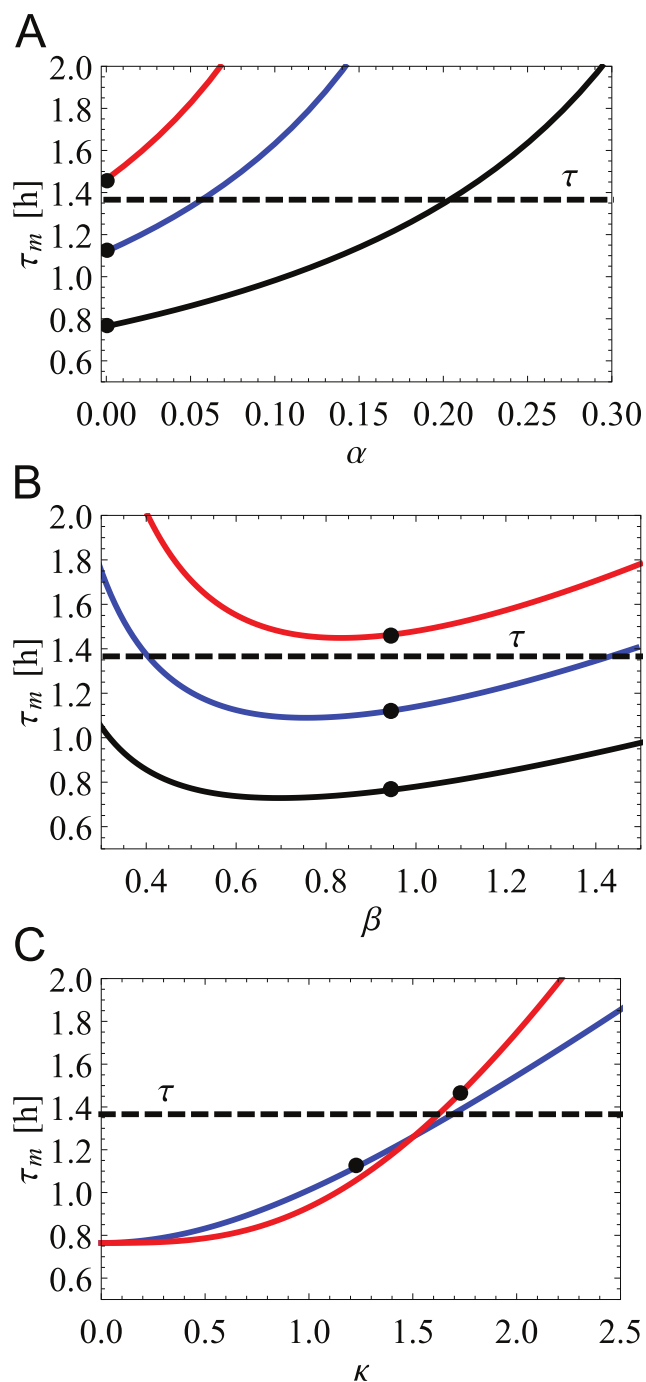
Figure 3.10: Dependencies between parameters of the p53 model. The p53 model is considered without (black) and with synthetically activated ($\nu = 2$, $\kappa = 1.23$ blue, $\nu = 3$, $\kappa = 1.73$ red) auto-inhibitory feedback. (A) τ_m and α. (B) τ_m and β. (C) τ_m and κ. Designations: dots – the fitted value of the parameter used in the p53 model, dashed line – the fitted value of τ (see Table B.1).
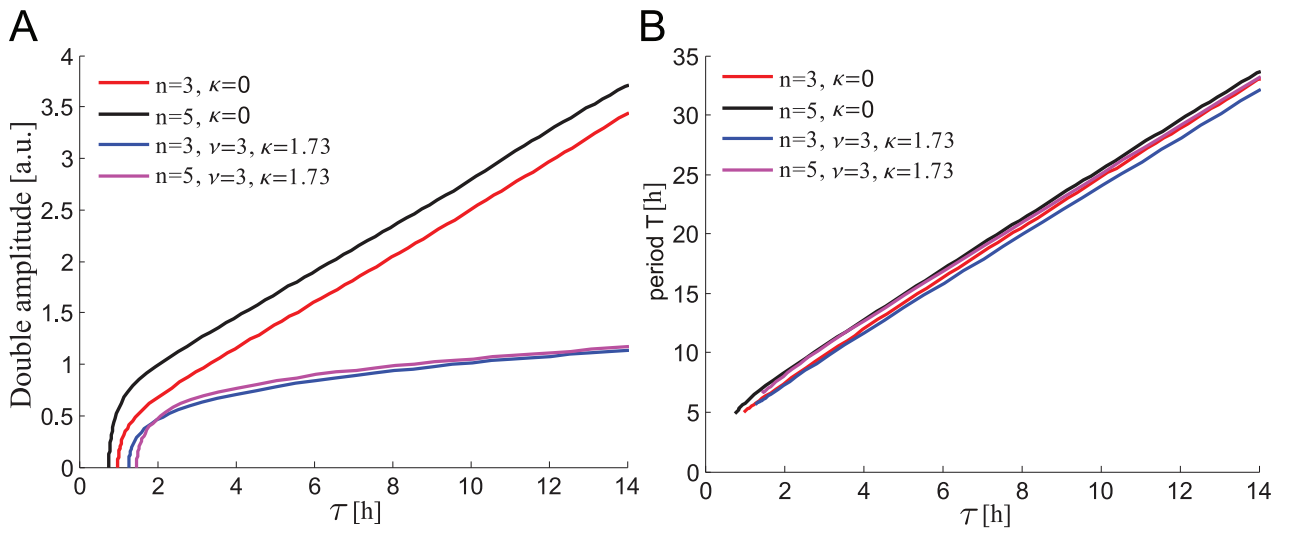
Figure 3.11: Amplitude/period curves of the p53 model under variation of
τ. (A) Dependence between the time delay τ and amplitude of oscillations. (B)
Dependence between the time delay τ and period of oscillations. The analysis
is performed for the p53 model (2.4) without and with synthetically activated
($\nu = 3$, $\kappa = 1.73$) auto-inhibitory feedback using values of the Hill coefficient
$n = 3$ and $n = 5$ (fitted value) of the DNF function $S_2(R)$ (1.10).

3.5 Discussion

In this chapter, I systematically studied design features of systems with delayed negative feedback (DNF), which tune the response patterns of biochemical components. To this end, I analysed models (2.1)-(2.6) containing a DNF differing in several aspects: presence of a nested negative feedback, presence of mass conservation for compounds and mechanism of DNF, i.e., input-inhibition or output-activation (see Fig. 2.1). These models were further subjected to computational and theoretical stability analyses.

I showed that

- nested auto-inhibitory feedback and overall DNF have opposing roles with respect to the characteristic response pattern. Nested auto-inhibitory feedbacks have the potential to suppress oscillatory behaviour, whereas increasing strength of the DNF promotes oscillations. Moreover, in oscillatory systems auto-inhibitory feedbacks de-couple amplitude and period of oscillations.

- mass conservation has a stabilizing effect on the system's equilibrium.

- depending on the parameter set, the type of DNF can also influence the response pattern. I found that input-inhibition can be more stabilizing compared to output-activation.

Thus, biochemical networks have a range of design possibilities shaping both their dynamic as well as their equilibrium properties. My systematic analysis of different design features allows predicting what kind of biochemical network underlies a certain characteristic response. For example, in designing oscillatory systems with a long time delay, it is reasonable to assume a limited number of post-translational modifications (mass conservation), no nested feedbacks and a strong overall negative feedback. Whereas adaptive systems with long time delay are likely to harbour nested negative feedbacks and post-translational modifications. Systems with a low number of components and short time delay that are meant to oscillate, will need an abrupt negative feedback with low activation threshold, whereas short time delay and a weak negative feedback are good design principles for adaptive systems.

My framework of delayed and non-delayed feedbacks can serve to support a design process for novel synthetic gene-regulatory networks. Indeed, my study allows to approximate the value of time delay and the structure of the DNF system for obtaining a certain type of the system dynamics. For example, in the p53 system I specified how a synthetic nested feedback should be designed to dampen p53 oscillations. It has been proposed that p53 oscillations have a physiological role. Thus, controlling such oscillations with a synthetic network may help to better understand their physiological role.

4 Experimental design for regulating a synthetic gene oscillator

4.1 Introduction

Synthetic biology is an engineering discipline, which combines biochemical and biophysical principles present in living organisms to engineer new systems [99, 106, 107]. The basic technique for constructing synthetic gene circuits is assembling DNA sequences with defined combinations of promoters and genes. As a result, the designed network contains prescribed activation and repression interactions [106]. Using special engineering techniques, the circuit can be placed in the living cell, where it is able to acquire the necessary resources to function [106, 107]. For controlling circuit activity one may apply external inputs called inducers. Inducers are small signalling molecules that are able to enter the cell wall after being added to the cell culture. Thus, inducers either activate or inhibit specific transcription factors. This leads to either mediating or blocking the transcription of certain genes [106, 107].

Nowadays, there are two main research directions that motivate scientists to construct and study synthetic networks. First, novel networks are able to perform new tasks and produce new substances [43, 106]. One of successful products of synthetic biology was the large scale production of insulin by utilizing *E. coli* bacteria as a cell factory [107, 108]. Second, synthetic biology enables understanding fundamental design principles of living systems through decoupling a simple network from its native and often complex setting [43, 106]. Applying this approach resulted in constructing fundamental two and three gene circuits including mono-stable [13] and bistable [33] systems. Interestingly, for a long period of time one of the major foci of research groups working in synthetic biology was to construct a circuit whose protein concentrations oscillate periodically in time [106]. As a result, several synthetic gene oscillators were designed and experimentally implemented [10, 27, 99].

Previous study presented an experimental design of a synthetic gene oscillator based on the combination of a positive feedback and a delayed negative feedback (DNF) [99]. This study showed that the time delay in the negative feedback loop is the key principle for inducing robust oscillations in gene networks. In the previous chapter, I showed analytically that the presence of nested negative feedbacks is able to repress oscillations in DNF systems. I wondered if including a nested negative feedback in this system will also result in repressing oscillations of gene products. In this chapter I construct a mathematical model of the synthetic gene oscillator presented in [99]. I parametrize

the model and show that it is able to recapitulate oscillatory dynamics of circuit components. Then, I modify the model by including a nested negative feedback acting through an additional component of the circuit. Using simulations of the resulting model I predict that suggested modifications may control the response pattern of the circuit. Namely, the circuit might be able to switch between sustained and damped oscillations and overdamped response in a controlled manner. Thus, the suggested model together with an experimental implementation of the circuit might become a novel approach for the regulation of the response of biochemical networks containing DNF.

4.2 Mathematical model of synthetic gene oscillator

One of studies [99] described an experimental design of a synthetic gene oscillator. In this section, I present a mathematical model of this synthetic gene oscillator using delay differential equations. The resulting model is fitted to experimental data. This model is further modified by including a nested negative feedback to control the model response.

Firstly, I introduce the original oscillator design. The synthetic gene oscillator was constructed using the bacteria *E. coli.* The network diagram of the circuit is depicted in Fig. 4.1. Briefly, the hybrid promoter consists of the activation operator site from the *araBAD* promoter and repression operator sites from the *lacZYA* promoter. Thus, the hybrid promoter is activated by the AraC protein in the presence of arabinose and repressed by the LacI protein in the absence of isopropyl β-D-1-thio-galactopyranoside (IPTG). Therefore, the addition of arabinose and IPTG to the medium leads to transcription of both genes. Increased production of AraC leads to a positive feedback loop, which increases promoter activity. Increased production of LacI releases the negative feedback inhibited by IPTG. As a result, the negative feedback through LacI decreases promoter activity. Oscillatory behaviour arises as a result of concurrent behaviour of two feedback loops, i.e., positive feedback loop through AraC and delayed negative feedback loop through LacI. For further details about the circuit design refer to [99].
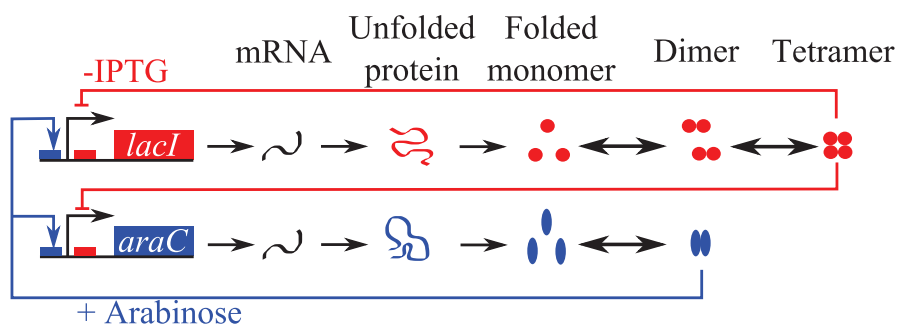

Figure 4.1: Network diagram of the synthetic gene oscillator including formation steps of functional forms of LacI and AraC proteins [99].

Next, I simplify the network diagram of the synthetic gene oscillator presented in Fig. 4.1. Namely, I replace transcription, translation and folding processes preceding formation of the functional form of proteins with time delay needed for their formation. The simplified diagram is presented in Fig. 4.2A. According to [99], transcription and translation of monomeric forms of both proteins AraC and LacI occur at similar rates. However, the functional AraC has a dimeric form, i.e., consists of two monomers, whereas the functional LacI has a tetrameric form, i.e., consists of four monomers (see Fig. 4.1). Hence, the formation of the functional LacI requires two times more monomers than the formation of the functional AraC. Since monomers are produced one by one, more time is required to produce the functional LacI than the functional AraC. This leads to the conclusion that the time delay τ_a needed for the formation of the functional AraC is less than the time delay τ_r needed for the formation of the functional LacI. In this way, negative feedback includes a greater time delay than positive feedback.

I convert the network diagram from Fig. 4.2A into the wiring scheme depicted in Fig. 4.2B. The wiring scheme has the following mathematical formulation by means of deterministic delay differential equations:

$$
\begin{aligned}
\frac{dA}{dt} &= k_0 + k_1 \frac{A(\cdot - \tau_a)^{n_1}}{K_{m1}^{n_1} + A(\cdot - \tau_a)^{n_1}} \cdot \frac{K_{m2}^{n_2}}{K_{m2}^{n_2} + L(\cdot - \tau_r)^{n_2}} - k_2\, A, \\
\frac{dL}{dt} &= k_1 \frac{A(\cdot - \tau_a)^{n_1}}{K_{m1}^{n_1} + A(\cdot - \tau_a)^{n_1}} \cdot \frac{K_{m2}^{n_2}}{K_{m2}^{n_2} + L(\cdot - \tau_r)^{n_2}} - k_2\, L.
\end{aligned}
\tag{4.1}
$$

Here, variables A and L represent abundances of functional proteins AraC and LacI, respectively. The parameter $k_0 > 0$ defines a constant stimulus that activates the gene transcription network. In this case, it corresponds to the sum of arabinose and IPTG concentrations. Parameters $k_1 > 0$ and $k_2 > 0$ mimic protein activation and degradation rates, respectively. Positive and negative feedbacks are modelled by Hill function (1.10) and reverse Hill function (1.9), respectively. Parameters $K_{m1} > 0$
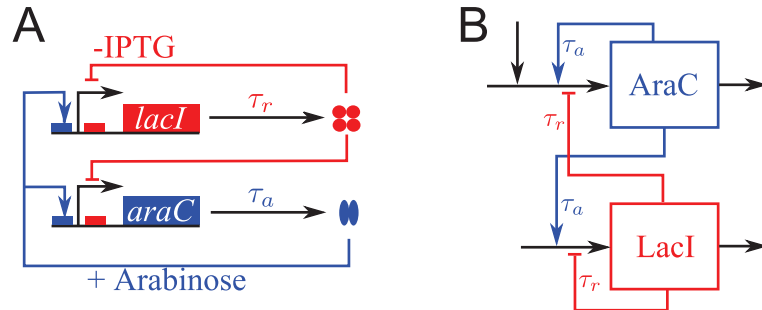

Figure 4.2: Simplified scheme of the synthetic gene oscillator. (A) Network diagram of the synthetic gene oscillator. Processes preceding formation of the functional form of proteins presented in Fig. 4.1 are replaced with the time delay, which is needed for their formation. (B) The wiring scheme of the synthetic gene oscillator.
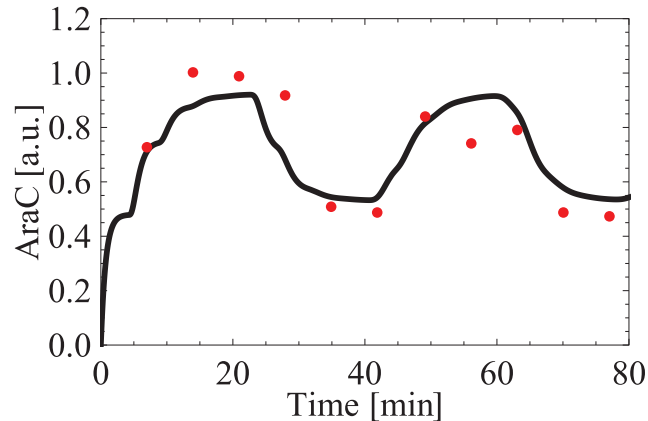
Figure 4.3: Simulation of the synthetic gene oscillator model (4.1)**.** Dots
designate experimental data obtained in the lab of Dr. Katja Bettenbrock from
Max-Planck Institute (Magdeburg). Oscillations were induced with 0.7% arabi-
nose and 2 mM IPTG. The experiment was performed one time according to the
protocol described in [99]. Fitted parameters from Table B.2 are used.

and $K_{m2} > 0$ define half-saturation constants beyond which positive and negative
feedbacks take effect, respectively. Parameters $n_1 \geq 1$ and $n_2 \geq 1$ represent Hill
coefficients defining the steepness of positive and negative feedbacks, respectively.

I fit parameters of the model (4.1) to experimental data obtained in the lab of
Dr. Katja Bettenbrock from Max-Planck Institute (Magdeburg). The experiment was
performed according to the protocol described in [99] with 0.7% arabinose and 2 mM
IPTG. The fitted parameter values are presented in Table B.2. The simulation of the
model (4.1) with fitted parameters is presented in Fig. 4.3. Thus, the parametrized
model (4.1) is able to recapitulate measured dynamics of the synthetic gene oscillator.

In the next section, I will demonstrate how a nested negative feedback may regulate
the characteristic response of this system.

4.3 Regulation of synthetic gene oscillator

In the previous chapter, I developed a theoretical framework showing that nested
negative feedbacks may repress oscillations in biochemical networks containing DNF.
I wondered if activating a nested negative feedback can also repress oscillations in the
synthetic gene oscillator described above. To this end I develop a modification of this
circuit by including a nested negative feedback. Namely, I suggest to add to hybrid
promoters one more repression operator site from the PLtetO1 promoter [27], which is
getting active in the presence of tetracycline. In addition, I suggest to create one more
promoter, which contains only the activation operator site from the *araBAD* promoter
and whose activation leads to the transcription of the *tetR* gene. The modification of
the synthetic gene oscillator from Fig. 4.2 is presented by dashed lines in Fig. 4.4.

Thus, the addition of arabinose and IPTG and the absence of tetracycline bring
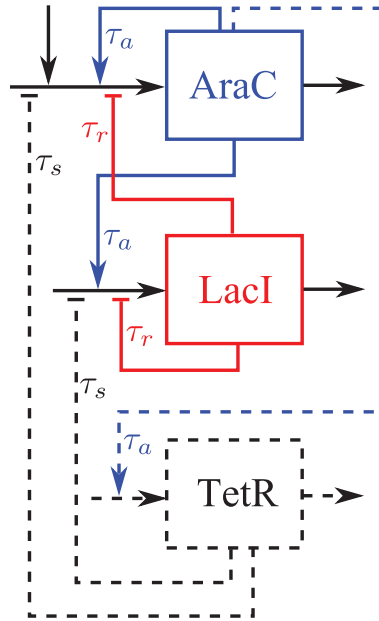
Figure 4.4: The wiring scheme of the modified synthetic gene oscillator.
With solid lines I designate proteins AraC and LacI and interactions, which construct the synthetic gene oscillator described in [99]. With dashed lines I designate an additional protein TetR and protein interactions, which I suggest to include in the system for regulation of oscillations in the synthetic gene oscillator.

the synthetic gene oscillator to the original form, i.e., network produces sustained oscillations of protein concentrations AraC and LacI as it was shown in Fig. 4.3. In the presence of tetracycline the negative feedback from TetR to AraC and LacI is getting active. Similar to the protein AraC, the protein TetR has a dimer functional form, which requires the presence of two monomers [87]. Note that monomers of considered proteins AraC, LacI and TetR are produced at similar rates. Since the formation of the functional TetR requires twice less monomers than the formation of the functional LacI, I may conclude that the production of the functional form for TetR needs less time than for LacI. This means that the negative feedback through TetR occurs faster than the negative feedback through LacI. Therefore, the feedback through TetR can be considered as a nested negative feedback whereas the feedback mediated by LacI can be considered as DNF.

According to the theoretical analysis presented in the previous chapter a nested negative feedback is able to suppress oscillations, which occur in biochemical DNF systems. To test this hypothesis I create a mathematical model of the modified synthetic gene oscillator presented in Fig. 4.4:

$$
\begin{aligned}
\frac{dA}{dt} &= k_0 + k_1 \frac{A(\cdot - \tau_a)^{n_1}}{K_{m1}^{n_1} + A(\cdot - \tau_a)^{n_1}} \cdot \frac{K_{m2}^{n_2}}{K_{m2}^{n_2} + L(\cdot - \tau_r)^{n_2}} \cdot \frac{1}{1 + (\kappa\, T(\cdot - \tau_s))^{\nu}} - k_2\, A, \\
\frac{dL}{dt} &= k_1 \frac{A(\cdot - \tau_a)^{n_1}}{K_{m1}^{n_1} + A(\cdot - \tau_a)^{n_1}} \cdot \frac{K_{m2}^{n_2}}{K_{m2}^{n_2} + L(\cdot - \tau_r)^{n_2}} \cdot \frac{1}{1 + (\kappa\, T(\cdot - \tau_s))^{\nu}} - k_2\, L, \\
\frac{dT}{dt} &= k_1 \frac{A(\cdot - \tau_a)^{n_1}}{K_{m1}^{n_1} + A(\cdot - \tau_a)^{n_1}} - k_3\, T.
\end{aligned}
$$

$$(4.2)$$

The model (4.2) differs from the model (4.1) by the inclusion of the variable T mimicking the concentration of the protein TetR and by the presence of the nested negative feedback through the protein TetR. I assume that the protein TetR has the same activation rate $k_1 > 0$ as AraC and LacI and the degradation rate $k_3 > 0$. The nested negative feedback through TetR is modelled by the reverse Hill function $F(T)$ (3.1) with parameters $\kappa \geq 0$, $\nu \geq 1$. I assume that the nested negative feedback through TetR occurs with time delay $\tau_s > 0$, where the relation $\tau_s < \tau_r$ holds.

I assume that the inclusion of the additional model component TetR does not affect the parameter values k_0, k_1, k_2, K_{m1}, K_{m2}, n_1, n_2, τ_a and τ_r common for the original and modified systems. In the model (4.2), the tetracycline activation of hybrid promoters, which regulate transcription of genes *araC* and *lacI*, acts through the parameter κ. In case tetracycline is absent, κ equals to 0 meaning $F(T) = 1$. As a result, in the absence of tetracycline AraC and LacI have the same dynamics for both models (4.1) and (4.2). Therefore, parameter values k_0, k_1, k_2, K_{m1}, K_{m2}, n_1, n_2, τ_a and τ_r fitted for the original model (4.1) are also valid for the modified model (4.2) (see Table B.2).

Further, I check how the nested negative feedback $F(T)$ with parameters κ, ν and τ_s and the degradation rate of the protein TetR, i.e., k_3, influence the dynamics of the model (4.2). For this I select some random parameter values $\kappa = 2$, $\nu = 2$ and $k_3 = 1.5$. As the value of time delay I select a random value $\tau_s = 1$ with the condition $\tau_s < \tau_r$. Then I vary each of these parameters in a certain range leaving the rest of the parameter values fixed. For obtained parameter sets I simulate the model (4.2) and depict the dynamics of AraC in Fig. 4.5. The colour of the simulation is turning from red to blue with the increasing parameter value.

Fig. 4.5 shows that increasing κ as well as decreasing ν and k_3 suppresses oscillations of the protein AraC. Fig. 4.5C demonstrates that the model (4.2) shows a low sensitivity with respect to the change in the time delay τ_s. Additionally, the variation of parameter values κ, ν and k_3 changes only the amplitude of oscillations leaving the period of oscillations unchanged.

Then, I show how the response of the model (4.2) can be regulated through the nested negative feedback using the parameter κ as a control. Recall that the positivity of κ indicates the presence of tetracycline in the system. Increasing κ suppresses oscillations of the model (4.2) (see Fig. 4.5A). Thus, my model (4.2) predicts the
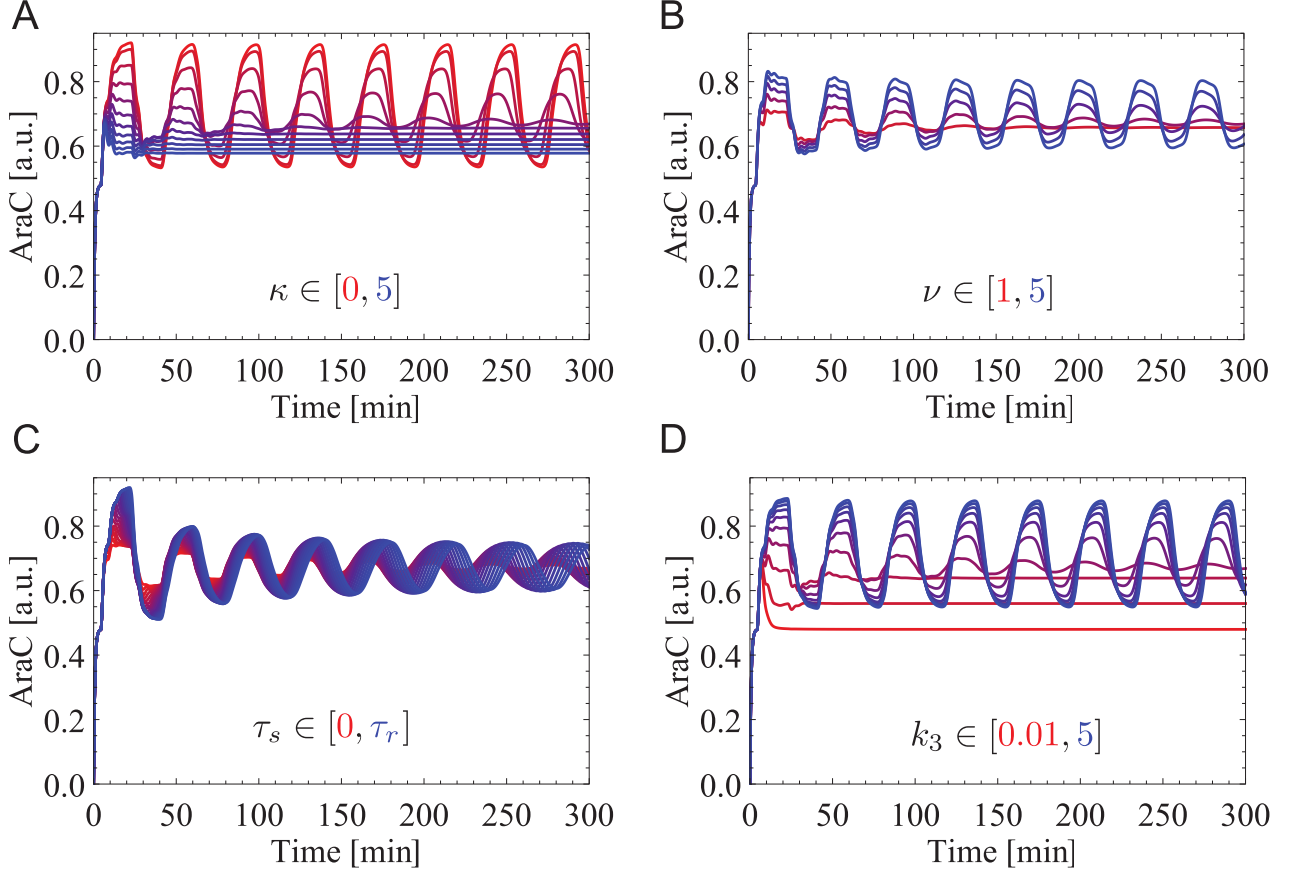
Figure 4.5: Simulations of the model (4.2) **with varied parameters.** Parameter values k_0, k_1, k_2, k_3, n_1, n_2, K_{m1}, K_{m2}, τ_a, τ_r are adopted from Table B.2. Parameter values $\kappa = 2$, $\nu = 2$, $\tau_s = 1$ and $k_3 = 1.5$ are chosen randomly. Then each of the parameters κ, ν, τ_s, k_3 is varied in the range $[0, 5]$, $[1, 5]$, $[0, \tau_a]$, $[0.01, 5]$, respectively, leaving the rest of the parameter values fixed. The model (4.2) is simulated for each obtained parameter set under variation of κ (A), ν (B), τ_s (C), k_3 (D). The colour of the simulation is turning from red to blue with increasing parameter value.

following response of the modified synthetic gene oscillator presented in Fig. 4.4 under the variation of κ (see Fig. 4.6):

- sustained oscillations for $\kappa = 0$ for $t \in [0, 200]$,

- damped oscillations for $\kappa = 2$ for $t \in [200, 400]$,

- sustained oscillations for $\kappa = 0$ for $t \in [400, 600]$,

- constant response for $\kappa = 4$ for $t \in [600, 800]$,

- sustained oscillations for $\kappa = 0$ for $t \in [800, 1000]$.

For simulations shown in Fig. 4.6 I use parameter values k_0, k_1, k_2, k_3, n_1, n_2, K_{m1}, K_{m2}, τ_a, τ_r adopted from Table B.2. Parameter values $\nu = 2$, $\tau_s = 1$ and $k_3 = 1.5$ are chosen randomly.
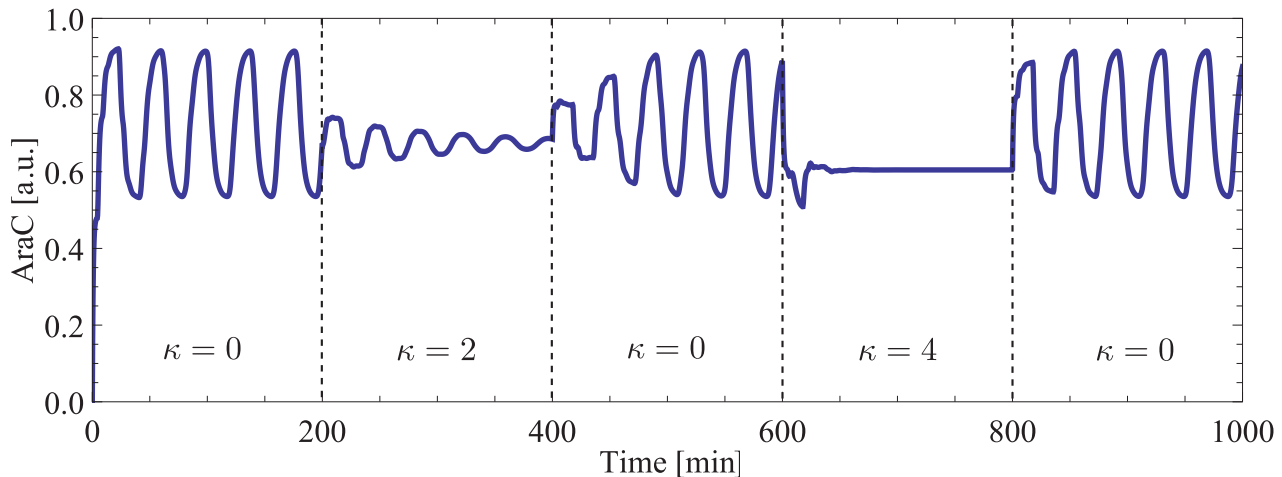
Figure 4.6: Simulations of the model (4.2) **with varied parameter κ during the simulation time.** For $t \in [0, 200]$ $\kappa = 0$ is used, for $t \in [200, 400]$ $\kappa = 2$ is used, for $t \in [400, 600]$ $\kappa = 0$ is used, for $t \in [600, 800]$ $\kappa = 4$ is used, for $t \in [800, 1000]$ $\kappa = 0$ is used. Parameter values k_0, k_1, k_2, k_3, n_1, n_2, K_{m1}, K_{m2}, τ_a, τ_r are adopted from Table B.2. Parameter values $\nu = 2$, $\tau_s = 1$ and $k_3 = 1.5$ are chosen randomly.

To summarize, I showed that including the nested negative feedback through the protein TetR in the presence of tetracycline may suppress oscillations of proteins AraC and LacI in the synthetic oscillating AraC-LacI system. In absence of tetracycline the modified AraC-LacI system is supposed to demonstrate the same response as the original one presented in [99].

4.4 Discussion

Synthetic genetic systems facilitate our understanding of cellular processes and assist us in studying system design principles [10]. For example, the analysis of the synthetic gene oscillator presented in [99] showed that a negative feedback loop in combination with time delay is the key design principle for constructing a robust oscillator. My theoretical study of delayed negative feedback (DNF) systems indicated that the presence of nested negative feedbacks in the system is able to suppress oscillatory behaviour of biochemical compounds. In order to confirm the derived theory experimentally, I suggested a modification of the mentioned synthetic gene oscillator by including a nested negative feedback acting through the additional component TetR (see Fig. 4.2).

In the modified circuit, I suggested to add to the hybrid promoter, which regulates the transcription of genes *lacI* and *araC*, one more, third, operator site from the PLtetO1 promoter. Up to now the technique of combining three operator sites for one promoter was not well established and caused a high level of noise in the gene expression [4, 46, 77]. However, a recent study [4] presented a construction of synthetic regulatory elements for the simultaneous recognition of three transcriptional

factors with the successful application in *E. coli*. This construction can be used for the experimental implementation of the modified circuit.

Further, I created a mathematical model of the modified synthetic gene oscillator. As a nested negative feedback function I used a reverse Hill function (3.1) with the Hill coefficient ν and with the transformed half-saturation constant κ. Then I analysed the dependence between the model dynamics and parameter values of the nested negative feedback. The analysis showed that damped oscillations of one of the model components turn into sustained oscillations with increasing ν (see Fig. 4.5B). This observation does not correspond well to my theoretical analysis presented in Section 3.3. There I proved that one may stabilize the equilibrium of a DNF model through increasing the slope of the nested negative feedback. For the reverse Hill function, an obvious choice to increase the slope is increasing the Hill coefficient ν. However, for this model the nested negative feedback suppresses oscillations rather through increasing κ than through increasing ν (see Fig. 4.5). This inconsistency can be explained by differences between the structure of generic models, which were subjected to the theoretical stability analysis, and the structure of the model, which was created for the modified synthetic gene oscillator.

Finally, simulations of the model with the nested negative feedback showed that the oscillatory dynamics of model components can firstly be damped and then turned into a constant by increasing κ (see Fig. 4.5A and Fig. 4.6). In order to verify this prediction the experimental implementation of the control for the half-saturation rate of the nested negative feedback is needed. Using this control one may induce various response patterns of the modified synthetic gene oscillator including sustained and damped oscillations and an overdamped response.

5 Approximation of DDEs by ODEs

5.1 Introduction

A system of delay differential equations (DDEs) is an obvious mathematical tool to model biochemical systems containing delayed negative feedback (DNF). Numerous theoretical approaches were developed for analysing systems of this kind [14, 21, 25, 28, 95]. However, the theoretical analysis of delay differential equations rapidly becomes complicated when including more and more details into the model [74]. In this case, DDE software packages might be helpful for numerical analysis of DDE systems [28]. However, the availability of the software for the computational analysis of DDEs is limited in comparison with the availability of the software for the analysis of ordinary differential equations (ODEs) [74]. In this context, the approximation of DDEs with a system of ODEs can be useful.

Various DDE approximation techniques were developed. One of them is the Padé approximation, which is based on Padé approximants represented by rational functions [11, 60]. The alternative approximation technique is based on Taylor series approximation of the delay term [47, 74]. Although both techniques work well for systems with small time delays, they do not preserve stability properties of delay differential equations [47, 74]. One more approximation technique is applicable for systems possessing Morse decomposition [34]. One of studies on approximation of delays in biochemical systems found this approximation method to be the most useful [74].

In this chapter, I describe the approximation method presented in [34, 74, 95] for DDE systems possessing Morse decomposition. Then I apply this technique to approximate adaptive HOG (2.2) and oscillating p53 (2.4) systems with DNFs introduced in previous chapters. I compare the error of approximation of these systems and investigate factors influencing the approximation quality. In this chapter, I designate DDE models as models with "discrete" time delay and approximated ODE models as models with "continious" time delay.

5.2 Approximation technique

Using special techniques allows approximation of a DDE system by the system of ODEs [34, 74]. Here, I describe an algorithm adopted from [34, 95] showing how to approximate a system of DDEs, which possesses a Morse decomposition, with a system
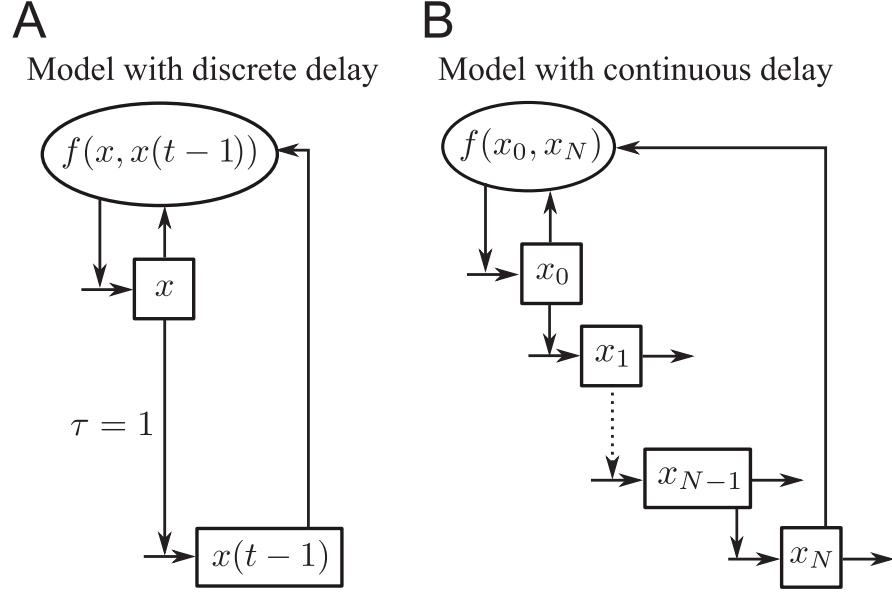
Figure 5.1: Wiring schemes of systems with delay. (A) The wiring scheme of the system (5.1) with discrete time delay. (B) The wiring scheme of the system (5.2) with continuous time delay.

of ODEs.

First, I introduce the following delay problem with the wiring scheme presented in Fig. 5.1A:

$$\begin{aligned} \frac{dx}{dt} &= f(x(t), x(t-1)), \\ x(t) &= \phi(t),\ t \in [-1, 0], \end{aligned} \tag{5.1}$$

where $f\colon \mathbb{R}^2 \to \mathbb{R}$ is C^∞ and represents a negative feedback function. The set of all bounded solutions of (5.1) is denoted as $\hat{A}_\infty \in C((-\infty, \infty), \mathbb{R})$. Thus, if $\hat{x} \in \hat{A}_\infty$, then $\phi := \hat{x}|_{[-1,0]} \in \hat{A}_\infty$ and $\hat{x}$ is the solution through initial condition ϕ.

I assume that the problem (5.1) admits a Morse decomposition. Morse decomposition is constituted by Morse sets. For the definition of Morse sets for the system (5.1) the study [71] introduced a discrete Lyapunov function on $\hat{A}_\infty$, i.e., $V : C((-\infty, \infty), \mathbb{R}) \to \mathbb{N}$, in the following way. Define $\sigma := \inf\{t \geq 0 : \hat{x}(t) = 0\}$ if it exists. Then, if σ exists, the function $V(\hat{x})$ is defined to be the number of zeroes, which counts the multiplicity of $\hat{x}$ in the interval $(\sigma - 1, \sigma]$. Otherwise, the function is defined as $V(\hat{x}) = 1$. The Morse sets for the system (5.1) will be sets in $\hat{A}_\infty$ on which the Lyapunov function is constant [34].

Now, I introduce a time discretization of the problem (5.1) presented in [34]. First, a positive integer N is fixed and used for the following annotation:

$$x_i(t) = x\left(t - \frac{i}{N}\right),\ \text{where}\ i = 0, 1, 2, \ldots, N.$$

Here, I designate $x_0(t) = x(t)$ and $x_N(t) = x(t-1)$.

Further, $\dfrac{dx_i}{dt}$ is represented using the definition of the derivative at the time point t:

$$\frac{dx_i}{dt} \approx \frac{x_i\left(t + \dfrac{1}{N}\right) - x_i(t)}{\dfrac{1}{N}} = N(x_{i-1}(t) - x_i(t)) \text{ for } t > \frac{i}{N}.$$

Thus, according to [34] the delay differential equation (5.1) can be approximated by the following system of $N + 1$ ODEs, which is depicted in Fig. 5.1B:

$$\begin{aligned}
\frac{dx_0}{dt} &= f(x_0(t), x_N(t)), \\
\frac{dx_i}{dt} &= N(x_{i-1}(t) - x_i(t)), \; i = 1, 2, \ldots, N, \\
x_i(0) &= \phi\left(-\frac{i}{N}\right), \; i = 0, 1, \ldots, N.
\end{aligned} \tag{5.2}$$

This conclusion is based on the fact that if $\{S_k{}^n\}_{k=1}^{N_\infty}$ are Morse sets for (5.1) and $\{S_k{}^n\}_{k=1}^{N_n}$ are Morse sets for (5.2), then, under certain assumptions, for any $\varepsilon > 0$, there exists N so that for all $n > N$, $S_k{}^n$ is in an ε-neighbourhood of $S_k{}^\infty$ for all $1 \leq k \leq N_\infty$ [34]. In other words, there exists N such that for all $n > N$ the solution of the continuous model (5.2) will converge to the solution of the discrete model for (5.1). For more details about this approximation technique refer to [34, 71].

5.3 Approximation of HOG and p53 models

In this section, I approximate HOG model (2.2) and p53 model (2.4) with discrete time delay by ordinary differential equations using the approximation approach presented in the section above.

First, I scale the time of the HOG model (2.2)

$$\begin{aligned}
\frac{dC}{dt} &= \tau\left(\mu\, S_1(I, R)(1 - C)\, F(C) - \alpha\, C\right), \\
\frac{dR}{dt} &= \tau\left(\eta\, C(\cdot - 1) - \beta\, R\right),
\end{aligned} \tag{5.3}$$

and p53 model (2.4)

$$\begin{aligned}
\frac{dC}{dt} &= \tau\left(I - \alpha\, C - \delta\, C\, S_2(R)\right), \\
\frac{dR}{dt} &= \tau\left(C(\cdot - 1) - \beta\, R\right).
\end{aligned} \tag{5.4}$$

to get time delay of both systems equal to 1.

Further, using the approach (5.2) I approximate the HOG model (5.3) by the system

of ODEs:

$$\frac{dC_0}{dt} = \tau \left(\mu \, S_1(I, R)(1 - C_0) \, F(C_0) - \alpha \, C_0 \right),$$
$$\frac{dC_i}{dt} = N \left(C_{i-1} - C_i \right), \, i = 1, 2, \ldots, N, \tag{5.5}$$
$$\frac{dR}{dt} = \tau \left(\eta \, C_N - \beta \, R \right),$$

and the p53 model (5.4) by the system of ODEs:

$$\frac{dC_0}{dt} = \tau (I - \alpha \, C_0 - \delta \, C_0 \, S_2(R)),$$
$$\frac{dC_i}{dt} = N \left(C_{i-1} - C_i \right), \, i = 1, 2, \ldots, N, \tag{5.6}$$
$$\frac{dR}{dt} = \tau (C_N - \beta \, R),$$

where N is some fixed positive integer number.

In Fig. 5.2A and B I demonstrate simulations of the component C of the HOG model (5.3) and p53 model (5.4), respectively, using black dashed lines. Here, for the HOG model I use $I = 0.4$ M as the representative stimulus level. Fig. 5.2A and B also present simulations of the component C_0 of approximated HOG model (5.5) and p53 model (5.6), respectively, for $N = 1, \ldots, 25$. With increasing N the colour of the simulation is turning from red to blue. For all models I use parameters from Table B.1. One may see that for the HOG model (see Fig. 5.2A) there is no significant difference between simulations of the model with discrete delay and the approximated model for all considered values of N. In comparison, for the p53 model (see Fig. 5.2B) the simulation of the component C_0 is approaching the simulation of the model component C of the p53 model (5.4) with increasing N.

Further, I calculate the error of approximation of DDE models by ODE models. For this I simulate the component C of HOG and p53 models with discrete time delay and the component C_0 of approximated HOG and p53 models for $N = 1, \ldots, 50$ for the time frame $[0, 25]$. Then I discretize the time frame $[0, 25]$ with the step equal to 0.33. At each obtained time point I calculate the absolute difference between values of the component C of the model with discrete time delay and the component C_0 of the approximated model. The obtained differences are summarized for all time points and depicted in Fig. 5.3. Analysing the error of approximation presented in Fig. 5.3 I may conclude that the approximation quality mainly depends on two factors:

- the number of auxiliary components. One may see that the higher the value of N, the lower the approximation error. Interestingly, for both HOG and p53 models the approximation error is rapidly decreasing for $N \in [1, 25]$ and stays constantly low for $N > 25$.

- the stability of the equilibrium of the model to be approximated with respect
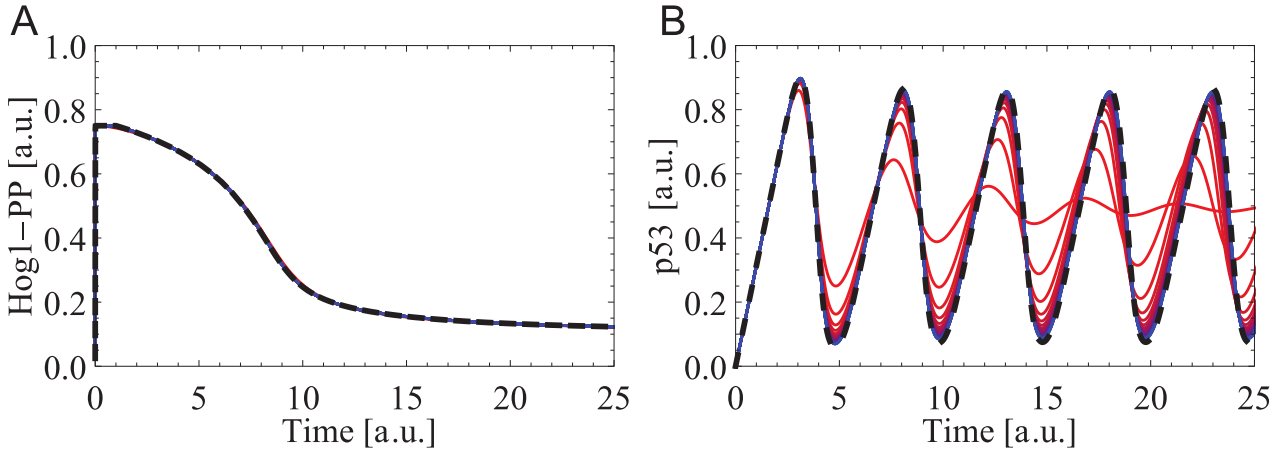
Figure 5.2: Approximation of the HOG model (5.3) **and p53 model** (5.4) **by ODEs.** (A) Simulation of the component C of the HOG model (5.3) and component C_0 of the approximated HOG model (5.5) for $I = 0.4$ M. (B) Simulation of the component C of the p53 model (5.4) and component C_0 of the approximated p53 model (5.6). I designate the simulation of the component C of models with discrete delay by black dashed lines. Approximated models are simulated for $N = 1, \ldots, 25$. With increasing N the colour of the simulated component C_0 is turning from red to blue. For simulations I use parameters from Table B.1.

to time delay. Indeed, the equilibrium of the HOG model (5.3) with parameters from Table B.1 and $I = 0.4$ M is asymptotically stable since $\tau = 3.58\,\text{min} \ll \tau_m = 113.5$ min holds. In comparison, the equilibrium of the p53 model (5.4) is unstable since $\tau = 1.37 > \tau_m = 0.76$ holds. For calculation of τ_m refer to Section 2.3.4. As a result, the approximation error for the HOG model is about 100 times less than the approximation error for the p53 model for $N = 1$ and stays less for all considered N.
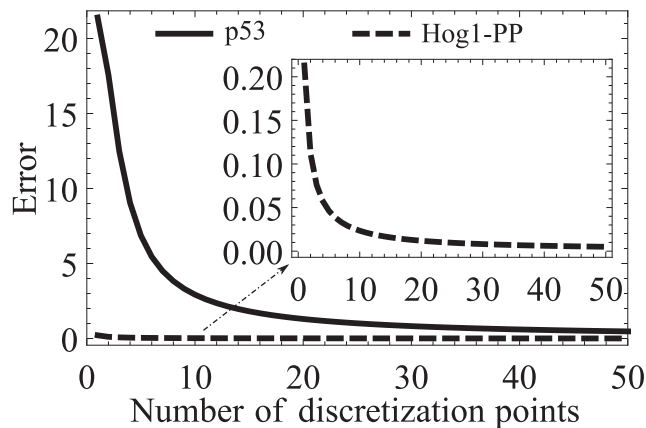

Figure 5.3: Errors of approximation of HOG and p53 models with discrete time delay. The error of approximation of the HOG model (5.3) and p53 model (5.4) with discrete time delay by the HOG model (5.5) and p53 model (5.6), respectively, for $N = 1, \ldots, 50$.

Finally, I compare the influence of parameter values of models with discrete and continuous time delay on the stability of the model equilibrium. I consider the p53 model with parameters from Table B.1 as the representative model for this analysis. In Fig. 5.4A-C I demonstrate the dependence between parameter values τ, I, K_m and the maximum real part of eigenvalues $\max(Re(\lambda_i))$ of the p53 model (5.4) with the discrete time delay and of the p53 model (5.6) with the continuous time delay, respectively.

Fig. 5.4A shows that for both models with discrete and continuous time delay $\max(Re(\lambda_i))$ increases with τ. For the model with discrete time delay $\max(Re(\lambda_i))$ equals to 0 at $\tau = \tau_m$ (see black dot). For the model with continuous time delay $\max(Re(\lambda_i))$ equals to 0 at values of τ, which are greater than τ_m and which decrease and approach τ_m from the right with increasing N.

In Fig. 5.4B and C I demonstrate the dependence between parameter values I and $\max(Re(\lambda_i))$ and K_m and $\max(Re(\lambda_i))$, respectively, for the p53 model with discrete time delay and p53 model with continuous time delay for $N = 25$. One may see that for both models with discrete and continuous time delay $\max(Re(\lambda_i))$ is increasing with I and decreasing with K_m. Moreover, for $N = 25$ there is no significant difference between values of $\max(Re(\lambda_i))$ calculated for models with discrete and continuous time delay, respectively.

Thus, I may conclude that the presented technique fits well for approximating a system of DDEs by a system of ODEs. The approximation quality depends on the number of used intermediate steps and the stability of the equilibrium of the model to be approximated.
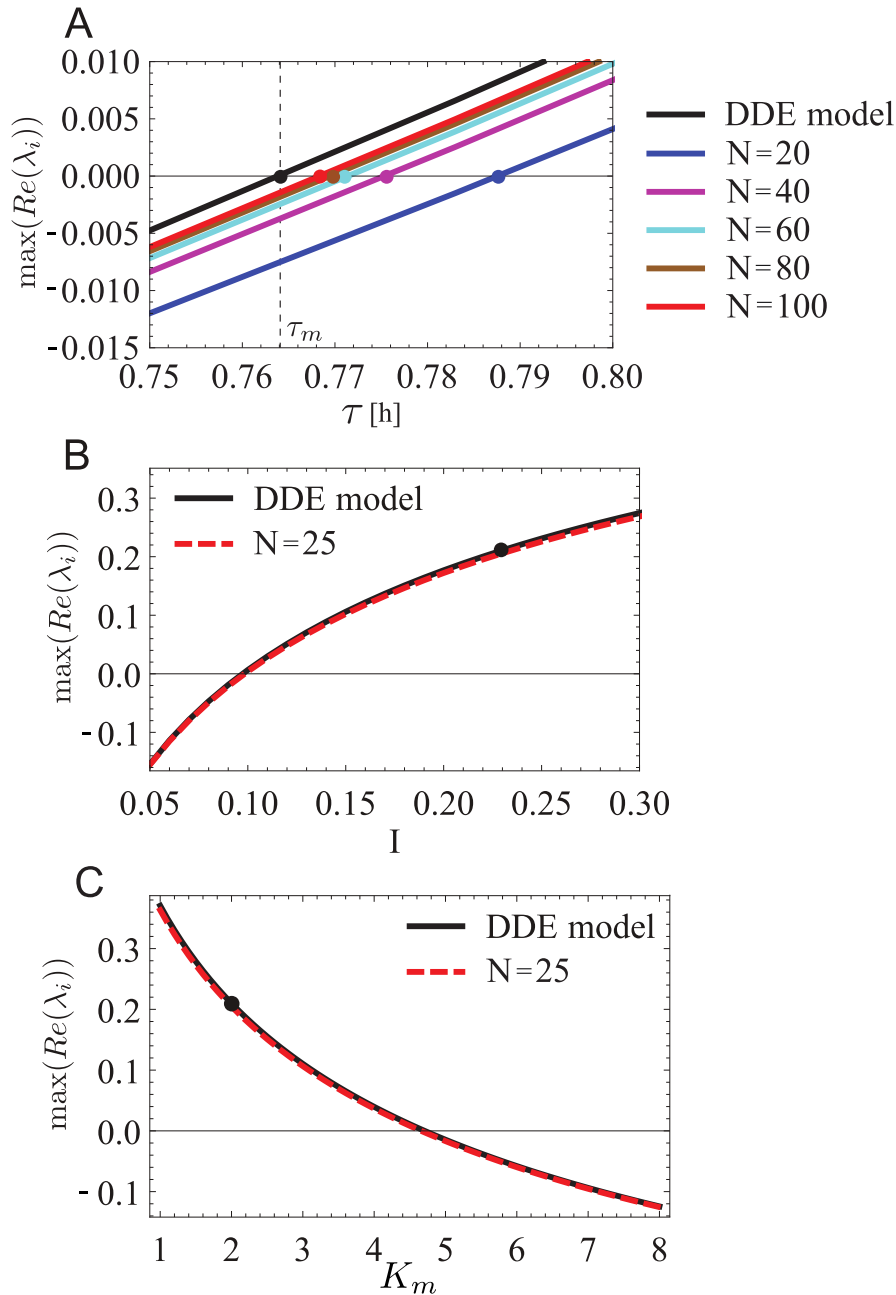
Figure 5.4: Influence of parameter values of p53 models with discrete (5.4) **and continuous** (5.6) **time delay on the stability of the model equilibrium.** (A) Dependence between time delay τ and $\max(Re(\lambda_i))$. For approximation the number of steps $N = 20, 40, 60, 80, 100$ are used. With the dashed line and black dot I designate the position of the marginal time delay τ_m of the p53 model (5.4). (B) Dependence between the stimulus level I and $\max(Re(\lambda_i))$. (C) Dependence between the parameter value K_m and $\max(Re(\lambda_i))$. For approximation in (B) and (C) the number of steps $N = 25$ are used. With $\max(Re(\lambda_i))$ I designate the maximum real part of eigenvalues $\max(Re(\lambda_i))$ of the p53 model with discrete and continuous time delay.

5.4 Discussion

Separation of time scales when modelling biochemical systems with delayed negative feedbacks (DNFs) is important for distinguishing between fast signal transduction processes and slow transcription, translation and translocation processes [74]. The time delay between sensing the stimulus and feeding back into the system can be explicitly included in the mathematical model by means of delay differential equations (DDEs) [21]. However, both theoretical and computational analyses of DDEs differ from the common widely used analysis of ordinary differential equations (ODEs). This makes modelling by DDEs complicated and unattractive.

In this chapter, I considered a technique for the approximation of DDE systems by ODEs through introducing auxiliary variables [95]. One of the advantages of this technique is its feasible biological interpretation. Thus, the auxiliary model components can be viewed as a signalling cascade presenting intermediate products of transcription, translation and formation processes preceding the formation of the system's response (see Fig. 5.1).

I applied this technique to approximate adaptive HOG model (2.2) and oscillating p53 model (2.4) both containing DNF. Using numerical analysis of HOG and p53 models with discrete and continuous time delays I concluded that the quality of approximation depends on two features:

- the number of auxiliary variables,

- the stability of the equilibrium of the DDE model to be approximated.

Further, I performed the stability analysis of p53 models with discrete and continuous time delays with respect to several parameters including time delay τ. The analysis showed that the threshold value of τ for the approximated model approaches the marginal value of time delay τ_m for the DDE model from the right with increasing number of auxiliary variables. I called these values of τ "approximated τ_m". Thus, as it was mentioned in [74] the absolute difference between τ_m and approximated τ_m can be an alternative measurement for the quality of approximation of the model with discrete time delay by the model with continuous time delay with a certain number of auxiliary steps.

Thus, I may conclude that applying the considered approximation technique allows the approximation of DNF systems modelled by DDEs by means of ODEs. This allows the application of the mathematical theory and computational software, originally developed for analysis of ODE systems, to the approximated system. The approximation quality can be regulated by the number of auxiliary steps.

6 Summary

6.1 Conclusions

Complex intracellular networks are formed from a small set of building blocks called network motifs. It is believed that understanding the dynamics of network motifs can provide insight into the dynamics of the entire network.

A very common network motif is a negative feedback loop. Negative feedback occurs when the output of the network, i.e., response, negatively influences the input. Often negative feedback operates in conjunction with time delay. Time delay happens due to the time needed to transduce a signal or to transcribe biochemical information into concentrations of relevant compounds. Delayed negative feedback (DNF) may cause adaptive as well as oscillatory behaviour of network components.

In this thesis, I considered time delay as a mechanism deciding on the response type of DNF systems, i.e., adaptive or oscillatory. Additionally, I investigated the ability of a range of network design features to suppress unwanted oscillations arising in DNFs. To approach time delay explicitly I applied mathematical modelling of DNF systems by means of delay differential equations (DDEs).

To generalise my research, I constructed mathematical models of several alternative DNF systems (Models 1-6 in Section 2.2). These alternatives differed in the type of DNF, i.e., input-inhibition and output-activation, and in the presence of signalling components, i.e., without mass conservation or with mass conservation for one or two network components. These models were further subjected to mathematical analysis. For all considered model structures I derived explicit formulas and criteria how model parameters determine characteristic response patterns like overdamped behaviour, critical damping, damped or sustained oscillations.

Performed theoretical research was further applied to study the role of time delay in concrete intracellular stress-response systems. Namely, I modelled the adaptive HOG system in yeast and the oscillating NF-κB system in mammals. For the HOG model I numerically calculated a value of time delay, which minimizes the adaptation time to osmotic stress. The obtained value appeared to be close to the actual time delay in the HOG system. Therefore, I concluded that the time delay in the HOG system serves to minimize the adaptation time to osmotic stress. This feature of the HOG system was called optimal adaptation. The analysis of the NF-κB model showed that the time delay in the NF-κB system is close to the bifurcation threshold. It means that the NF-κB system is able to demonstrate both damped and sustained oscillatory responses upon small changes in the value of time delay. Thus, by controlling the time

delay the cell may tune fate decisions.

The systematic study of design features of DNF systems showed that nested auto-inhibitory and delayed negative feedbacks act in an opposite way with respect to the response pattern of the system. Namely, nested auto-inhibitory feedbacks have the potential to suppress oscillations, whereas increasing the strength of the DNF promotes oscillations. In contrast to ODEs [80, 92], it is the steepness of the nested negative feedback that shapes response patterns rather than its strength. This discovery was further applied to design a synthetic nested negative feedback, which may dampen oscillations in the mammalian p53 system. It was proposed that oscillations in the p53 system have a physiological role. Implementing synthetic auto-inhibitory feedback may control oscillations in the p53 system and help to better understand their physiological role. By the example of the p53 system I also showed numerically that both period and amplitude of oscillations increase with increasing time delay. However, in comparison with the DNF, the auto-inhibitory feedback may decouple the increase of amplitude and period with respect to time delay.

Using Monte-Carlo analysis I demonstrated that mass conservation has a stabilizing effect on the system's equilibrium. In addition, depending on the parameter set input-inhibition has a higher potential to suppress oscillations than output-activation. Thus, the analysis of considered design features allows the prediction of a characteristic response of a concrete DNF system. In particular, this information is useful for designing novel synthetic gene-regulatory networks.

As a result, I suggested a design of a synthetic network, which may switch between sustained and damped oscillations and overdamped response in a controlled manner. For this I considered the existing synthetic gene-regulatory network containing DNF and producing artificial sustained oscillations in bacteria [99]. Then, I constructed a mathematical model of this system and fitted to experimental data. I modified the model by including a nested negative feedback through the additional network component. The numerical analysis of the modified system indicated that the nested negative feedback may suppress sustained oscillations of network compounds resulting in a damped oscillatory or an overdamped response.

Finally, I analysed an approach on how to approximate DDEs by introducing auxiliary variables described by ordinary differential equations (ODEs) [34]. The approximation of DDEs by ODEs has several advantages. Namely, for analysing ODEs the investigator can apply common well-developed theory. In addition, there exist various available computational packages for simulating ODEs and performing numerical analysis. Additionally, this technique has a feasible biological interpretation. Indeed, auxiliary variables can be considered as a signalling cascade presenting processes, which precede the formation of the system's response, e.g., transport, transcription, translation, etc. I applied this method to approximate DDE models of the HOG and the p53 system. As a result, I concluded that the quality of approximation depends on the number of intermediate variables and the stability of the equilibrium of the model

to be approximated.

Taken together, mathematical modelling is a powerful tool for revealing and analysing new mechanisms in functioning biological systems. Indeed, constructing generic models of DNFs allowed a deeper understanding of how the system's response depends on time delay and on network design features. Additionally, mathematical modelling assisted in designing a novel synthetic network, which may switch the response type in a controlled manner.

6.2 Outlook

In this thesis, I investigated the role of time delay in biochemical systems containing delayed negative feedbacks (DNFs). Using my theoretical framework I showed that time delay in the high osmolarity glycerol pathway in yeast minimizes the adaptation time to osmotic stress. It would be interesting to see whether this feature of optimal adaptation also applies to other adaptive biochemical networks.

In addition, I checked if a range of network design features are able to suppress oscillations arising in DNF systems. Performed computational analysis of these systems indicated that input-inhibition as a feedback mechanism can be more stabilizing than output-activation. The rigorous theoretical stability analysis of DNF models with respect to the kind of feedback mechanism could verify this hypothesis.

In comparison, I theoretically proved that nested auto-inhibitory feedbacks are able to suppress oscillatory behaviour of DNF sytems. Using this inference I designed a nested negative feedback to suppress oscillations in the mammalian p53 system. Simulations of the modified p53 model showed that nested auto-inhibitory feedback can decouple the amplitude and period of oscillations. Experimental validation is needed to prove this ability of the nested auto-inhibitory feedback.

Based on derived theoretical results, I suggested a modification of the synthetic oscillatory network presented in [99] by including a nested negative feedback. According to performed simulations the modified system may switch between sustained and damped oscillations and overdamped response in a controlled manner. The experimental implementation of the modified synthetic circuit could confirm this behaviour. For creating the modified synthetic circuit I suggest to use the experimetal technique of combining three operator sites for one promoter presented in [4]. Also it could be an interesting problem for the future research to derive a criterion for DNF models with a different architecture showing in which case half-saturation rate or steepness of the nested feedback control the stability of the model equilibrium.

Finally, I presented an approximation approach of delay differential equations (DDEs) by means of ordinary differential equations (ODEs). It would be useful to derive a mathematical relation for the stability of equilibria of initial DDE and approximating ODE models. In [21] it was shown that both DDE and approximating

ODE Goodwin's models have the same necessary condition for producing sustained oscillations of model components. Deriving the common sufficient condition could be helpful to understand the connection between stability properties of DDEs and ODEs.

A Materials and methods

Used experimental data

I used the following data to parametrize and analyse concrete cellular systems:

- for the HOG pathway I took data from [69] as described in [92]. The dataset consists of time series of phosphorylated Hog1 under several hyper-osmotic shock conditions for wild-type yeast and different mutants for up to 2 h after hyper-osmotic shock.

- the dataset that I used to parametrize NF-κB model was digitized from the supplementary material of [44] from Fig. S1. It shows the oscillatory profile of nuclear NF-κB over time up to 6 hours in IκBβ-/- IκBϵ-/- mice fibroblasts in response to TNF-α stimulation.

- the dataset used for the parametrization of the p53 model was digitized from the supplementary material of [36] from Fig. S6 as described in [92]. It represents an averaged oscillation pattern that was meant to resemble an idealized undamped oscillation with peak characteristics that correspond to the average peak characteristics of oscillating cells.

- experimental data of the synthetic gene oscillator were obtained in the lab of Dr. Katja Bettenbrock (Max-Planck Institute, Magdeburg). JS011 cells were cultured in LB0 with Kanamycin and Ampicillin. A single colony was taken and inoculated into LB0 with Ampicillin and Kanamycin and cultured overnight. This overnight culture was diluted to an OD600 of about 0.05 into fresh medium again with antibiotics. Cells were incubated at 37°C for about 3 hours and then 2mM IPTG and 0.7% arabinose were added. At the indicated time points samples were taken and green fluorescent protein (GFP) production was stopped by addition of chloramphenicol. Samples were analysed immediately by flow cytometry on a Partec CyFlow Space. The experiment was performed one time.

Model simulation and analysis

All simulations of the delay differential equations were carried out in Mathematica 9 using the function *NDSolve* based on the method of steps. I used DDE-BIFTOOL v. 2.00 [28] and MATLAB R2008b to calculate dependencies between the value of time delay τ and amplitude and period of oscillations of the p53 model. Monte-Carlo analysis was performed in Mathematica 9.

Robustness of optimal solutions of the HOG model, NF-κB model and p53 model.

I analyzed the robustness of the optimal solutions for the HOG model, the NF-κB and p53 model with respect to noise. To this end, I randomly sampled parameter values within $\pm10\%$ of their respective fitted values using a uniform distribution for 100 times. Then I simulated considered models with perturbed parameters and calculated 0.05 and 0.95 quantiles of obtained simulations (see *gray regions* in Fig. A.1). Fig. A.1 shows that the model solutions with fitted parameters are located between 0.05 and 0.95 quantiles for all considered time points.

Further, for each model and each perturbed parameter set I calculated the relative variation of the integral of the first transient response after the stimulation:

$$var_i = \frac{\left| \int_0^{t_{Int}} C(t)dt - \int_0^{t_{Int}} C_p^i(t)dt \right|}{\int_0^{t_{Int}} C(t)dt} \cdot 100\%,$$

where $C(t)$ corresponds to the model solution with fitted parameters, $C_p^i(t)$ corresponds to the model solution with i^{th} perturbed parameter set ($i = 1, 2, 3, ..., 100$). For the HOG model t_{Int} corresponds to the time point, where the Hog1 activation decreases to 50% of its maximum (see Fig. A.1A). For the NF-κB and the p53 system, t_{Int} corresponds to the time of the first minimum after initial stimulation (see Fig. A.1B and C).

This way, the robustness of both initial activation amplitude and timing of the first transient response, two characteristic measures of system dynamics, can be estimated concomitantly.

As the measure of robustness I calculated the mean value $< var >$ and standard deviation sd of obtained relative variations var_i:

- for HOG model (I considered $I = 0.4$ M as the representative stimulus value) $< var > \pm sd = 11.3 \pm 8.3\%$,

- for NF-κB model $< var > \pm sd = 6.4 \pm 4.8\%$,

- for p53 model $< var > \pm sd = 8.7 \pm 6.4\%$.

One may see that for the considered models values of $< var >$ and sd do not exceed 12%. Thus, the fitted solutions turned out to be very robust with respect to noise in the parameters, also indicating that the fitted solutions are in a well-defined local minimum.
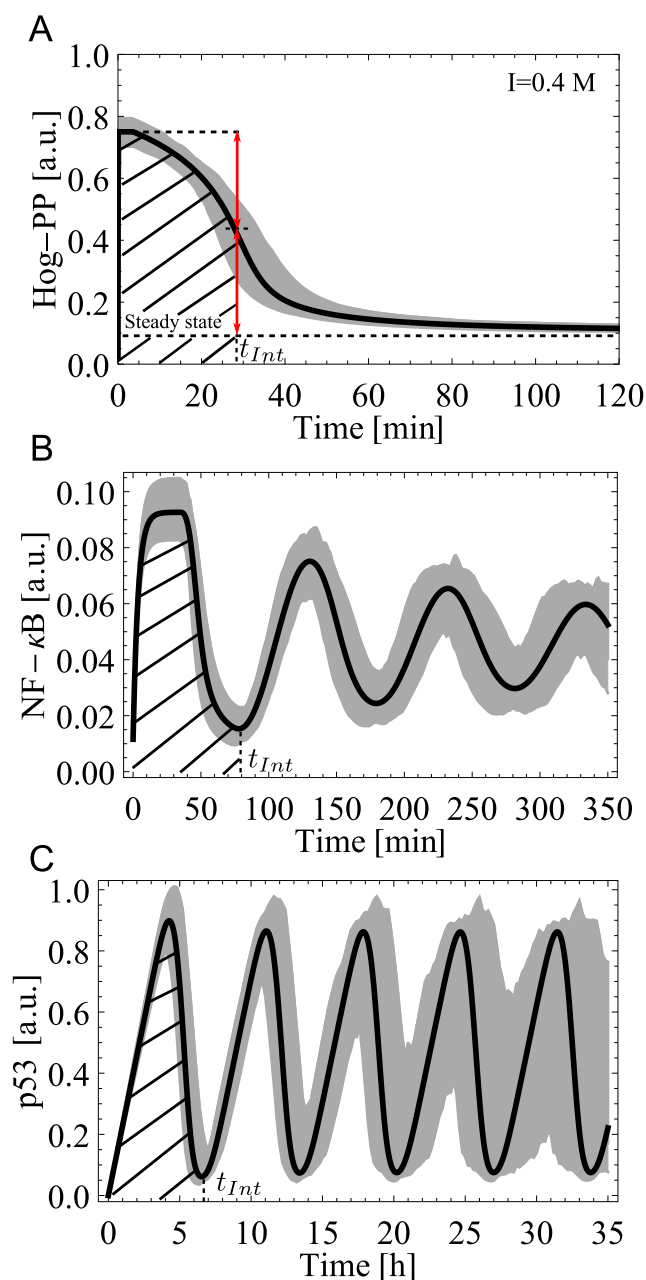
Figure A.1: Robustness of optimal solutions of the HOG model, NF-κB model and p53 model. (A) HOG model with $I = 0.4$ M. (B) NF-κB model. (C) p53 model. Fitted parameter values of models were perturbed 100 times and used for model simulations. Gray region: 0.05-0.95 quantiles of simulations of the parametrized model with perturbed parameters. Black solid line: simulations of models with fitted parameters from Table B.1. Dashed areas correspond to integral values $\int_0^{t_{Int}} C(t)dt$ used for calculating relative variations var_i.

B Estimated parameter values

Table B.1: Best-fit parameters used for the HOG model (2.2), NF-κB model (2.4) and p53 model (2.4).

Parameters	HOG model	NF-κB model	p53 model
I	-	$I^* = 10$ ng/ml	$0.23\,[a.u.]$
T_0	0.07 M	$1.43\,\mu$M	-
τ	4.22 min	34.5 min	1.37 h
ξ	$0.57\,\mathrm{min}^{-1}$	-	-
μ	$733.52\,[a.u.]$	$0.002\,[a.u.]$	-
α	$2668.34\,\mathrm{min}^{-1}$	$0.26\,\mathrm{min}^{-1}$	$5.9 \times 10^{-13}\,\mathrm{h}^{-1}$
η	$0.034\,\mathrm{min}^{-1}$	$0.045\,\mathrm{min}^{-1}$	$1.16\,\mathrm{h}^{-1}$
β	$0.004\,\mathrm{min}^{-1}$	$0.052\,\mathrm{min}^{-1}$	$0.94\,\mathrm{h}^{-1}$
δ	-	$141.7\,\mathrm{min}^{-1}$	$176\,\mathrm{h}^{-1}$
ρ	$0.03\,\mathrm{min}^{-1}$	-	-
K_m	$0.064\,\mu$M	$0.4\,\mu$M	$2\,\mu$M
n	-	2.6	4.97
$C(t \leq 0)$	$0.025\,[a.u.]$	$0.012\,[a.u.]$	$0\,[a.u.]$
$R(t \leq 0)$	$0.2\,[a.u.]$	$0.01\,[a.u.]$	$0\,[a.u.]$
SSR	0.11	1.7×10^{-3}	2.16

Designations: SSR - the sum of squared residuals

Table B.2: Best-fit parameters used for the synthetic gene oscillator model (4.1).

Parameters	Values
k_0	$0.66\,[a.u.]$
k_1	$0.73\,\mathrm{min}^{-1}$
k_2	$1.37\,\mathrm{min}^{-1}$
n_1	2.39
n_2	3.34
K_{m1}	$0.48\,\mu$M
K_{m2}	$0.28\,\mu$M
τ_a	4.25 min
τ_r	17.67 min
$AraC(t \leq 0)$	$0\,[a.u.]$
$LacI(t \leq 0)$	$0\,[a.u.]$

Bibliography

[1] L. Allen. *An Introduction to Stochastic Processes with Applications to Biology.* Pearson/Prentice Hall, 2003.

[2] U. Alon. *An introduction to systems biology: design principles of biological circuits*, volume 10. Chapman & Hall/CRC, 2006.

[3] U. Alon. Network motifs: theory and experimental approaches. *Nat. Rev. Genet.*, 8(6):450–461, 2007.

[4] G. R. Amores, M.-E. Guazzaroni, and R. Silva-Rocha. Engineering synthetic cis -regulatory elements for simultaneous recognition of three transcriptional factors in bacteria. *ACS Synth. Biol.*, 4(12):1287–1294, August 2015.

[5] D. Angeli, J. E. Ferrell, and E. D. Sontag. Detection of multistability, bifurcations, and hysteresis in a large class of biological positive-feedback systems. *Proceedings of the National Academy of Sciences*, 101(7):1822–1827, feb 2004.

[6] D. Angeli and E. D. Sontag. Oscillations in I/O monotone systems under negative feedback. *IEEE Transactions on Automatic Control*, 53(Special Issue):166–176, jan 2008.

[7] L. Ashall, C. A. Horton, D. E. Nelson, P. Paszek, C. V. Harper, K. Sillitoe, S. Ryan, D. G. Spiller, J. F. Unitt, D. S. Broomhead, et al. Pulsatile stimulation determines timing and specificity of NF-κB-dependent transcription. *Science Signalling*, 324(5924):242, 2009.

[8] F. M. Asl and A. G. Ulsoy. Analysis of a system of linear delay differential equations. *J. Dyn. Sys., Meas., Control*, 125(2):215, 2003.

[9] K. Aström and R. Murray. *Feedback Systems: An Introduction for Scientists and Engineers.* Princeton University Press, 2010.

[10] M. R. Atkinson, M. A. Savageau, J. T. Myers, and A. J. Ninfa. Development of genetic circuitry exhibiting toggle switch or oscillatory behavior in escherichia coli. *Cell*, 113(5):597–607, May 2003.

[11] G. Baker and P. Graves-Morris. *Padé Approximants.* Encyclopedia of Mathematics and its Applications. Cambridge University Press, 1996.

[12] E. Batchelor, A. Loewer, C. Mock, and G. Lahav. Stimulus-dependent dynamics of p53 in single cells. *Mol. Syst. Biol.*, 7:488, May 2011.

[13] A. Becskei and L. Serrano. Engineering stability in gene networks by autoregulation. *Nature*, 405(6786):590–593, Jun 2000.

[14] R. Bellmann and K. L. Cooke. *Differential-difference equations.* Mathematics in

Science and Engineering. Elsevier Science, 1963.

[15] S. Bernard, B. Cajavec, L. Pujo-Menjouet, M. C. Mackey, and H. Herzel. Modelling transcriptional feedback loops: the role of Gro/TLE1 in Hes1 oscillations. *Philosophical Transactions of the Royal Society A: Mathematical, Physical and Engineering Sciences*, 364(1842):1155–1170, 2006.

[16] M. A. Blätke, M. Heiner, and W. Marwan. Chapter 7 - biomodel engineering with petri nets. In R. S. Robeva, editor, *Algebraic and Discrete Mathematical Methods for Modern Biology*, pages 141 – 192. Academic Press, Boston, 2015.

[17] N. Blüthgen. Transcriptional feedbacks in mammalian signal transduction pathways facilitate rapid and reliable protein induction. *Mol. Biosyst.*, 6(7):1277–1284, 2010.

[18] G. E. P. Box and N. R. Draper. *Empirical Model-building and Response Surface*. John Wiley & Sons, Inc., New York, NY, USA, 1986.

[19] A. Börsch and J. Schaber. How time delay and network design shape response patterns in biochemical negative feedback systems. *BMC Systems Biology*, 10(1), 2016.

[20] A. Coddington. *An Introduction to Ordinary Differential Equations*. Dover Books on Mathematics. Dover Publications, 2012.

[21] K. L. Cooke and Z. Grossman. Discrete delay, distributed delay and stability switches. *Journal of Mathematical Analysis and Applications*, 86(2):592 – 627, 1982.

[22] C. Cosentino and D. Bates. *Feedback control in systems biology*. CRC Press, 2011.

[23] R. M. M. Domitilla Del Vecchio. *Biomolecular Feedback Systems*. Princeton University Press, 2014.

[24] G. S. Downs, Y.-M. Bi, J. Colasanti, W. Wu, X. Chen, T. Zhu, S. J. Rothstein, and L. N. Lukens. A developmental transcriptional network for maize defines coexpression modules. *Plant Physiology*, 161(4):1830–1843, Feb 2013.

[25] R. Driver. *Ordinary and delay differential equations*. Applied mathematical sciences. Springer-Verlag, 1977.

[26] T. Eißing, F. Allgöwer, and E. Bullinger. Robustness properties of apoptosis models with respect to parameter variations and intrinsic noise. *IEE Proceedings-Systems Biology*, 152(4):221–228, 2005.

[27] M. B. Elowitz and S. Leibler. A synthetic oscillatory network of transcriptional regulators. *Nature*, 403(6767):335–338, 2000.

[28] K. Engelborghs, T. Luzyanina, and G. Samaey. DDE-BIFTOOL v. 2.00: a matlab package for bifurcation analysis of delay differential equations. Technical Report TW-330, Department of Computer Science, K.U.Leuven, Belgium, 2001.

[29] L. Evans. *Partial Differential Equations.* Graduate studies in mathematics. American Mathematical Society, 2010.

[30] J. E. Ferrell, T. Y.-C. Tsai, and Q. Yang. Modeling the cell cycle: why do certain circuits oscillate? *Cell*, 144(6):874–885, 2011.

[31] A. S. C. Figueiredo. *Mathematical models of IL-10 regulation in macrophages stimulated with immunomodulatory molecules of parasitic nematodes - a systems biology approach.* PhD thesis, 2012.

[32] J. A. Freyre-Gonzalez and L. Trevino-Quintanilla. Analyzing regulatory networks in bacteria. *Nature Education*, 3(9):24, 2010.

[33] T. S. Gardner, C. R. Cantor, and J. J. Collins. Construction of a genetic toggle switch in escherichia coli. *Nature*, 403(6767):339–342, Jan 2000.

[34] T. Gedeon and G. Hines. Upper semicontinuity of morse sets of a discretization of a delay-differential equation: An improvement. *Journal of Differential Equations*, 179(2):369–383, Mar 2002.

[35] S. Gerondakis, M. Grossmann, Y. Nakamura, T. Pohl, and R. Grumont. Genetic approaches in mice to understand Rel/NF-κB and IκB function: transgenics and knockouts. *Oncogene*, 18(49):6888–6895, Nov 1999.

[36] N. Geva-Zatorsky, N. Rosenfeld, S. Itzkovitz, R. Milo, A. Sigal, E. Dekel, T. Yarnitzky, Y. Liron, P. Polak, and G. Lahav. Oscillations and variability in the p53 system. *Mol. Syst. Biol.*, 2(1):2006.0033, 2006.

[37] B. Goodwin. *Temporal organization in cells: a dynamic theory of cellular control processes.* Academic Press, 1963.

[38] B. C. Goodwin. Oscillatory behavior in enzymatic control processes. *Adv. Enzyme Regul.*, 3(0):425 – 437, 1965.

[39] J. Griffith. Mathematics of cellular control processes i. negative feedback to one gene. *J. Theor. Biol.*, 20(2):202 – 208, 1968.

[40] M. Hafner, H. Koeppl, M. Hasler, and A. Wagner. Global robustness analysis and model discrimination for circadian oscillators. *PLoS Comput Biol*, 5(10):e1000534, Oct 2009.

[41] L. H. Hartwell, J. J. Hopfield, S. Leibler, and A. W. Murray. From molecular to modular cell biology. *Nature*, 402(6761 Suppl):C47–C52, Dec 1999.

[42] J. Hasty, M. Dolnik, V. Rottschäfer, and J. J. Collins. Synthetic gene network for entraining and amplifying cellular oscillations. *Phys. Rev. Lett.*, 88(14):148101, 2002.

[43] J. Hasty, F. Isaacs, M. Dolnik, D. McMillen, and J. J. Collins. Designer gene networks: Towards fundamental cellular control. *Chaos*, 11(1):207–220, Mar 2001.

[44] A. Hoffmann, A. Levchenko, M. L. Scott, and D. Baltimore. The IκB-NF-

κB signaling module: Temporal control and selective gene activation. *Science*, 298(5596):1241–1245, 2002.

[45] S. Hohmann. Osmotic adaptation in yeast-control of the yeast osmolyte system. *Int. Rev. Cytol.*, 215:149 – 187, 2002.

[46] S. Hooshangi, S. Thiberge, and R. Weiss. Ultrasensitivity and noise propagation in a synthetic transcriptional cascade. *Proceedings of the National Academy of Sciences*, 102(10):3581–3586, Feb 2005.

[47] T. Insperger. On the approximation of delayed systems by Taylor series expansion. *J. Comput. Nonlinear Dynam.*, 10(2):024503, Jan 2015.

[48] B. N. Kholodenko. Negative feedback and ultrasensitivity can bring about oscillations in the mitogen-activated protein kinase cascades. *Eur. J. Biochem.*, 267(6):1583–1588, 2000.

[49] B. N. Kholodenko, J. F. Hancock, and W. Kolch. Signalling ballet in space and time. *Nat. Rev. Mol. Cell Biol.*, 11(6):414–426, 2010.

[50] J. Kim, D. Bates, I. Postlethwaite, L. Ma, and P. Iglesias. Robustness analysis of biochemical network models. *Systems Biology, IEE Proceedings*, 153(3):96–104, May 2006.

[51] H. Kitano. Biological robustness. *Nat Rev Genet*, 5(11):826–837, Nov 2004.

[52] H. Kitano. Towards a theory of biological robustness. *Mol Syst Biol*, 3, Sep 2007.

[53] E. Klipp, W. Liebermeister, C. Wierling, A. Kowald, H. Lehrach, and R. Herwig. *Systems Biology.* Wiley, 2011.

[54] E. Klipp, B. Nordlander, R. Krüger, P. Gennemark, and S. Hohmann. Integrative model of the response of yeast to osmotic shock. *Nat. Biotechnol.*, 23(8):975–982, 2005.

[55] M. Kollmann, L. Løvdok, K. Bartholomé, J. Timmer, and V. Sourjik. Design principles of a bacterial signalling network. *Nature*, 438(7067):504–507, 2005.

[56] M. H. Kubbutat, R. L. Ludwig, M. Ashcroft, and K. H. Vousden. Regulation of Mdm2-directed degradation by the C terminus of p53. *Mol. Cell. Biol.*, 18(10):5690–5698, Oct 1998.

[57] P. Kunkel and V. Mehrmann. *Differential-algebraic Equations: Analysis and Numerical Solution.* EMS textbooks in mathematics. European Mathematical Society, 2006.

[58] Y. Kuznetsov. *Elements of Applied Bifurcation Theory*, volume 112 of *Applied Mathematical Sciences.* Springer-Verlag New York, 2004.

[59] G. Lahav, N. Rosenfeld, A. Sigal, N. Geva-Zatorsky, A. J. Levine, M. B. Elowitz, and U. Alon. Dynamics of the p53-Mdm2 feedback loop in individual cells. *Nat. Genet.*, 36(2):147–150, 2004.

[60] J. Lam. Model reduction of delay systems using pade approximants. *Interna-*

tional Journal of Control, 57(2):377–391, Feb 1993.

[61] J. Lambert. Observationes variae in mathesin puram. *Acta Helvetica, physico-mathematico-anatomico-botanico-medica*, III:128–168, 1758.

[62] A. Lapytsko and J. Schaber. The role of time delay in adaptive cellular negative feedback systems. *Journal of Theoretical Biology*, 398:64–73, 2016.

[63] S. Legewie, H. Herzel, H. V. Westerhoff, and N. Blüthgen. Recurrent design patterns in the feedback regulation of the mammalian signalling network. *Mol Syst Biol*, 4:190, 2008.

[64] R. Lev Bar-Or, R. Maya, L. A. Segel, U. Alon, A. J. Levine, and M. Oren. Generation of oscillations by the p53-Mdm2 feedback loop: A theoretical and experimental study. *Proceedings of the National Academy of Sciences*, 97(21):11250–11255, 2000.

[65] L. Ljung. *System Identification: Theory for the User*. Pearson Education, 1998.

[66] D. M. Longo, J. Selimkhanov, J. D. Kearns, J. Hasty, A. Hoffmann, and L. S. Tsimring. Dual delayed feedback provides sensitivity and robustness to the nf-κb signaling module. *PLoS Comput Biol*, 9(6):e1003112, 2013.

[67] L. Ma and P. A. Iglesias. Quantifying robustness of biochemical network models. *BMC Bioinformatics*, 3(1):38, 2002.

[68] W. Ma, A. Trusina, H. El-Samad, W. A. Lim, and C. Tang. Defining network topologies that can achieve biochemical adaptation. *Cell*, 138(4):760–773, 2009.

[69] J. Macia, S. Regot, T. Peeters, N. Conde, R. Solé, and F. Posas. Dynamic signaling in the Hog1 MAPK pathway relies on high basal signal transduction. *Sci Signal*, 2(63):ra13, 2009.

[70] J. Mahaffy and C. Pao. Models of genetic control by repression with time delays and spatial effects. *J. Math. Biol.*, 20(1):39–57, 1984.

[71] J. Mallet-Paret. Morse decompositions for delay-differential equations. *Journal of Differential Equations*, 72(2):270–315, Apr 1988.

[72] D. McCloskey, B. O. Palsson, and A. M. Feist. Basic and applied uses of genome-scale metabolic network reconstructions of escherichia coli. *Molecular Systems Biology*, 9(1):661–661, Jan 2013.

[73] R. Milo. Network motifs: Simple building blocks of complex networks. *Science*, 298(5594):824–827, Oct 2002.

[74] W. Mocek, R. Rudnicki, and E. Voit. Approximation of delays in biochemical systems. *Mathematical Biosciences*, 198(2):190–216, Dec 2005.

[75] U. M. Moll and O. Petrenko. The MDM2-p53 Interaction. *Molecular Cancer Research*, 1(14):1001–1008, December 2003.

[76] N. A. Monk. Oscillatory expression of hes1, p53, and NF-κB driven by transcriptional time delays. *Curr. Biol.*, 13(16):1409 – 1413, 2003.

[77] K. F. Murphy, R. M. Adams, X. Wang, G. Balazsi, and J. J. Collins. Tuning and controlling gene expression noise in synthetic gene networks. *Nucleic Acids Research*, 38(8):2712–2726, Mar 2010.

[78] J. A. Nelder and R. Mead. A simplex method for function minimization. *The Computer Journal*, 7(4):308–313, jan 1965.

[79] D. Nelson, A. Ihekwaba, M. Elliott, J. Johnson, C. Gibney, B. Foreman, G. Nelson, V. See, C. Horton, D. Spiller, et al. Oscillations in NF-κB signaling control the dynamics of gene expression. *Science Signalling*, 306(5696):704, 2004.

[80] L. K. Nguyen. Regulation of oscillation dynamics in biochemical systems with dual negative feedback loops. *J. R. Soc. Interface*, 9(73):1998–2010, Aug 2012.

[81] X. Y. Ni, T. Drengstig, and P. Ruoff. The control of the controller: molecular mechanisms for robust perfect adaptation and temperature compensation. *Biophys. J.*, 97(5):1244–1253, 2009.

[82] D. Noble. *The Music of Life: Biology beyond genes*. OUP Oxford, 2008.

[83] B. Novak, O. Kapuy, M. R. Domingo-Sananes, and J. J. Tyson. Regulated protein kinases and phosphatases in cell cycle decisions. *Curr. Opin. Cell Biol.*, 22(6):801–808, 2010.

[84] B. Novak, J. J. Tyson, B. Gyorffy, and A. Csikasz-Nagy. Irreversible cell-cycle transitions are due to systems-level feedback. *Nat. Cell Biol.*, 9(7):724–728, 2007.

[85] H. L. Pahl. Activators and target genes of Rel/NF-κB transcription factors. *Oncogene*, 18(49):6853–6866, Nov 1999.

[86] J. E. Purvis, K. W. Karhohs, C. Mock, E. Batchelor, A. Loewer, and G. Lahav. p53 dynamics control cell fate. *Science Signalling*, 336(6087):1440, 2012.

[87] J. L. Ramos, M. Martinez-Bueno, A. J. Molina-Henares, W. Teran, K. Watanabe, X. Zhang, M. T. Gallegos, R. Brennan, and R. Tobes. The tetr family of transcriptional repressors. *Microbiology and Molecular Biology Reviews*, 69(2):326–356, Jun 2005.

[88] S. Rastgou Talemi, G. Kollarovic, A. Lapytsko, and J. Schaber. Development of a robust DNA damage model including persistent telomere-associated damage with application to secondary cancer risk assessment. *Scientific Reports*, 5:13540, Sep 2015.

[89] D. J. Robbins, D. L. Fei, and N. A. Riobo. The hedgehog signal transduction network. *Science Signaling*, 5(246):re6–re6, Oct 2012.

[90] H. H. M. Sauro and B. B. N. Kholodenko. Quantitative analysis of signaling networks. *Prog. Biophys. Mol. Biol.*, 86(1):5–43, 2004.

[91] J. Schaber, R. Baltanas, A. Bush, E. Klipp, and A. Colman-Lerner. Modelling reveals novel roles of two parallel signalling pathways and homeostatic feedbacks in yeast. *Mol. Syst. Biol.*, 8:622, 2012.

[92] J. Schaber, A. Lapytsko, and D. Flockerzi. Nested autoinhibitory feedbacks alter the resistance of homeostatic adaptive biochemical networks. *J. R. Soc. Interface*, 11(91):20130971, Feb 2014.

[93] G. Seber and C. Wild. *Nonlinear Regression*. Wiley Series in Probability and Statistics. Wiley, 2003.

[94] S. S. Shen-Orr, R. Milo, S. Mangan, and U. Alon. Network motifs in the transcriptional regulation network of escherichia coli. *Nat. Genet.*, 31(1):64–68, Apr 2002.

[95] H. Smith. *An Introduction to Delay Differential Equations with Applications to the Life Sciences*. Texts in Applied Mathematics. Springer Science+Business Media, LLC, 2010.

[96] J. Stelling, U. Sauer, Z. Szallasi, F. J. Doyle, and J. Doyle. Robustness of cellular functions. *Cell*, 118(6):675–685, Sep 2004.

[97] U. Stelzl, U. Worm, M. Lalowski, C. Haenig, F. H. Brembeck, H. Goehler, M. Stroedicke, M. Zenkner, A. Schoenherr, S. Koeppen, and et al. A human protein-protein interaction network: A resource for annotating the proteome. *Cell*, 122(6):957–968, Sep 2005.

[98] R. Storn and K. Price. Differential evolution–a simple and efficient heuristic for global optimization over continuous spaces. *Journal of global optimization*, 11(4):341–359, 1997.

[99] J. Stricker, S. Cookson, M. R. Bennett, W. H. Mather, L. S. Tsimring, and J. Hasty. A fast, robust and tunable synthetic gene oscillator. *Nature*, 456(7221):516–519, Nov 2008.

[100] S. Strogatz. *Nonlinear Dynamics and Chaos: With Applications to Physics, Biology, Chemistry, and Engineering*. Advanced book program. Westview Press, 1994.

[101] O. E. Sturm, R. Orton, J. Grindlay, M. Birtwistle, V. Vyshemirsky, D. Gilbert, M. Calder, A. Pitt, B. Kholodenko, and W. Kolch. The mammalian MAPK/ERK pathway exhibits properties of a negative feedback amplifier. *Science Signalling*, 3(153):ra90, 2010.

[102] H. S. Tharp and W. W. Zhang. Robust control of a nonlinear time-delay system. *Dynamics and Control*, 4(1):21–38, Jan 1994.

[103] P. Trairatphisan, A. Mizera, J. Pang, A. Tantar, J. Schneider, and T. Sauter. Recent development and biomedical applications of probabilistic boolean networks. *Cell Commun Signal*, 11(1):46, 2013.

[104] T. Y.-C. Tsai, Y. S. Choi, W. Ma, J. R. Pomerening, C. Tang, and J. E. Ferrell. Robust, tunable biological oscillations from interlinked positive and negative feedback loops. *Science*, 321(5885):126–129, 2008.

[105] J. J. Tyson, K. C. Chen, and B. Novak. Sniffers, buzzers, toggles and blinkers:

dynamics of regulatory and signaling pathways in the cell. *Curr. Opin. Cell Biol.*, 15(2):221–231, 2003.

[106] D. Vecchio and R. Murray. *Biomolecular Feedback Systems.* Princeton University Press, 2014.

[107] D. D. Vecchio and R. M. Murray. Synthetic biology. *Encyclopedia of Systems and Control*, pages 1–8, 2013.

[108] L. Villa-Komaroff, A. Efstratiadis, S. Broome, P. Lomedico, R. Tizard, S. P. Naber, W. L. Chick, and W. Gilbert. A bacterial clone synthesizing proinsulin. *Proceedings of the National Academy of Sciences*, 75(8):3727–3731, Aug 1978.

[109] W. Weber, M. Fussenegger, et al. Engineering of synthetic mammalian gene networks. *Chemistry & biology*, 16(3):287, 2009.

[110] E. Yeger-Lotem, S. Sattath, N. Kashtan, S. Itzkovitz, R. Milo, R. Y. Pinter, U. Alon, and H. Margalit. Network motifs in integrated cellular networks of transcription-regulation and protein-protein interaction. *Proceedings of the National Academy of Sciences*, 101(16):5934–5939, Apr 2004.

[111] T.-M. Yi, Y. Huang, M. I. Simon, and J. Doyle. Robust perfect adaptation in bacterial chemotaxis through integral feedback control. *Proceedings of the National Academy of Sciences*, 97(9):4649–4653, 2000.